Abstract

Teaching Vector Control for Induction Motors by Implementing Simulation and Real-Time FPGA Tools

by Joycer Osorio

Detailed explanation and implementation of complex control laws as vector control for AC electric drives are quite important for academic formation of new candidate engineers and researchers interested in learning and improving control laws for AC electric motors. Alternative energy sources are quite important for different application and it is presented in this thesis work the implementation in an electric motor of intelligent and conventional vector controllers by means of simulation, co-simulation and experimental tools. It is also the aim of this work to be useful for other researchers as a knowledge source in order to keep improving on control techniques for AC electric drives. Also, this work has the potential to contribute to students and researchers to have a complete detailed theory, design and implementation guide of vector control to AC induction motors. This can help to green energy transportation and to keep developing science in favor of alternative energy implementation for several applications.

The designing phases are aided by Mathworks Matlab and National Instruments LabVIEW tools, and validated with real time experimentation and within co-simulation environment. All the work involved in this thesis is well documented in order to provide useful guidelines to design and implement the vector control technique for electric drives control applications.

The vector control technique is used for AC motors applications and its main goal is to decoupling the rotor magnetic flux and torque components based on coordinate framework transformations and mathematical equations computation. The latter, contribute to the vector control complexity because a relevant quantity of calculations need to be carried out in order to perform a control action. In this work, two vector control designs are tested by simulation and experimentation. From these tests and evaluations relevant points are noted in order to highlight the key points of a control/motor system performance for electric motor control.

The design of an intelligent vector control technique is implemented in this work, which is complemented by artificial intelligence and robust control techniques in order to achieve an intelligent vector control for EV powertrain. Real-time implementation tools are used to achieve a better understanding of how a vector control works and how can other control techniques and methods can be applied for improvement.

Fuzzy Logic and Sliding Mode Control (SMC) techniques are implemented with the vector control in order to have a good performance of a motor/control system performance and therefore EV powertrain operation in a simulation and co-simulation environments. The second important part of this thesis is reflected in the implementation of different tools that helps to improve the design of an AC motor controller; this last part is deeply explained throughout chapter two to four with the intention to depict step by step the details of an EV model, induction motor model, a conventional and an intelligent vector control.

Table of Contents

List of figures

Chapter 1: Introduction and State of the Art

Teaching control theory for electric machines requires well knowledge foundation on electromagnetics, control laws based on the electric motors, modulation techniques and stability analysis, just to mention a few topics. Beside this, a set of tools needs to be deployed to execute the required analysis steps to accomplish a final control law design. In this work is presented the theory behind the design and implementation method of FOC. This technique is use to control three-phases electric machines and is one of the most used techniques for a wide range of applications (e.g. automotive, industry, energy, etc.).

FOC and AC electrical machine theories are topics primary taught in university careers such as electrical engineering and graduate studies on this field. Several types of research have proposed innovating tools with access through the internet (Sepe and Short 2000; Sepe, Chamberland, and Short 1999; Veiga et al. 2012; Ernest et al. 2007) as interactive motor control laboratories to ease students experience with experimentation and practices with motor control. Other studies have been focused on developing scaled platform to test motor control for applications such as hybrid electric vehicles (Tant et al. 2012; Timmermans et al. 2009). Virtual approaches (Zorzano et al. 2007; Goldberg, Horton, and Agayoff 2001; Fraile-Ardanuy et al. 2011) have been also proposed in order to set interactive virtual environments to develop tests related to electric motor control. Those studies support the practical application by setting remote connections with environments where experimentation can be carried out. From the perspective presented in this study, the theoretical explanation along with the implementation of FOC in simulations and real-time execution will contribute to students to link theory with experimentation.

Modeling and real-time design tools have been used in some studies with the aim of proposing a more realistic experience to students with the implementation of power electronics and electric machine control as presented in (Chen and Wei 2008; Banerjee et al. 2015; Zhao and Wang 2005; Pacheco, Batista, and Petry 2012; Pérez et al. 2008). Where software like Matlab/Simulink, Modelica and LabVIEW, and real-time hardware such as DSP, FPGA and PSPICE are implemented to develop electric drives control and help to analyze control response by using post processing tools of the software mentioned. A modular approach is presented in (Ponce, Pacas, and Molina 2012) based on a set of blocks to rapidly design induction motor control to have a laboratory setup to proceed with simulation and full real-time tests. In this work, the focus is to present the theoretical explanation of FOC applied to induction motors and tested in a simulation environment Matlab/Simulink and real-time implementation using LabVIEW. This approach can contribute to improve teaching experience in courses such as Electric Machine Laboratory, Power Electronic Control and Energy Transformation Laboratory in the careers of Mechatronics and Electrical Engineering at Tecnológico de Monterrey-Mexico

A potential result from improving control and electric motor understanding is the implementation of enhanced control theories for AC induction motors in electric motor applications. In this work is presented the EV operation and relation with electric drives and power electronics, since it is an important application for AC electric drives. Also, engineer students interested in control of AC motors are encourage to pursuit the implementation of vector control and induction motors in EV applications to keep developing novel control strategies for this type of application. In this study the theory, design and implementation of vector control and induction motors will be supported with simulations of the vehicle and powertrain models, the co-simulation and experimentation will be carried out just for the induction motor.

In order to provide a better comprehension of EV, this introductory chapter will present relevant information related to EVs. For a very long time EVs have been in existence. They give very low acoustic noise and zero emissions in their tailpipes. Even though they once competed favorably with the highly inefficient internal combustion engine vehicles, the latter gained upper hand because of the poor battery capacity which made the driving range of electric vehicles short before recharging.

Inter Combustion Vehicles (ICVs) are the main competitor of EVs and HEVs, therefore different alternative solutions have been proposed in order to tackle internal combustion issues by means of EV and HEV improvements. However, the fundamental disadvantage of EVs is storage capability. The fuel tank for an ICV can store far more energy, in a much smaller space than a battery pack, at a much lower initial cost. The storage disadvantage of EVs becomes much less important when the vehicles are driven at low average speeds within urban areas. At such speeds, it can take a long time to deplete the battery pack. Further, as average speed declines, the average energy requirement per hour of operation drops off considerably more rapidly than for conventional gasoline and diesel engines, extending the hours that can be driven on a full charge (Santini 2011).

This chapter present a state of the art of the most relevant research works related to HEV and EV. This will be divided in the following subjects:

- Energy management
- Power electronics
- Powertrain and Intelligent Control

The list above gathers the main parts of EVs and HEVs. Besides, it is important to know how other researchers are tackling EV improvements in order to lead correctly the contributions resulted from this thesis.

1.1 Energy Management

EV and HEVs rely mainly on the power of their battery supply, therefore it is important to work on the power units in order to minimize weights, increase thermal isolation, increase efficiency and so on; with the creation of an intelligent power unit (IPU) the EV/HEVs get a reduction of weight and an increment of efficiency, functionality and reliability (Majumdar et al. 2001). The IPU is created with power chips, a DC capacitor, and a processor that monitors the current and voltage; this new IPU include the power phase which contains the rectifier and inverter components. The latter plays a quite important role in the correct operation of AC drives, actually the inverter is the core for an AC driver operation and now the 5th generation inverters are implemented in order to address higher performance

One of the most important parts of an EV and HEV is the energy storage unit; this could be batteries, ultracapacitors and/or fuel cells. On this field several works have been proposed regarding storage unit configuration and control algorithms in order to optimize energy efficiency. Amjadi and Williamson proposed (Amjadi and Williamson 2010) for a plug-in HEV (PHEV) a combined energy storage unit (i.e. batteries, ultracapacitors and regenerative fuel cells (RFC)), this unit is determined by a current loop controller and PI-type regulators are used for both the RFC generator and battery power stage regulation. To achieve the correct operation of the vehicle, it was proposed a multiple-input dc/dc power converter (MIPEC), which is devoted to combine the power flows of multiple energy sources of the on-board EV/PHEV energy storage systems.

Another form to tackle issues related to EV and HEV's energy management is based on driving cycle sensitivity identification, Liang *et al* (Liang et al. 2009) proposed a control strategy using support vector machine (SVM) to identify driving cycles and then optimize the energy management for an HEV. The results obtained by Liang *et al* demonstrates that the proposed control improved the fuel economy and reduced emissions.

Yi and Liang (Yi et al. 2009) proposed an intelligent control based on Fuzzy and Neural Network methods for an intelligent energy management of parallel HEV. It includes using fuzzy neural to identify the different cities' driving cycles and changing the working area of engine according to the identify results.

The obtained control was proved to identify the driving cycle of the cities of Guangzhou and Shanghai, the results were successful and the intelligent energy management based on driving cycle identification could make the engine and motor work effectively and improve fuel economy and reduce emissions.

Danhong *et al* (Zhang et al. 2009) proposed an intelligent energy management for a PHEV based on fuzzy logic and genetic algorithms (GA). The State of Charge (SOC), the desired vehicle power and battery power, were the variables to control. The GA-fuzzy logic controller was implemented in a PHEV model and simulated in ADVISOR. The simulations results demonstrate a significant fuel consumption improvement using a GA-fuzzy controller rather than a fuzzy controller.

Rosario and Luk (L. C. Rosario and Luk 2006) presented a modular power and energy management system (PEMS) for an electric vehicle with hybrid storage unit, battery-ultracapacitor. The PEMS is comprised by three main parts: the energy management shell (EMS), which handles the long-term decisions of energy usage in relation to the longitudinal dynamics of the vehicle; power management shell (PMS) which handles the fast decisions to generate power split ratios between the batteries and ultracapacitors; and power electronics shell (PES) which handles the ultra-fast switching functions that facilitate the active power sharing between the two sources. Since the EMS defines the values of maximum and minimum battery and ultracapacitor power, battery positive and negative slew coefficient, and ultracapacitor charging power; it was proposed a fuzzy inference system in order to maintain the vehicle kinetic to electric energy balance correlation by regulating the SOC of the ultracapacitor bank as a function of the vehicle velocity. Also, based on the fuzzy controller for the EMS, the battery power is regulated, and the desired energy levels are achieved based on the vehicle power and speed demands. The PEMS was implemented in an electric go-kart vehicle; the modular PEMS proposed in (L. C. Rosario and Luk 2006) provides a novel framework to develop and test the electric vehicle in a consistent and systematic manner.

In other research work Luk and Rosario (Luk and Rosario 2006) proposed another design structure for electric vehicle with dual energy storage units, battery-ultracapacitor. This structure is based on special sequential decision process, which determines the power split ratio and reference energy levels of the dual battery-ultracapacitor as well as the optimal SOC throughout the drive cycle. The energy management policy proposed in (Luk and Rosario 2006) was experimentally verified with effective results. In a more recent work the researchers Rosario and Luk (L. Rosario, Chi, and Luk 2007) continue with their research line and proposed an improvement of the PEMS proposed in (L. C. Rosario and Luk 2006).

Esposito *et al* (Esposito, Isastia, and Meo 2010) proposed the implementation of an optimization algorithm called particle swarm optimization (PSO) for the energy management of an EV with dual energy storage units, battery-ultracapacitor. The proposed approach is able to split the power demand between battery and ultracapacitor maximizing the driving range and the performances of the vehicle, this also increases the life cycle of the battery. The variable to control is the SOC for both storage units and in order to prove the proposed PSO energy management strategy, simulations were carried with Lead-acid, NiMH and Li-ion batteries for different driving cycles. The suggested strategy achieved energy saving of +13%, 9.9% and +1.7% respectively with each battery.

1.2 Power Electronics

The power electronics components of a EV is mainly composed by energy source and storage units, electric motors, inverter and rectifier. These components define the correct operation of the powertrain systems, which is comprised by electric motor, storage unit, gearbox and wheels. Therefore, the relation among the power electronic components and the powertrain defines the EV performance. Hence several research works have been developed in order to guarantee the efficient of the mentioned relation.

1.2.1 Energy Sources and Storages

These units represent the EV core and based on the storage capacity and efficiency the EV will be able to reach longer distances and better power delivered by storage units to the vehicle. Since this thesis is focused on EV, in this subsection will be presented two of the most important energy storage units used for EV applications.

1.2.1.1 Batteries and Ultracapacitors

The efficient performance of EV is based on the energy sources capabilities, this means, how long can work a vehicle in an electric regime using the primary energy source (e.g. batteries and/or ultracapacitors).

- **Batteries**

For EVs and HEVs nickel metal hybrid (NMH) batteries have been most popular implemented storage unit until 2006. Now, the development of lithium-ion batteries has progressed to the point that strong consideration is being given to the use of those batteries in EVs and HEVs. For EVs there are some considerations that must be fulfilled by the battery, those are:

1. The battery must be sized to meet the specified range of the vehicle.
2. Life cycle for deep discharges is a key consideration and it is essential that the battery meets a specified minimum requirement.
3. The weight and volume are calculated from the energy consumption (Wh/km) of the vehicle and the energy density (Wh/kg, Wh/L) of the battery discharged over the appropriate test cycle.
4. The battery sized by range can meet the power (kW) requirement for a specified power demand acceleration performance, gradeability, and top cruising speed of the vehicle.

The current technology for batteries implements materials like: lead-acid, nickel metal hybride and lithium-ion. Depending on the application (HEV or EV) the batteries will have certain specific characteristics, which means that based on several experiments and researches were detected the main differences to take into account for the battery design. Table 1 was taken from (Burke 2007) and it shows the characteristic values for HEV and EV.

Table 1. Various Technologies/Types of Batteries for EV and HEV (Burke 2007)

Battery Technology	Application	Ah	V	Wh/kg At C/3	Resist mOhm	W/kg Match. Imped.	W/kg 95%eff.	SOC
Lead-acid								
Panasonic	HEV	25	12	26.3	7.8	389	77	28%
Panasonic	EV	60	12	34.2	6.9	250	47	---
Nickel Metal Hydride								
Panasonic EV	EV	65	12	68	8.7	240	46	---
Panasonic EV	HEV	6.5	7.2	46	11.4	1093	207	40%
Ovonic	EV	85	13	68	10	200	40	---
Ovonic	HEV	12	12	45	10	1000	195	30%
Saft	HEV	14	1.2	47	1.1	900	172	30%
Lithium-ion								
Saft	HEV	12	4	77	7	1550	256	20%
Saft	EV	41	4	140	8	476	90	---
Shin-Kobe	EV	90	4	105	0.93	1344	255	---
Shin-Kobe	HEV	4	4	56	3.4	3920	745	18%

From Table 1 is possible to note some important features from EV and HEV batteries. For the EV batteries the cell size (Ah) is significant larger than that of the HEV batteries, this is because the EV batteries need to store more energy than HEV batteries. Another difference important to remark is the power capability of the batteries designed for HEVs is much higher than batteries for EVs, the reason behind this is the lower weight of the HEV batteries and the need to transfer energy in and out of the HEV batteries at high efficiency. In this order, is identified that the energy densities of the HEV batteries are significantly lower than that of the EV batteries of the same chemistry.

- **Ultracapacitors**

Electric double-layer capacitors, also known as supercapacitors, electrochemical double layer capacitors (EDLCs), or ultracapacitors. This energy storage unit is frequently used for power delivering optimization, in other words, ultracapacitors are combined with batteries for EVs in order to compensate the low power capabilities of EV but using their high energy.

In a conventional capacitor, energy is stored by the removal of charge carriers, typically electrons, from one metal plate and depositing them on another. This charge separation creates a potential between the two plates, which can be harnessed in an external circuit. The total energy stored in this fashion is proportional to both the number of charges stored and the potential between the plates. In contrast with traditional capacitors, electric double-layer capacitors do not have a conventional dielectric. Rather than two separate plates separated by an intervening substance, these capacitors use "plates" that are in fact two layers of the same substrate, and their electrical properties, the so-called "electrical double layer", result in the effective separation of charge despite the vanishingly thin (on the order of nanometers) physical separation of the layers.

Currently most development has been on double-layer capacitors using microporous carbon in both of the electrodes. Electrochemical capacitors that have an unusually high energy density compared to common capacitors, typically on the order of thousands of times greater than a high capacity electrolytic capacitor. These elements can be used in HEV sustaining charge, for ultracapacitors the energy storage unit is sized by the energy storage (Wh) requirement because the energy density (Wh/kg) of ultracapacitors is relatively low (5-10 Wh/kg) and the useable power density is high (1-2 kW/kg).

Ultracapacitors have several disadvantages and advantages relative to batteries:

Disadvantages

- The amount of energy stored per unit weight is considerably lower than that of an electrochemical battery (3-5 W.h/kg for an ultracapacitor compared to 30-40 W.h/kg for a battery). It is also only about 1/10,000th the volumetric energy density of gasoline.

- The voltage varies with the energy stored. To effectively store and recover energy requires sophisticated electronic control and switching equipment.

- Has the highest dielectric absorption of all types of capacitors.

Advantages

Very high rates of charge and discharge.

Little degradation over hundreds of thousands of cycles.

Good reversibility

Low toxicity of materials used.

High cycle efficiency (95Vo or more)

The ultracapacitors represent a distinct technology, which is remarkable in their power and life cycle characteristics significantly better than the high power batteries because the energy density of the capacitors will be significantly less than that of batteries. From (Burke 2007) is taken The characteristics of different ultracapacitors technologies and are presented in Table 2.

Table 2. Characteristics of Carbon/Carbon Ultracapacitors, (Burke 2007)

Device	V rated	C (F)	R (mOhm)	RC (sec)	Wh/kg (1)	W/kg (95%) (2)	W/kg Match. Imped.	Wgt. (kg)	Vol.lit.
Maxwell**	2.7	2800	0.48	1.4	4.45	900	8000	0.475	0.32
Ness	2.7	10	25	0.25	2.5	3040	27000	0.0025	0.0015
Ness	2.7	1800	0.55	1	3.6	975	8674	0.38	0.277
Ness	2.7	3640	0.3	1.1	4.2	928	8010	0.65	0.514
Ness	2.7	5085	0.24	1.22	4.3	958	8532	0.89	0.712
Asahi Glass (propylene carbonate)	2.7	1375	2.5	3.4	4.9	390	3471	.210 (estimated)	0.151
Panasonic (propylene carbonate)	2.5	1200	1	1.2	2.3	514	4596	0.34	0.245
Panasonic	2.5	1791	0.3	0.54	3,44	1890	16800	0.31	0.245
Panasonic	2.5	2500	0.43	1.1	3.7	1035	9200	0.395	0.328
EPCOS	2.7	3400	0.45	1.5	4.3	760	6750	0.6	0.48
Okamura Power Sys.	2.7	1350	1.5	2	4.9	650	5785	0.21	0.151
ESMA	1.3	10000	0.275	2.75	1.1	156	1400	1.1	0.547

(1) Energy density at 400 W/kg constant power, Vrated - 1/2 Vrated (2) Power based on P=9/16*(1-EF)* V2/R, EF= efficiency of discharge **Except where noted, all the devices use acetonitrile as the electrolyte

The Table 2 presents the characteristics of ultracapacitors in terms of capacitance, density and weight among others. It is possible to note the lower energy density respect to energy density of batteries (see Table 1).

Currently, the application of ultracapacitors is more restricted to mild HEV because the energy storage capacity; for PHEV the ultracapacitors are not suitable as the primary energy storage technology because dangerous implications during the charge process.

1.2.2 Electric Motors

Electric motors play an important role in the success of EVs, HEVs, PHEV and FCVs (Chan 2007). There are three major types of electric motors that are suitable for EV, HEV and FCV applications: 1) induction motors; 2) PM synchronous; and 3) switched reluctance motors. Typical requirements for electric motors for EV applications are:

1. High torque density and power density.
2. Wide speed range including constant torque and constant power operations.
3. High efficiency over wide speed range, high reliability, and robustness.
4. Reasonable cost.

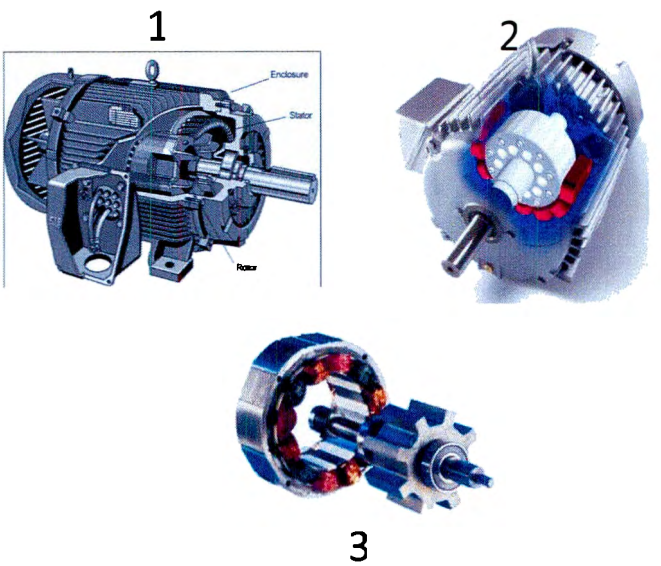

Figure 1. 1) Induction motor, 2) Permanent magnet AC motor 3) Switched reluctance motor

Induction machines are used for EV, HEV and FCV powertrain due their simplicity, robustness, and wide speed range. Besides, induction machines do not have back emf to deal with at high speeds. Field-oriented control (known also as vector control) makes an induction machine behave just like the way a dc machine behaves. Induction motors are classified based on their characteristics. One of them, is based on their rotor type, that is: (1) Squirrel-cage rotor: for this kind of induction motors the rotor is completely isolated. (2) Slip-ring rotor: current is provided to the rotor directly through electrical contacts called commutators and slip rings. This electric motor type will be explained in detail in the following chapter.

Permanent magnet (PM) machines possess unique characteristics such as high efficiency, high torque, and high power density. However, PM motors inherently have a short constant power range due to its rather limited field weakening capability, resulting from the presence of the PM field, which can only be weakened through production of a stator field component, which opposes the rotor magnetic field. Besides, the back emf can be an issue at high speed: the inverter must be able to withstand the maximum back emf generated by the stator winding. In the case of a stator winding short circuit fault, the system can run into problems due to the existence of a rotor PM field.

The switched reluctance motor (SRM) is gaining interest as a candidate of electric propulsion for EVs, HEVs, and FCVs because of its simple and rugged construction, simple control, ability of extremely high

speed operation, and hazard-free operation. These prominent advantages are more attractive for traction application than other kinds of machines. However, since SRM is not yet widely produced as a standard motor, its cost may be higher than the induction motor.

1.2.3 Inverters, Rectifiers and Control Methods

Power electronics is an enabling technology for the development of EVs and implementing the advanced electrical architectures to meet the demands for increased electric loads.

Inverters can be classified in Voltage Source Inverter (VSI) and Current Source Inverter (CSI) (Vandermeulen and Maurin 2010).

- Current Source Inverter: the converter section uses silicon-controlled rectifiers (SCRs), gate commutated thyristors (GCTs), or symmetrical gate commutated thyristors (SGCTs). This converter is known as an active rectifier or active front end (AFE). The DC link uses inductors to regulate current ripple and to store energy for the motor. The inverter section comprises gate turn-off thyristor (GTO) or symmetrical gate commutated thyristor (SGCT) semiconductor switches. These switches are turned on and off to create a pulse width modulated (PWM) output regulating the output frequency.

Voltage Source Inverter: uses a diode rectifier that converts utility/line AC voltage (60 Hz) to DC. The converter is not controlled through electronic firing like the CSI drive. The DC link is parallel capacitors, which regulate the DC bus voltage ripple and store energy for the system. The inverter is composed of insulated gate bipolar transistor (IGBT) semiconductor switches. There are other alternatives to the IGBT: insulated gate commutated thyristors (IGCTs) and injection enhanced gate transistors (IEGTs). This paper will focus on the IGBT as it is used extensively in the MV VSI drives market. The IGBT switches create a PWM voltage output that regulates the voltage and frequency to the motor.

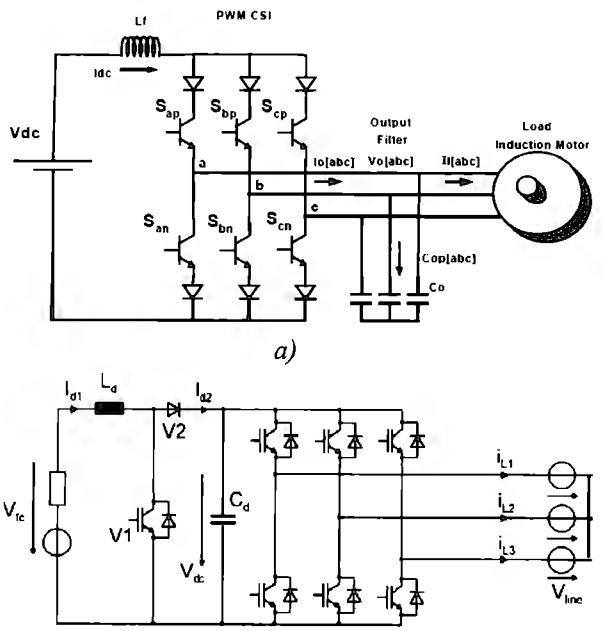

Figure 2. *a)* CSI topology and *b)* VSI topology, (Vandermeulen and Maurin 2010)

From the Figure 2, Vdc represents the DC voltage source, Lf works as a current filter, Ld and Cd compose the DC-Link. Multilevel converters are considered today as the state-of-the-art power-conversion systems for high -power and power- quality demanding applications. Multilevel converters are currently considered as one of the industrial solutions for high dynamic performance covering a power range from 1 to 30 MW (Lai and Peng 1996; Teodorescu et al. 1999; Franquelo et al. 2008). Among the reasons for their success are the higher voltage operating capability, lower common-mode voltages, reduced voltage derivatives (dv/dt), voltages with reduced harmonic contents, near sinusoidal currents, increased efficiency and in some cases possible fault-tolerant operation.

The number of levels of a converter can be defined as the number of steps or constant voltage values that can be generated by the converter between the output terminal and any arbitrary internal reference node within the converter. Typically, it is a dc-link node, and it is usually denoted by N and called neutral. To be called a multilevel converter, each phase of the converter has to generate at least three different voltage levels. This differentiates the classic two-level voltage source converter (2L-VSC) from the multilevel family. Some single-phase examples of this concept and their respective waveforms are given in Figure 3 for different number of levels. It is worth mention that, generally, the different voltage levels are equidistant from each other in multiples of Vdc.

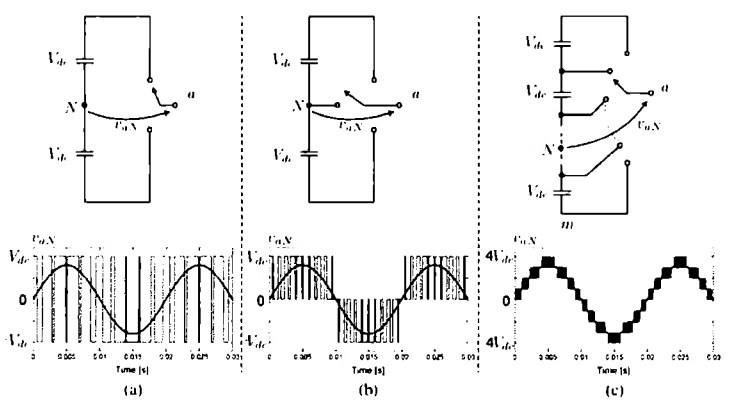

Figure 3. Converter output voltage waveform: a) two level, b) three level, c) nine level

From Figure 3 is possible to note how the waveform is composed by better resolution pulse modulation in proportion to the inverter level. Two-level converters can generate a variable frequency and amplitude voltage waveform by adjusting a time average of their two voltage levels. This is usually performed with pulse-width modulation (PWM) techniques (Holtz 1994). On the other side, multilevel converters add a new degree of freedom, allowing the use of the voltage levels as an additional control element and giving more alternatives to generate the output waveform. For this reason, multilevel inverters have intrinsically improved power quality, characterized by: lower voltage distortion (more sinusoidal waveforms), reduced dv/dt, and lower common-mode volt-ages, which reduce or even eliminate the need of output filters.

The problem with multilevel converters is related to the control complexity added for the voltage-level clamping nodes; this is possible to see in Figure 4 where is possible to note that the number of clamping diodes needed to share the voltage. This increase the difficulty to control the dc-link capacitor unbalance, reason by which the industrial acceptance of the multilevel NPC topologies (just to mention a specific inverter type, but for other multilevel inverters happen a similar case with the control complexity) is quite low keeping with until 3-level inverters.

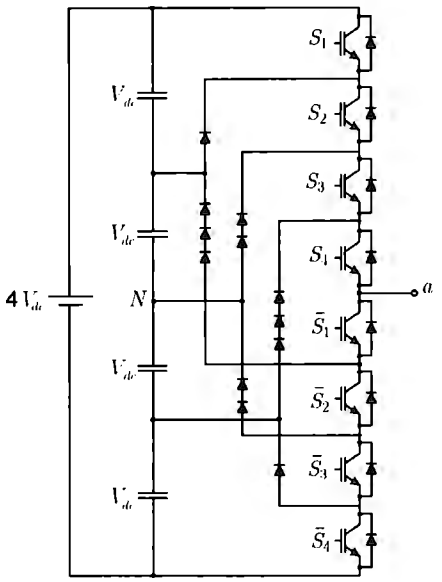

Figure 4. Five-level Inverter NPC

For convention inverter topologies there are several modulation methods, like: Space vector PWM, Sine PWM, SHE-PWM, Hysteresis PWM, Six-step PWM, etc. But for multilevel inverter topologies the convention modulation methods need to be improved, this implies an inherent additional complexity of having more power-electronics devices to control, and the possibility to take advantage of the extra degrees of freedom provided by the additional switching states generated by these multilevel topologies. For these topologies the more common modulation methods are depicted in Figure 5

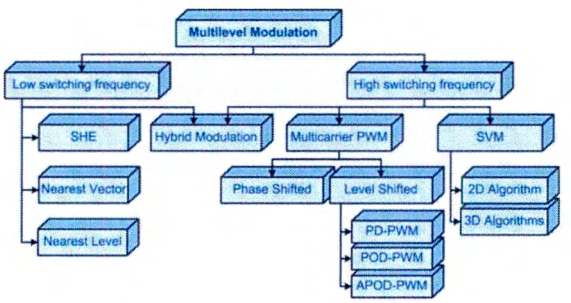

Figure 5. Multilevel inverter modulation methods (Rodriguez et al. 2009)

Some PWM methods for conventional (2-level) and multilevel (more than 2-level) converters are:

- Space Vector PWM for multilevel inverters (SVM): This method is basically also a PWM strategy with the difference that the switching times are computed based on the three-phase space vector representation of the reference and the inverter switching states rather than the per-phase in time representation of the reference and the output levels as in previous methods. This method can be classified into:
  - SV PWM for Multilevel Balanced Systems
  - SV PWM for Multilevel Unbalanced Systems
    - 3-D SVM for multilevel inverters

- Selective Harmonic Elimination (SHE-PWM): Selective harmonic elimination (SHE) is a low switching frequency PWM method developed for traditional converters in which a few (generally from three to seven) switching angles per quarter fundamental cycle are predefined and pre-calculated via Fourier analysis to ensure the elimination of undesired low-order harmonics (Holtz 1994). For converters with a higher number of levels, like CHB, SHE is also known as staircase modulation because of the stair-like shape of the voltage waveform. The basic idea is identical to SHE; the difference is that each angle is associated to a particular cell. The operating principle of this technique is to connect each cell of the inverter at specific angles to generate the multilevel output waveform, producing only a minimum of necessary commutations.
- Phase Shifted (PS-PWM): this method is specially implemented for Flying Capacitor (FC) inverter and Cascaded H-bridge (CHB).
- Level Shifted (LS-PWM): this method is an extension of bipolar PWM for multilevel inverters. This modulation method is especially useful for neutral point clamped (NPC) inverters. This methods includes three modulation methods based on the carrier signals arrangement, there are (Carrara et al. 1992):
  - Phase disposition (PD-PWM): carriers arranged in vertical shifts.
  - Phase opposite disposition (POD-PWM): the positive carriers in phase with each other and in opposite phase of the negative carriers.
  - Alternate phase opposition disposition (APOD-PWM): alternating the phase between adjacent carriers.
- Hybrid PWM Modulation (H-PWM): implemented for CHB. The main challenge is to reduce the switching losses of the inverter by reducing the switching frequency of the higher power cells.

Another important of the power electronic devices and directly related with the inverter is the rectifier. This allows the correct power supply to the inverter and as is logical with the inverter evolution to multilevel inverter, it is necessary to implement rectifiers for multilevel inverters. The rectifiers for multilevel inverters can be classified into (Rodriguez et al. 2009):

- Non-regenerative rectifiers: These rectifiers are based on diodes as is depicted in Figure 6. In this kind of rectifier, the energy is not regenerated to the grid.

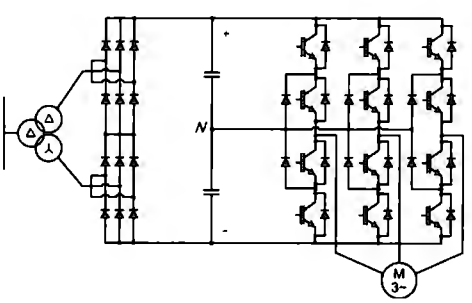

Figure 6. Double diode-based rectifier in combination with a delta-wye transformer, (Rodriguez et al. 2009)

- Regenerative rectifiers: Regenerative converters based on active rectifiers can take the energy provided by the load and put it back on the ac network, increasing the efficiency of the power-conversion system, especially when the load regenerates constantly, like downhill conveyors (Rodríguez et al. 2001). An example of a regenerative rectifier with a multilevel inverter is depicted in

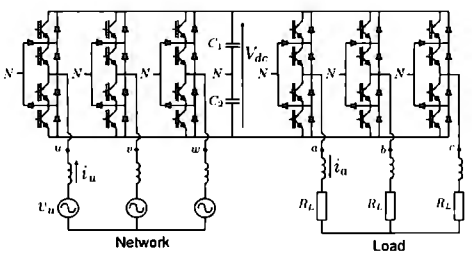

Figure 7. Regenerative rectifier with NPC multilevel inverter, (Rodríguez et al. 2001)

For an EV operation all this equipment need to be installed and their parameters change depending on the power requirement. Therefore, the power electronic design, installation and control play a preponderant part for EV developments.

1.3 Powertrain and Intelligent Control Techniques

The implementation of Artificial Intelligence (AI) control techniques for automotive applications has reached important design levels in order to avoid negative environmental and economic impacts. Nowadays, the problems that affect the environment have a serious impact over humanity, e.g.: acid rain, greenhouse effect, respiratory failures, chronic diseases, and even cancer. The current technology in the auto-industry has a lot of fault on this environmental problem. Since some years ago, one of the most important solutions proposed by industry and academia has been the implementation of new green energy sources in order to decrease the levels of pollution. It is known that one of the biggest pollution sources in the world comes from the gas vehicles emissions. For this reason, many different solutions have been proposed with the intention to manufacture vehicles with fewer gas emission and desirable rates of fuel consumption.

In this order, different academic, auto-industry and other research groups involved in vehicles' development performance area have been working in the improvement of different Engine Control Units (ECU) to achieve higher power engine performance and fewer gas exhaust emission, better control techniques, innovation in power train systems and design of new hybrid vehicle concepts. In this way, several research works have been developed about AI systems for automotive applications.

Hybrid vehicles work in two stages, one motor, powered by fuel, starts the engine and a battery which keeps the vehicle rolling; the vehicle has to manage perfectly the alternation of these stages so the vehicle works smoothly and stable. For achieving this goal a fuzzy logic controller is proposed (Majdi, Ghaffari, and Fatehi 2009). The controller manages the power train, and thanks to the nonlinearity the fuzzy input-output working is a suitable. After making the simulations, the results were not very significant because a little improvement on fuel-spending was done, leading to a poor proposal that can be redone for getting better results.

A distinct solution is using the Particle Swarm Optimization (PSO) algorithm (Xiaolan et al. 2008), which enhances the non-linearity of the power train, this algorithm consists on a series of particles (solutions of the problem) which enters the solution space. Different to the previous problem, this solution is easier to apply and far more effective with the simulations done.

Implementing artificial intelligence techniques for the energy sources management of an HEV Wang et al (Wang, Tang, and Yang 2004) proposed an adaptive hierarchical supervisory control strategy based on fuzzy logic and neural networks. The proposed control aim was to optimize an HEV system and its subsystems using a plan of a class of multiple model with an intelligent hierarchical supervisory control. Good results were obtained from the implementation of this control strategy to a complex system structure such as the HEV structure.

Electric Vehicles are still in development and the HEV's have not really got a proper definition. The term degree of hybridization is introduced taking into account the number of mechatronic systems. A fuzzy control system is also proposed for the power train control, this fuzzy control type is very suitable, because its capabilities to domain the nonlinear functions and systems (M. K. Park et al. 1996). With the introduction of this fuzzy control system the car achieves better fuel economy, and lower emissions. It is also proposed a future research for the possibilities of combining a fuzzy system with a neural network for the best performance of the vehicles. Simulations are done for getting more approach-to-reality results.

One of the HEV's, as well as other vehicles, parts is the steering. The steering is very important, because is one of the primordial functions of a vehicle. With the new advances in technology, the steering got some improvements in technology such as a yaw feedback, but this is not enough for getting the best response while steering. While steering, multiple factors intervene for getting each time a different reaction; the main factors involve the highway, and the tire. For this variation, a fuzzy intelligent system, a neural network with a complex algorithm for separating the drive wheels and the steering ones (considering a four wheel vehicle), is proposed and simulated mathematically (M. K. Park et al. 1996). One of the principal innovations is the separation of the input-output response and the fuzzy system and the neural network for getting an error (kind of uncertainty).

For conventional vehicles the Direct Torque Control (DTC) offers many advantages like faster torque control, but due to the motor array for HEV's this system creates torque ripple. This is why a new intelligent control system is proposed, based on a six-step control algorithm which offers better performance (Gupta et al. 2009). This system is called, neural network and was simulated using MATLAB, this is the big problem of the proposal. Not having real-world tests for this new control-torque system may be a risky offer for HEV's manufacturers to include.

In 2005, M. Mohebbi & M. Charhgard (Mohebbi, Charkhgard, and Farrokhi 2005) developed a control strategy based on an adaptive neuro-fuzzy inference system method that was applied to parallel hybrid electric vehicles. The objective was to adjust the throttle in the combustion engine to achieve the maximum output torque of the vehicle while minimizing fuel consumption used by the internal combustion engine. The inputs of the system were the desired torque and the battery pack SOC (state of charge). The results showed a significant performance improvement of the vehicle with the ANFIS model proposed in comparison with Mohebbi's previous work (Farrokhi, M. Mohebbi 2005) where it was implemented a fuzzy control system to achieve the same objective proposed with the ANFIS model (Mohebbi, Charkhgard, and Farrokhi 2005).

For an adaptable intelligent control to the different loads of an engine's requirements, it is useful to implement an Adaptive Neuro-Fuzzy Inference System (ANFIS) that combines the benefits of an AI network with the benefits of the fuzzy inference system in a single model. This structure allows having two intelligent approaches achieving good reasoning in quality and quantity. In other words, this structure has fuzzy reasoning and AI network calculation (Jiang and Xia 2002). The vector control is implemented to control the electromagnetic torque and rotor flux in a Permanent Magnets Synchronous Motor (PMSM). It is known that vector control is widely implemented for AC asynchronous and/or synchronous machines used as industrial drives or to any other power application. The idea with vector control is to control AC machines as DC machines by means of a decoupled control of the rotor flux magnitude and the torque-

producing current (Shoorehdeli, Teshnehlab, and Sedigh 2006). Thus, the ANFIS model is used to learn the vector control responses and later on makes the replacement of the convectional controller by the S-ANFIS controller, then the system responses with the conventional and S-ANFIS controllers are compared and evaluated.

Power electronics, electric drives, control theories, modulation techniques and artificial intelligence methods are part of the main body to obtain a solid electric motor/control system for EV powertrain control Next will be explained the structure, motivations and objective points for the present work.

1.4 Motivation

The automotive industry is putting large amount of resources in terms of monetary investments and research efforts into one goal; achieving high performance in EV and HEV. This is a well-known fact and it is leading the new green technology paradigm.

Numerous companies such as Toyota, Honda, Nissan, Chevrolet, Honda, Audi, Hyundai, General Motors, Ford, Tesla Motors among others, are offering several industry careers in areas related to power electronics, battery design, R&D electronics and control, all these related to EV and HEV applications. These industry careers require engineers and technicians with high job qualification, which encourages to undergraduate, post graduate MSc and/or PhD students to fulfill the automakers' demands.

Therefore, around the world governments, and entities are interested in technological developments, for examples: The USA government has a strong commitment with green technologies, in 2011 the president Barack Obama said "With more research and incentives, we can break our dependence on oil with biofuels, and become the first country to have 1 million electric vehicles on the road by 2015". The Japan industry Nissan invested in 2012 the amount of 2000 million dollars in Mexico-Aguascalientes, this plant will fulfill part of the Nissan's demands in North America (Mexico, USA and Canada) and also several researches and developments for electric vehicles (specifically the Nissan Leaf) will be achieved in this plant. In 2010 the company of microchips, power electronics and circuits Freescale formed joint lab with Chinese automakers, Foton/Freescale Automotive Joint Lab in Beijing, this laboratory will be focused on power electronics, microcontrollers and sensor into automotive control systems. There is more and more news related to governments and/or industries initiatives for EV and HEV.

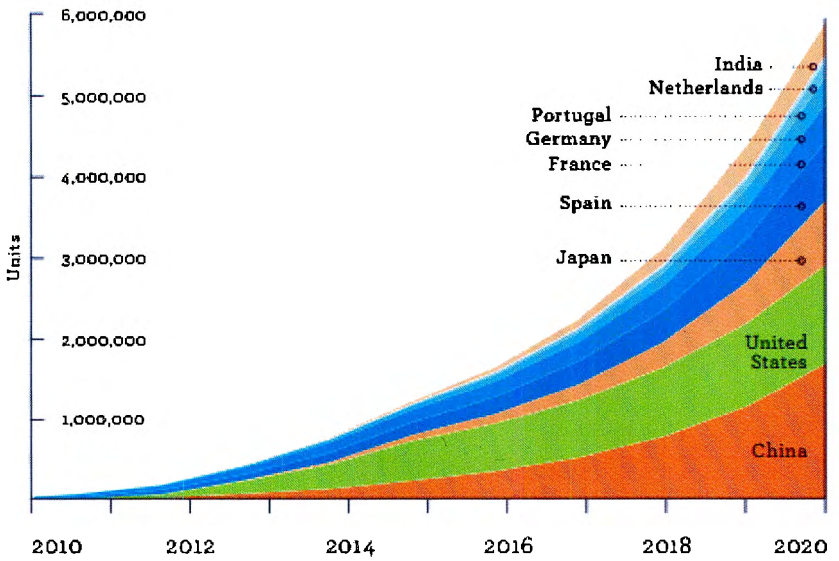

Figure 8. Sales targets 2020, (Trigg et al. 2013)

The mentioned facts are part of the strength of green technologies in the automotive industry and the importance of keeping working in this field. Thus, this thesis synthesizes the knowledge acquired during years of academic studies (undergraduate and MSc) and the labor as a researcher at the Instituto Tecnológico y de Estudios Superiores de Monterrey- CCM. Also, the main motivation of this thesis is to present how intelligent and robust control techniques improve electric machine control performance, which comes along with a detailed theoretical and practical implementation in order to guide future generations interested in electric machine control applied to EV powertrain. In this work is also presented a deployment of different tools that can be used for simulation and rapid control design and implementation. All this work implies knowledge regarding power electronics, control techniques, electric vehicles and programming skills. The opportunity to contribute to the automotive world and keep working with electric and hybrid vehicles is enough motivation.

1.5 Problem Statement

Environment deterioration, human health and economy issues are some of the different problems that the humanity is now facing. All these problems have different sources (e.g. manufacturing industry, chemistry industry, and vehicles pollution to mention a few.), and each source needs to be handled in order to minimize negative effects against the humanity and environment.

The automotive industry with internal combustion vehicles (ICVs) represent one of the biggest pollution sources with its consequences in respiratory diseases and ozone layer deterioration, to mention a few. In response to this, alternative energies have been implemented as main power sources. This becomes a solution to reduce vehicle contamination; however, improvements on this field are still in progress in order to address high standards in terms of vehicle performance and energy management. These need to be achieved with the intention to reach ICV performance but without hazards implications.

Now, delimiting the statement "alternative energies as main power sources for vehicle" to one kind of energy power source, electric vehicles, it is possible to delimit the problem to techniques and technology

development useful to improve electric vehicles performance. The latter is the main problem which establishes the bases of this thesis.

Summarizing, the problem to solve is related to the improvement of electric vehicle performance by means of the powertrain control. This is not an easy task, and need to be handled based on the powertrain features and performance requirements.

1.6 Objectives

- Present a complete documentation of vector control for induction motor from the different design software and real time platforms. All this in order to contribute to the academy with a complete guide to design and implement vector control in AC induction motors.
- Implementation of a control technique based on intelligence artificial methods for AC electric motor
- Show the design process of a vector control technique for AC induction electric motor.
- Present experimental and simulation results of an indirect vector control technique on a squirrel cage induction AC motor.

1.7 Methodology

The methodology followed to reach a successful thesis is:

- Literature review and state of the art
- Objective definitions
- First approach to the solution
- Development of the solution
- Implementation of the solution
- Testing and refining
- Real time Implementation
- Documentation of results

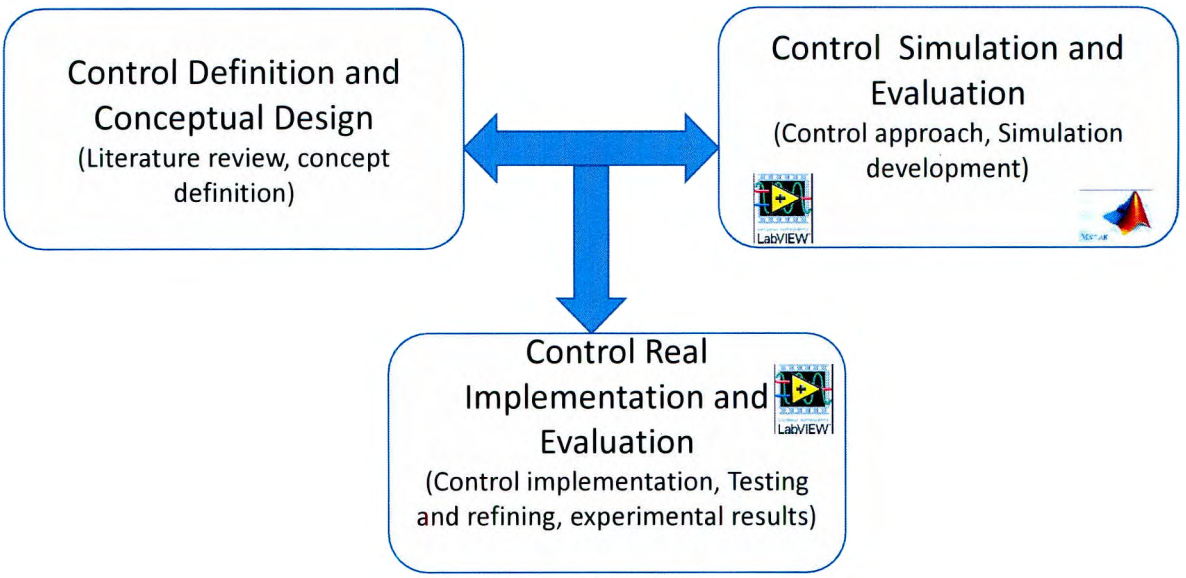

Figure 9. Control Implementation Strategy

Figure 9 represents the methodology implemented in this thesis work and also it depicts the software that will aid the control design and implementation processes. The interaction among Matlab and LabVIEW it is quite useful for the rapid control implementation and study, which is presented and explained in this thesis work.

1.8 Justification

This thesis presents the design process of an indirect vector control implemented on an AC induction motor. It is also depicted the interaction among control design tools capable to ease the motor control evaluation, design and implementation stages. The latter points are part of the contribution deliver by this work, since it will help to other researchers and new engineering students to understand and study vector control in order to promote future work developed around EV/HEV powertrain applications. Figure 10 depicts the description of the content presented in this thesis, this illustrates the among of information gathered in this thesis and the implementation of real time vector control and co-simulation intelligent vector control.

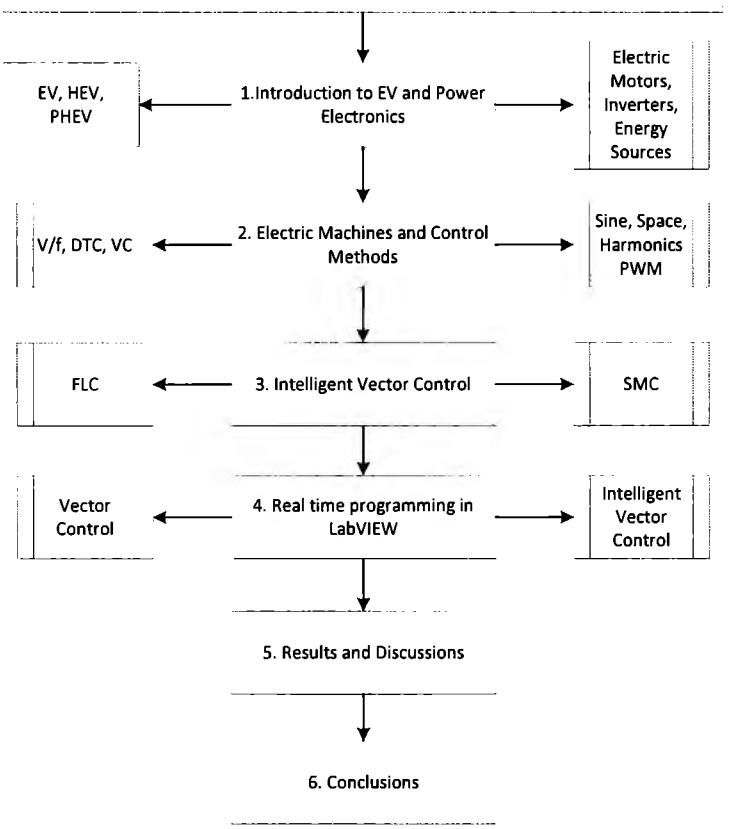

Figure 10. Thesis content description

In the following chapters and sections will be presented the theoretical bases of electric vehicles, electrical motors and AC motor control techniques, after that will be depicted artificial intelligence techniques that are used for control applications. This work has the intention to present the transition from the theory to simulation in the Matlab environment, co-simulation of a intelligent vector control in the LabVIEW environment with Multisim (a software of National Instruments, where all the power electronic and electric drive are modelled) and finally the practice in real time in the LabVIEW environment (FPGA programming to implement in the real world).

Chapter 2: Electric Machines, Electric Vehicle and Control Models

In this chapter the models for the main components of the EV powertrain and the conventional control models will be presented and explained in detail. As it was mentioned before the main components of the EV powertrain are:

- Electric motor
- Energy storage unit
- Inverter and rectifier
- Transmission

The interaction of these components into an EV will define the powertrain operation, therefore is quite important to understand how each element of the powertrain works, its dynamics, responses to variations and disturbances and how all work together as a system. All this will dictate the guidelines to design the correct controller for the EV powertrain. In this thesis the intelligent vector controller will be applied to an EV with an AC asynchronous motor also known as induction motor, so the model and control will be designed for this electric motor.

The order in which will be structured this chapter is:

1. Induction motor model and control
2. EV powertrain model and control implementation

2.1 Induction Motor Model and Control

The induction motor is one of the most rugged and most widely used machines in the industry. The main parts of this motor are: the stator and the rotor. These parts are depicted in Figure 11Figure 12 (Thornton and Armintor 2003).

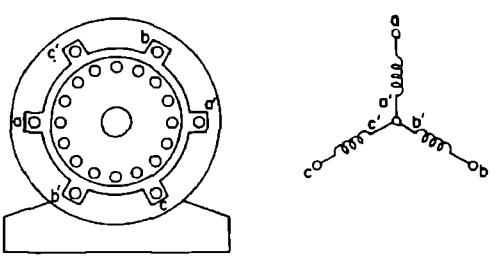

Figure 11. Stator and rotor schematic representation, (Thornton and Armintor 2003)

The rotating magnetic field is produced by the contributions of space-displaced phase winding carrying appropriate time displaced currents. The application of three-phase currents through a balanced three phase winding produces a rotating magnetic field that is both constant in amplitude and speed. This happens if the following conditions are met:

- There is a space displacement between balanced phase windings of 120 electrical degrees.
- The currents flowing through the phase windings are balanced and time-displaced by 120 electrical degrees.

Figure 12 shows the relationship of three phase currents and rotating magnetic field over 360 electrical degrees in time.

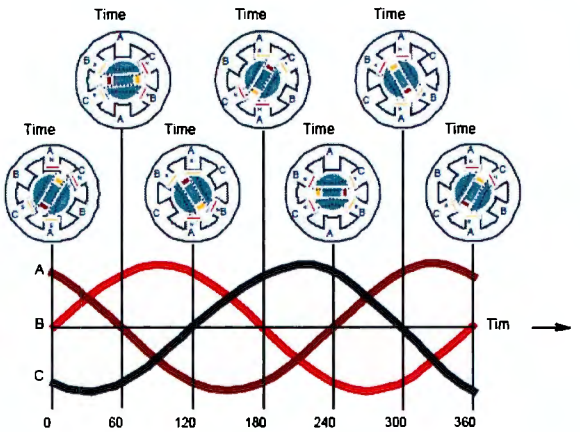

Figure 12. Three phase currents and rotating magnetic field, (Thornton and Armintor 2003)

A physical representation of an induction motor with its main parts is depicted in the Figure 13.

Figure 13. Physical representation of an induction motor

Induction motors are designed based on torque applications. NEMA designs define the torque and current characteristics of the motor. Alphabetic letters are used to define categories; the next table explained the most used categories.

Table 3. Standard NEMA Designs for Various Torque Characteristics

NEMA Design	Starting Torque	Starting current	Breakdown Torque	Full Load Slip	Typical sine wave Applications
A	Normal	High	High	Low	Mach. Tools, Fans
B	Normal	Normal	Normal	Normal	General industrial
C	Normal	Normal	Normal	Normal	Loaded compressor Loaded Conveyor
D	Normal	Low		High	Puch Press or Hoists

Torque is the main characteristic to take into account for electric motor application, this one represents the turning effect developed by the motor. There are four important points that need to be considered, these are depicted in the following figure.

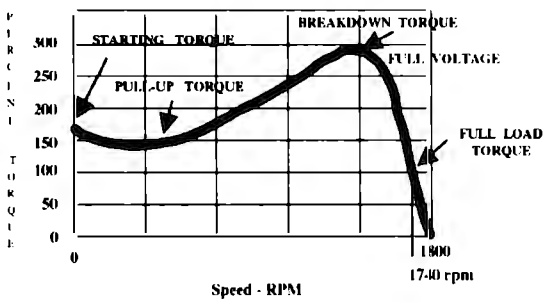

Figure 14. Typical NEMA Speed-Torque curve for induction motor, (Thornton and Armintor 2003)

- Full load torque: is the torque required to produce rated horsepower at full speed
- Breakdown torque: is the maximum torque that can be developed by the motor at rated voltage and frequency without a sudden loss of speed. This represents the ability of the motor to maintain operation under peak-load conditions.
- Pull-up torque: is the minimum torque developed by an induction motor during the period of acceleration from zero to the speed at which breakdown occurs.
- Starting torque: is the torque delivered by a motor at the instant it is energized. Starting torque is often higher than rated running or full load torque.

Next, the induction motor model is explained in the following subsection.

2.1.1 Induction Motor Model

The induction motor model is referred to the equivalent circuit showed in Figure 15.

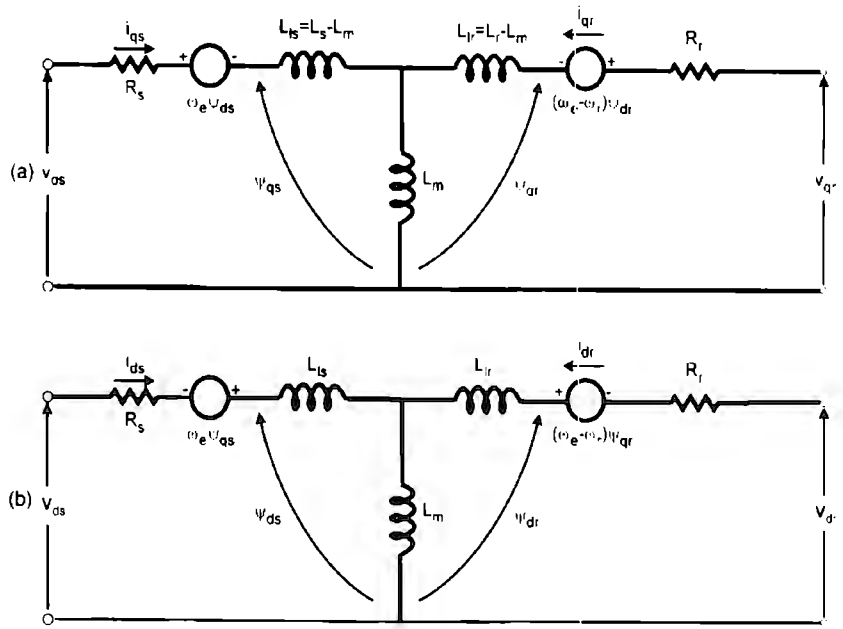

Figure 15.Synchronous Rotating Dynamic d-q Equivalent Induction Motor Circuit Model

In order to be able to control an AC induction motor is required to take into account the transient response. This one, can be evaluated with the dynamic d-q model. The dynamic behavior of an AC motor may be complex to explain, since it is related to the three phase rotor windings moving respect to the three phase stator windings. Hence, the AC asynchronous motor has stator and rotor flux linkages, currents and voltages rotating at different rates. Thus, some coordinate manipulations are required in order to obtain a model in the same reference framework. These are the Park's and Clarke's transforms developed during 1920's and 1930 by Robert H. Park and H. C. Stanley.

The parameters in the right part of the circuit in Figure 15, are the rotor parameters that have been referred to the stator through the ideal transformer in the machine model. The dynamic equations of the induction motor can be described from the balanced voltage equation of the stator phases as, bs and cs and the spatial vector of the stator flux (Ponce and Sampé 2008), which is defined as:

$$\bar{V}_s = \frac{2}{3}[v_{as} + av_{bs} + a^2 v_{cs}] \quad (2.1)$$

The right part of the equation (2.1) represents the contribution of each phase, where $a = e^{j2\pi/3}$ and $a^2 = e^{-j2\pi/3}$. This equation can be physically interpreted as the spatial vector magnitude and direction of the net stator voltage sinusoidal distribution. In the same way, the rotor components cab be represented.

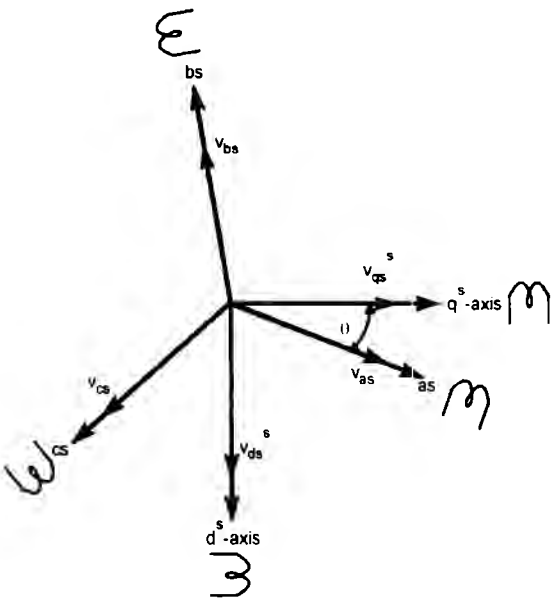

Figure 16.Stationary frame a-b-c to ds-qs axes transformation

In order to transform from the three phase stationary reference to the two phase stationary reference the Clarke transformation is applied based on Figure 16

$$\begin{bmatrix} v_{ds}^{s} \\ v_{qs}^{s} \\ v_{os}^{s} \end{bmatrix} = \frac{2}{3}\begin{bmatrix} \cos(\theta) & \cos(\theta - \frac{2\pi}{3}) & \cos(\theta + \frac{2\pi}{3}) \\ -\sin(\theta) & -\sin(\theta - \frac{2\pi}{3}) & -\sin(\theta + \frac{2\pi}{3}) \\ 1/2 & 1/2 & 1/2 \end{bmatrix}\begin{bmatrix} v_{as} \\ v_{bs} \\ v_{cs} \end{bmatrix}$$

For convenience if θ is set to zero. The q^s axis will be aligned with as-axis. The final transformation, ignoring the zero sequence v_o, the transformation is simplified to as:

$$v_{qs}^{s} = \frac{2}{3}v_{as} - \frac{1}{3}v_{bs} - \frac{1}{3}v_{cs}$$

$$v_{ds}^{s} = -\frac{1}{\sqrt{3}}v_{bs} + \frac{1}{\sqrt{3}}v_{cs} \qquad (2.2)$$

Now the stationary voltage components are referred to the synchronously rotatory frame thanks to the Park's transformation.

$$v_{qs} = v_{qs}^{s}\cos\theta_e - v_{ds}^{s}\sin\theta_e$$

$$v_{ds} = v_{qs}^{s}\sin\theta_e + v_{ds}^{s}\cos\theta_e \quad (2.3)$$

where $\theta_e = \omega_e t$, which is the synchronously rotating angle.

Now the dynamic induction motor model in the synchronous rotating frame, also known as the Kron equation, (Bose 2002).

- Stator

$$v_{ds} = R_S i_{ds} + \frac{d}{dt}\psi_{ds} - \omega_e \psi_{qs} \quad (2.4)$$
$$v_{qs} = R_S i_{qs} + \frac{d}{dt}\psi_{qs} + \omega_e \psi_{ds} \quad (2.5)$$

- Rotor

$$v_{dr} = R_r i_{dr} + \frac{d}{dt}\psi_{dr} - (\omega_e - \omega_r)\psi_{qr} \quad (2.6)$$
$$v_{qr} = R_r i_{qr} + \frac{d}{dt}\psi_{qr} + (\omega_e - \omega_r)\psi_{dr} \quad (2.7)$$

The third component of the Kron equations, corresponds to the induced EMF and Back-EMF for the stator and rotor respectively. These equations are based on the model circuit in Figure 15, this circuit also helps to define the flux linkages such as:

$$\psi_{qs} = L_{ls} i_{qs} + L_m (i_{qs} + i_{qr}) \quad (2.8)$$

$$\psi_{qr} = L_{lr} i_{qr} + L_m (i_{qs} + i_{qr}) \quad (2.9)$$

$$\psi_{qm} = L_m (i_{qs} + i_{qr}) \quad (2.10)$$

$$\psi_{ds} = L_{ls} i_{ds} + L_m (i_{ds} + i_{dr}) \quad (2.11)$$

$$\psi_{dr} = L_{lr} i_{dr} + L_m (i_{ds} + i_{dr}) \quad (2.12)$$

$$\psi_{dm} = L_m (i_{ds} + i_{dr}) \quad (2.13)$$

The matrix equation presented is in terms of stator, rotor and common inductances and stator and rotor currents. The impedances in (2.3) are defined as:

$$L_S = L_{LS} + L_m$$
$$L_R = L_{LR} + L_m$$

Where L_S and L_R are the impedances that links the stator winding with the rotor winding. The impedances L_{LS} and L_{LR} are the stator and rotor leakage respectively, they are defined as:

$$L_{LS} = \frac{X_{LS}}{\omega_b}$$
$$L_{LR} = \frac{X_{LR}}{\omega_b}$$

where ω_b is the rate motor speed. It is important to mention that the rotor's voltages equations v_{dr} and v_{qr} are equal to zero for a squirrel cage machine.

From the equations (2.4) - (2.7) if the synchronous speed $\omega_e = 0$. Then the stationary model, also known as the Stanley equation is obtained.

$$v_{ds} = R_S i_{ds} + \frac{d}{dt}\psi_{ds} \quad (2.14)$$

$$v_{qs} = R_S i_{qs} + \frac{d}{dt}\psi_{qs} \quad (2.15)$$

$$v_{dr} = R_r i_{dr} - \omega_r \lambda_{qr} + \frac{d}{dt}\psi_{dr} \quad (2.16)$$

$$v_{qr} = R_r i_{qr} + \omega_r \lambda_{dr} + \frac{d}{dt}\psi_{qr} \quad (2.17)$$

Finally, in order to have the complete set of equations to model an induction motor. It is taking into account the mechanical implications, that is:

$$T_m = \frac{3}{2}(P/2)(\lambda_{ds} i_{qs} - \lambda_{qs} i_{ds}) \quad (2.18)$$

where P is the number of poles. The electrical rotor speed is defined as:

$$\frac{dw_r}{dt} = \frac{P}{2}\frac{(T_e - T_L)}{J} \quad (2.19)$$

The induction motor model is completed. The equations (2.14) - (2.17) represent the stator and rotor voltages components, and the equations (2.18) and (2.19) represent the electromagnetic torque and rotor speed.

Now is simulated the induction motor based on its dynamic equations presented. The motor parameters to use are:

- P= 4 (Number of poles)
- Rs= 0.435 ohms (Stator resistance)
- Rr= 0.816 ohms (Rotor resistance)
- Lm= 0.06931 (Magnetizing impedance [H])
- Lls= 0.002 (Stator side leakage impedance [H])
- Llr= 0.002 (Rotor side leakage impedance [Ohms])
- we= 377. (Base electrical frequency [rads/s])
- J= 0.0089 (Rotor inertia [Kg m^2])
- B1= 0 (Load damping coefficient)
- Nema A
- cos φ =0.676 (Power factor)
- Pr=1.1kw (Real power)
- vds= 0 (D axis stator voltage)
- vqs=180 (Q axis stator voltage)
- vqr= 0 (D axis rotor voltage)
- vdr= 0 (Q axis rotor voltage)
- T_L= 0 (Load torque, initial condition)

Initially the load torque T_L is set to zero and the results obtained are presented from Figure. 17 to Figure. 20.

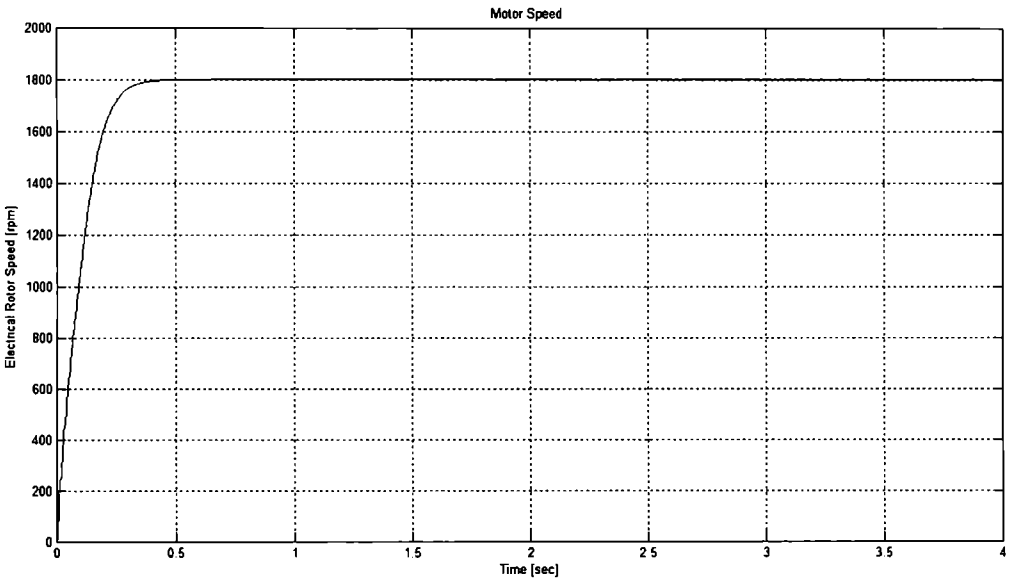

Figure. 17. Rotor Speed, $T_L = 0$

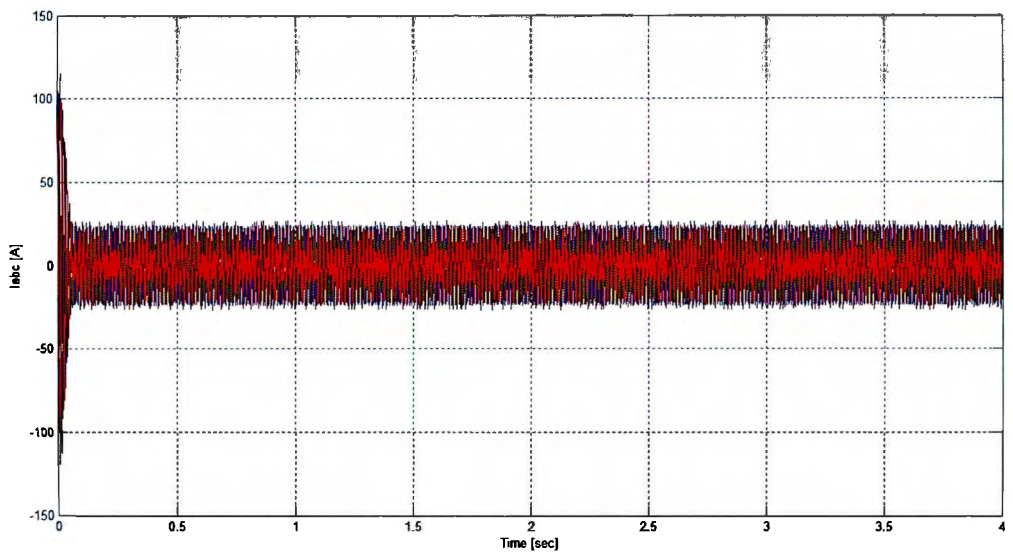

Figure. 18. Stator currents, $T_L = 0$

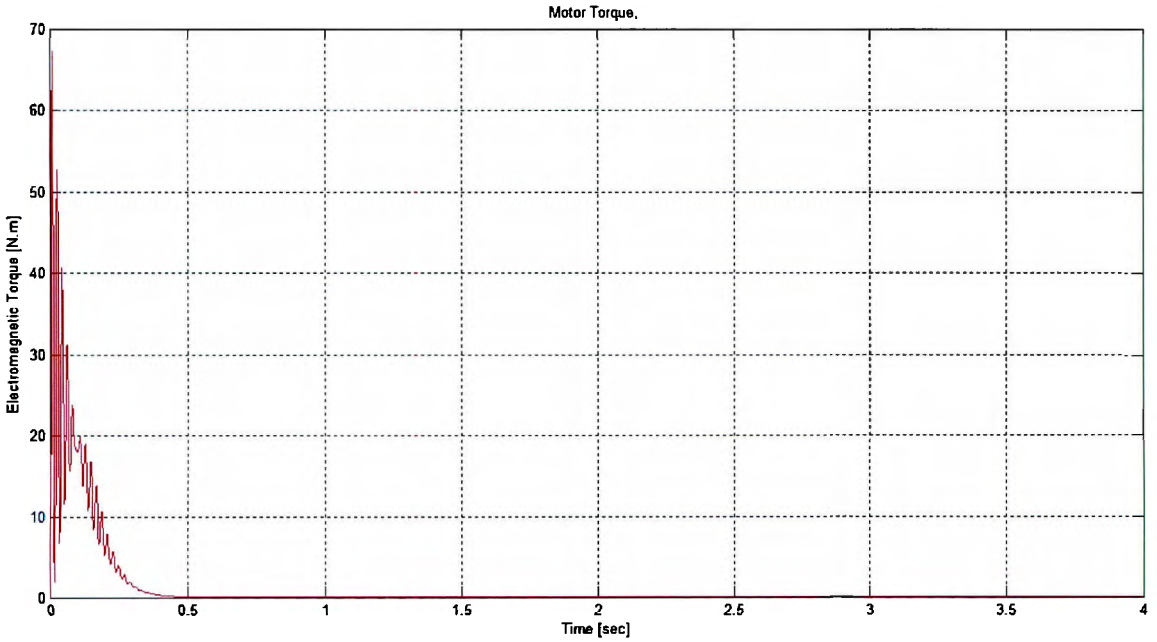

Figure. 19. Electromagnetic Torque, T_L= 0

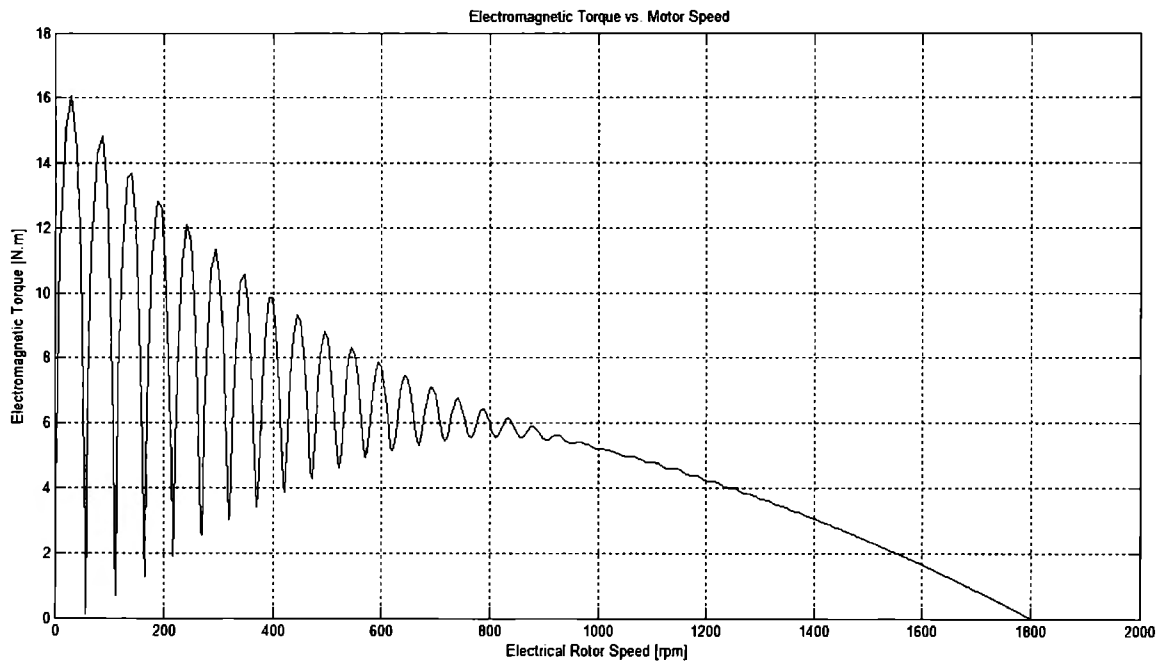

Figure. 20. Electromagnetic Torque vs. Motor Speed, T_L= 0

The second simulation is to evaluate the results in terms of electromagnetic torque, speed and the relation among torque and speed, when it is applied different load torque values to the induction motor. ~~in~~ Figure. 21 and Figure. 22 shown the results.

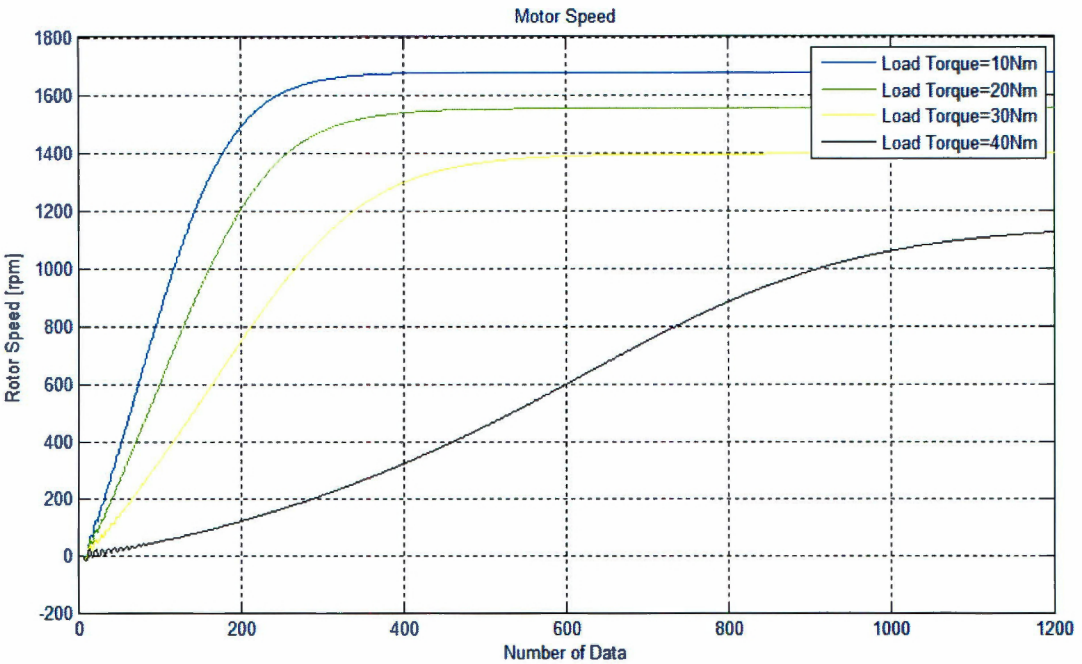

Figure. 21. Rotor Speed Results for different T_L

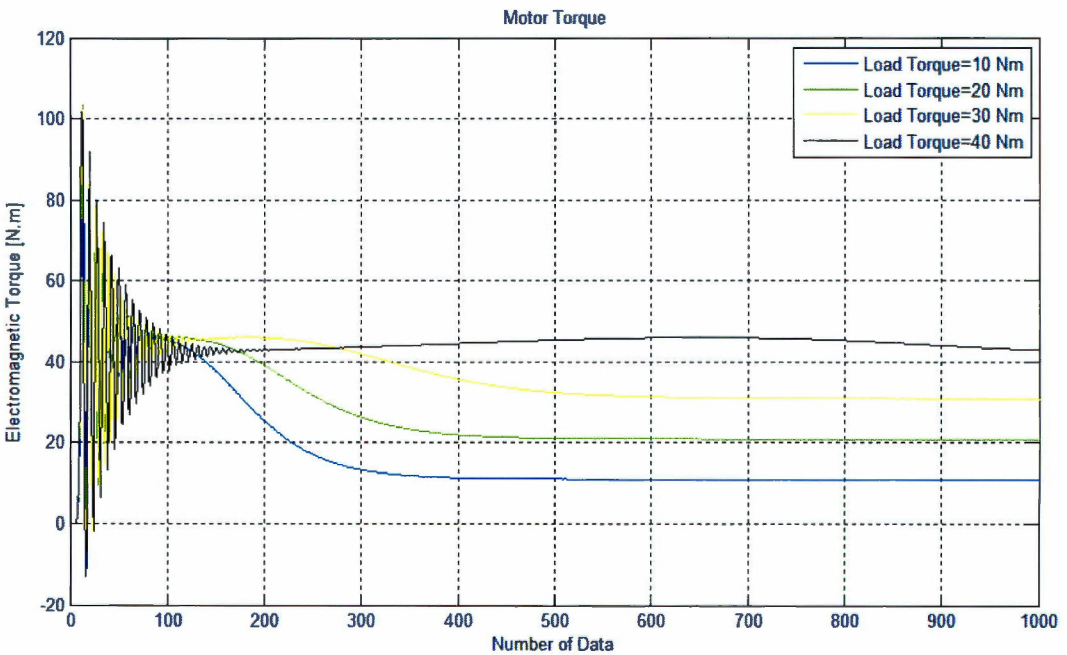

Figure. 22. Electromagnetic Torque Results for different T_L

The Figure. 22 shows load toque applied at 25%, 50%, 75% and 100% of the motor nominal toque (40 Nm). Note that for some load torque changes the transitory response maintains almost the same and the changes are for the stable response to the different stabilization torque points. The induction motor has a high non-linear model and involves current and magnetic flux components for the stator and rotor parts. Therefore, must be established a control law capable to handle the relations among torque-magnetic flux,

speed-currents and torque-speed. The latter implies that there is a logical relation among currents and magnetic flux. This relation established the problem faced time ago by several researchers in order to control an induction motor, this led researchers to solve this issue with a solution similar as the one used for the DC motors. Next will be explained the control methods designed for AC motors.

2.1.2 Control of AC motors

In order to explain the control techniques implemented for the AC motors is convenient to understand first how DC are controlled. DC motors were popular for their easy control method. Figure 23 shows the equivalent circuit of the separately excited DC

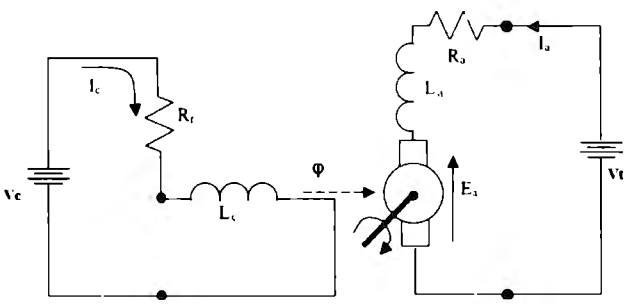

Figure 23. Separately excited DC motor equivalent circuit

Based on this motor circuit the dynamic model is developed (Ponce and Sampé 2008), which dictates the control design for this kind of motor.

From Figure 23 the right part represents the rotor and the left side the stator. Then from the rotor is obtained:

$$V_t = I_a R_a + L_a\left(\frac{dI_a}{dt}\right) + E_a \quad (2.20)$$

And from the stator is obtained:

$$V_c = I_c R_c + L_c\left(\frac{dI_c}{dt}\right) \quad (2.21)$$

The electromagnetic torque is formulated as:

$$T = k\phi I_a = KI_a \quad (2.22)$$

The mechanical equation of the DC motor is:

$$T_e = KI_a = J\left(\frac{d\omega}{dt}\right) + \beta\omega + T_L \quad (2.23)$$

Where J is the inertia coefficient, β is the friction coefficient and T_L is the load torque.

From equation (2.22) that K is a constant which includes the magnetic flux (Φ). Therefore, it is possible to maintain constant one power supply in order to linearize the model. Then, for the stator power supply maintains constant and the EMF of the rotor is defined as:

$$E_a = k\phi\omega = K_1\omega \quad (2.24)$$

Where $k\phi$ is constant, k is defined as

$$k = \frac{PN}{2\pi q} \quad (2.25)$$

Where P is the number of pole pairs, N is the number of active conductors and q is the number of parallel circuit pairs.

Thus the electromagnetic torque is now:

$$T_e = k\phi I_a = K_2 I_a \quad (2.26)$$

And now the rotor and the mechanical equations are:

$$V_t = I_a R_a + L_a\left(\frac{dI_a}{dt}\right) + K_1\omega \quad (2.27)$$

$$K_2 I_a = J\left(\frac{d\omega}{dt}\right) + \beta\omega + T_L \quad (2.28)$$

Finally, from equations (2.27) and (2.28), is possible to obtain the space state model of the separately excited DC motor

$$\begin{bmatrix} \dot{I}_a \\ \dot{\omega} \end{bmatrix} = \begin{bmatrix} -\frac{R_a}{L_a} & -\frac{K_1}{L_a} \\ \frac{K_2}{J} & \frac{\beta}{J} \end{bmatrix} \begin{bmatrix} I_a \\ \omega \end{bmatrix} + \begin{bmatrix} \frac{1}{L_a} & 0 \\ 0 & -\frac{1}{J} \end{bmatrix} \begin{bmatrix} V_t \\ T_L \end{bmatrix}$$
$$[y] = [1 \quad 0] \begin{bmatrix} I_a \\ \omega \end{bmatrix} \quad (2.29)$$

From the DC motor model is conceivable to see the simplicity of this kind motor in terms of control, because while one power supply maintains constant (i.e. there is power supply for the stator and other for the rotor, from there the name of this motor) the other can change and the torque and speed control is achieved. This is synthesized in the equation (2.26) where is possible to note that by means of the variable I_a (rotor current) the electromagnetic torque can be manipulated. Also, it is now possible to understand better why the DC motor was for many years an attractive solution for industrial and automotive applications among others.

Based on the DC motor control and more specifically the equation (2.26) which establishes the main idea of the electric machines control, that is, to be able to separate the relation among magnetic flux, currents, speed and electromagnetic torque. Therefore, the basic idea is to achieve in an AC motor that the rotor magnetic flux and stator current decouple, in order to be able to control an AC motor as a DC motor. This was not an easy task to achieve and it implied a lot of work and years of development by several researchers, but at the beginnings of the 70's in Germany Occidental the researchers Hasse and Blaschke established the field-oriented control technique for AC motors (Blaschke 1972) also known as vector control. After other techniques were proposed to control AC motors as DC motors.

Nowadays there are several control techniques implemented for AC motors, those are: scalar control, vector control and direct torque control. In this thesis will be developed an intelligent control techniques based on vector control for an EV motor. Nevertheless, the author of this thesis considered important to explain the main important control techniques used for AC motors.

2.1.2.1 Scalar control

This technique is also known as voltage/frequency (V/f) control (Ponce and Sampé 2008) and is based on the equivalent circuit of the induction motor (see Figure 15) which implies that this control technique works good in steady-state region. For the mathematical explanation of the scalar control technique is neglected the voltage drop in the stator, so it is possible to establish that the input voltage is equal to the EMF induced. This assumption helps to define a direct relation among the supply voltage and the generated torque, so it is obtained:

$$\Phi(t) = \phi_{max} sen(w_s t) \quad (2.30)$$

Defining the EMF generated as $E = \frac{d\phi(t)}{dt}$, it is possible to derivate the equation (2.30) obtaining

$$E = 2\pi f_s \phi_{max} \cos(\omega_s t) \quad (2.31)$$

Resolving (2.31) for the RMS values, it is obtained:

$$E = \frac{2\pi f_s}{\sqrt{2}} \phi_{max} \eta \quad (2.32)$$

where η is a motor design constant. Based on the assumption $Vs=E$, it is possible to define Vs as:

$$\frac{V_s}{f_s} = K\phi_{max} \quad (2.33)$$

The expression (2.33) is the core of the scalar control technique and this can be demonstrated with the analysis of the induction motor torque expression (2.34)

$$T = \frac{3|V_s|^2}{\omega_s} \frac{\frac{R_r}{s}}{\left(R_s + \frac{R_r}{s}\right)^2 + X_T^2} \quad (2.34)$$

From the equation (2.34) is possible to note the direct relation between the torque and the square of the supply voltage, also the torque is inversely proportional to the synchronous speed. Therefore, the correct voltage/frequency relation of the equation (2.33) dictates the motor performance.

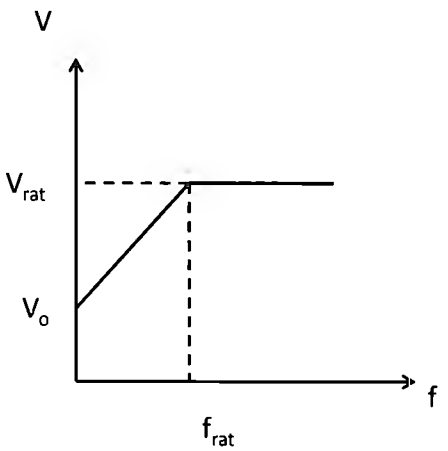

Figure 24. Scalar Control

Figure 24 depicts the scalar control operation regions, where f_{rat} and V_{rat} are the voltage and frequency rate. The first part with slope different of zero is known as constant torque region and the second region with voltage constant is known as the constant power (weak field) region. It is important to remark two things of this control technique:

- The scalar control technique assumes that the voltage drop in the stator is neglected, and then a compensation voltage ($V_{s,0}$) has to be included. This voltage depends on the load connected to the motor.
- The scalar control is based on the steady state equations which mean that the motor will have a bad operation in the transitory state.

This technique is very useful for applications where is needed an AC motor operating with constant torque. Actually companies such as Siemens and Schneider Electric have developed frequency variator for AC motors which can be implemented in open and closed loop. Figure 25 depicts a scalar control closed loop implementation for an induction motor.

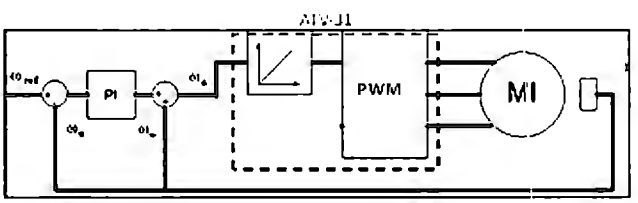

Figure 25. Scalar Control Closed loop for induction Motor

The scalar control technique is a useful tool for electric motor control; however, several applications need a good operation under transitory state, for instance electric vehicles. This control technique can be more reliable with the implementation of adaptive control techniques (Yang and Fang 1994) in order to estimate on-line the load connected to the motor with the aim to calculate the compensation voltage, this combination can improve the scalar control implementation.

2.1.2.2 Direct Torque Control (DTC)

This control technique was born as a competitive solution for the control of AC motors years after the vector control was proposed by Blaschke. In 1984 Manfred Depenbrock presented the DTC patent (Depenbrock 1987), which was originally known as Direct Self-control (DSC). Months before Takahashi and Noguchi presented a journal paper (Takahashi and Noguchi 1986) with a similar idea for an induction motor, thus DTC is credited to all three researchers.

This technique gained popularity for industry applications thanks to its simplicity, the first major commercial application was the ACS600 variable speed drive developed by the Swedish-Swiss multinational corporation ABB. Several publications and books presents a deep theoretical explanation of DTC and ACS600 implementation (Tiitinen 1996; Nash 1997; Vas 1998).

In principle, the DTC technique selects one of the six active voltage space phasors and one of the two zero voltage space phasors generates by the voltage source inverter (VSI) in order to keep stator magnetic flux and torque within the limits of two hysteresis bands (see Figure 26).

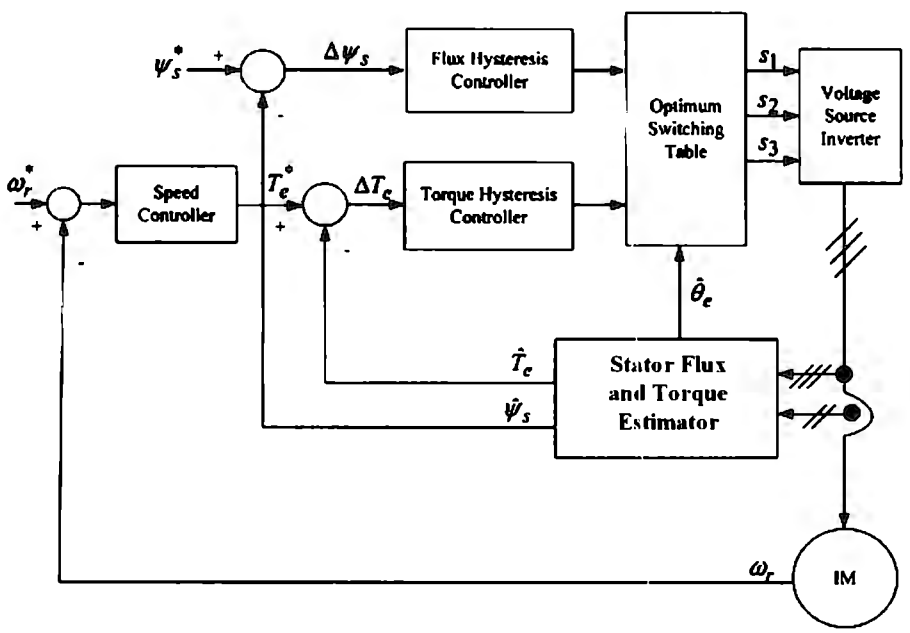

Figure 26. Simplified DTC Scheme

DTC is based on the dynamic equations of the induction motor for the estimation of the stator magnetic flux and torque. Thus, this control technique can operate in transitory and steady states. One advantage of this technique is the mathematical simplicity over the vector control technique and the motor is decoupled by means of the power electronics. Common disadvantages of DTC are high torque ripple and slow transient response to the step changes in torque during start-up.

DTC is a powerful tool for AC motors control and it has a wide application in industry with lesser mathematical complexity than vector control, but it requires extra power electronics in order to achieve

motor decupled. The latter is not desire for EV applications, since major power electronics components imply higher electronic complexity. Thus, in this thesis is implemented an intelligent control based on vector control rather DTC, because the mathematical complexity that vector control adds to the EV motor control can be compensated by improvements thanks to artificial intelligence methods.

2.1.2.3 Field Oriented Control or Vector Control

This control technique has two main categories: the first one was developed by Felix Blaschke in 1968 but commercially available until the early 80's when microprocessors where capable to support vector control operation. Blaschke presented in his work (Blaschke 1972) a deep explanation of how the direct vector control works. And the second one was invented by Karl Hasse, who developed the indirect vector control theory in his doctoral thesis in 1969 (Hasse 1968; Hasse 2001; Hasse 1969). Until now these techniques have been largely implemented for industry application and most important EV applications.

The vector control consists of controlling the stator currents or stator voltage represented by a vector. The basic idea is to play with projections between different frameworks, first a transformation from a three phase time and speed dependent system into a two co-ordinates (d and q co-ordinates) time invariant system and later the opposite transformation. The vector control needs two constants as input references, the torque component (q co-ordinate) and the flux component (d co-ordinate). Some advantages for the vector control implementation are:

- The ease of reaching constant reference (torque component and flux component of the stator current)
- The ease of applying direct torque control because in the (d,q) reference frame the expression of the torque is:

$$T \propto \psi_R i_{qs} \quad (2.35)$$

By maintaining the amplitude of the rotor flux (ψ_R) at a fixed value it is possible to have a linear relationship between torque and torque component (i_{sq}). We can then control the torque by controlling the torque component of stator current vector.

It is important to remember that the induction motor works with a slip between the rotor and stator speed (from there the induction motor is also known as asynchronous motor). Hence, the vector control for the induction motor establishes transformations between time variant to time invariant frameworks. These transformations are achieved by means of the Clarke's and Park's transformation (Tao and Liang 2011):

- Clarke's transformation

Change the three-phase AC system to two-phase system is called Clarke transformation, the inverse is used to transform from 3 phase to 2 phase

$$\begin{bmatrix} i_\alpha \\ i_\beta \end{bmatrix} = \sqrt{\frac{2}{3}} \begin{bmatrix} 1 & -\frac{1}{2} & -\frac{1}{2} \\ 0 & \frac{\sqrt{3}}{2} & -\frac{\sqrt{3}}{2} \end{bmatrix} \begin{bmatrix} i_A \\ i_B \\ i_C \end{bmatrix} \quad (2.36)$$

➢ Park's transformation

Change the two-phase AC system to rotating DC system is called Park transformation

$$\begin{bmatrix} i_{ds} \\ i_{qs} \end{bmatrix} = \begin{bmatrix} cos\theta & sin\theta \\ -sin\theta & cos\theta \end{bmatrix} \begin{bmatrix} i_{\alpha} \\ i_{\beta} \end{bmatrix} \quad (2.37)$$

These transformations are depicted in Figure 27 and the complete vector control scheme is presented in Figure 32

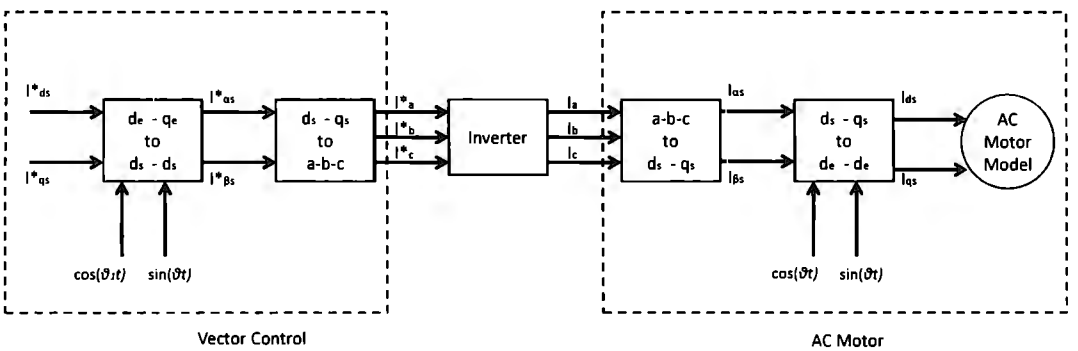

Figure 27. Transformation Processes in Vector Control

The main difference among direct and indirect vector control is the calculation of the unit vector $(\cos(\theta_e), sin(\theta_e))$. Depending on the application and accuracy of control is possible to select between these techniques.

2.1.2.3.1 Direct Vector Control

This technique also known as feedback method because generates a unit vector signal from feedback flux vector. Figure 28 depicts the direct vector control scheme; note that for this explanation the flux signals are referred as $\hat{\psi}_r$ and $\hat{\psi}_s$ which are vector quantities.

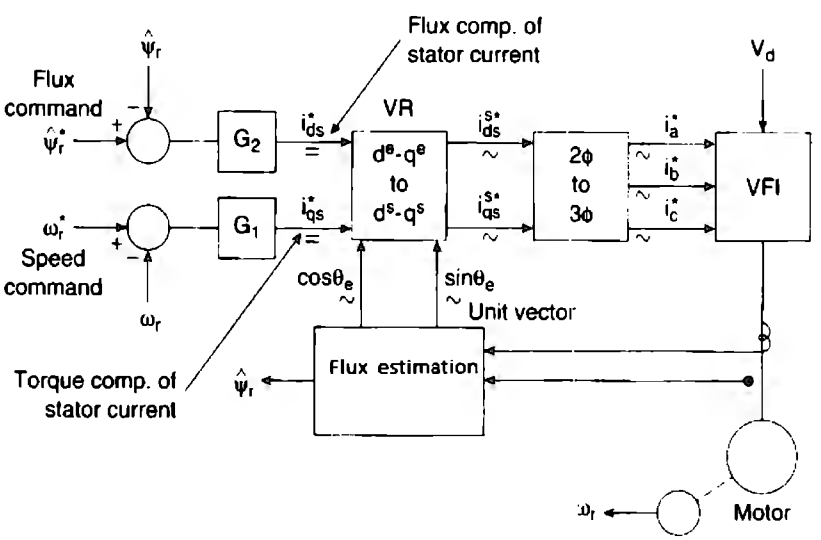

Figure 28. Direct Vector Control, (Bose 2002)

For the unit vector calculation, the following equations are implemented

$$\hat{\psi}_r = \sqrt{{\psi_{dr}^s}^2 + {\psi_{qr}^s}^2} \quad (2.38)$$

$$\psi_{dr}^s = \hat{\psi}_r \cos(\theta_e) \quad (2.39)$$

$$\psi_{qr}^s = \hat{\psi}_r \sin(\theta_e) \quad (2.40)$$

From equations (2.39) and (2.40) is possible to obtain the unit vector. Consequently, these equations imply the rotor flux components calculation.

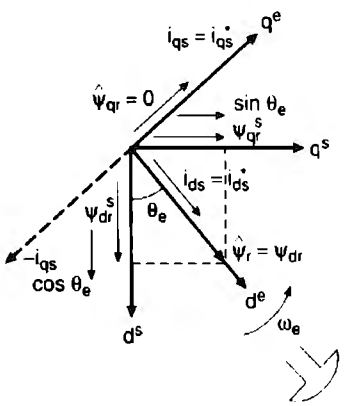

Figure 29. Phasor Scheme and Rotor Flux Orientation, (Bose 2002)

The estimation of the rotor flux vector can be achieved by a voltage method or by a current method (Blaschcke equations). Both methods are explained (Bose 2002).

2.1.2.3.1 Voltage Model

This model uses the direct and quadrature components of the stator voltage in order to calculate the stator fluxes components and then rotor fluxes components. This model computes the following equations:

Using Clark's transform (2.36) to calculate i_{ds}^s - i_{qs}^s and v_{ds}^s - v_{qs}^s then the stator flux components are calculated as follow:

$$\psi_{ds}^s = \int (v_{ds}^s + R_s i_{ds}^s)\, dt \quad (2.41)$$

$$\psi_{qs}^s = \int (v_{qs}^s + R_s i_{qs}^s)\, dt \quad (2.42)$$

$$\hat{\psi}_s = \sqrt{{\psi_{ds}^s}^2 + {\psi_{qs}^s}^2} \quad (2.43)$$

$$\psi_{dm}^s = \psi_{ds}^s - L_{ls} i_{ds}^s = L_m (i_{ds}^s + i_{dr}^s) \quad (2.44)$$

$$\psi_{qm}^s = \psi_{qs}^s - L_{ls} i_{qs}^s = L_m (i_{qs}^s + i_{qr}^s) \quad (2.45)$$

$$\psi_{dr}^s = L_m i_{ds}^s + L_r i_{dr}^s \quad (2.46)$$

$$\psi_{qr}^{s} = L_m i_{qs}^{s} + L_r i_{qr}^{s} \quad (2.47)$$

Substituting (2.44) and (2.45) in (2.46) and (2.47) to eliminate the rotor currents, it is obtained:

$$\psi_{dr}^{s} = \frac{L_r}{L_m}(\psi_{ds}^{s} - \sigma L_s i_{ds}^{s}) \quad (2.48)$$

$$\psi_{qr}^{s} = \frac{L_r}{L_m}(\psi_{qs}^{s} - \sigma L_s i_{qs}^{s}) \quad (2.49)$$

where $\sigma = 1 - \frac{L_m^2}{L_r L_s}$

The electromagnetic torque is defined by

$$T_e = \frac{3}{2}\frac{P}{2}\frac{L_m}{L_r}(\psi_{dr}^{s} i_{qs}^{s} - \psi_{qr}^{s} i_{ds}^{s}) \quad (2.50)$$

Using (2.48) and (2.49) is possible to calculate the rotor flux vector in order to calculate the unit vector. The direct vector control technique with the vector model has the following difficulties:

- At low frequency, voltages signals v_{ds}^{s} and v_{qs}^{s} are very low. In addition, ideal integration becomes difficult because DC offset tends to build up at the integrator output.
- Variations of R_s, L_{ls}, L_{lr} and L_m because of temperature. These variations are more significant at low voltage and frequency.

In automotive applications induction drives are often required to operate from zero speed (stand still vehicle). For these cases the direct vector control with voltage model signal estimation cannot be used.

2.1.2.3.2 Current Model

In the low speed region, the rotor flow components can be synthesized more easily with the help of speed and current signals. This model is based on the stationary d^s-q^s equivalent circuit.

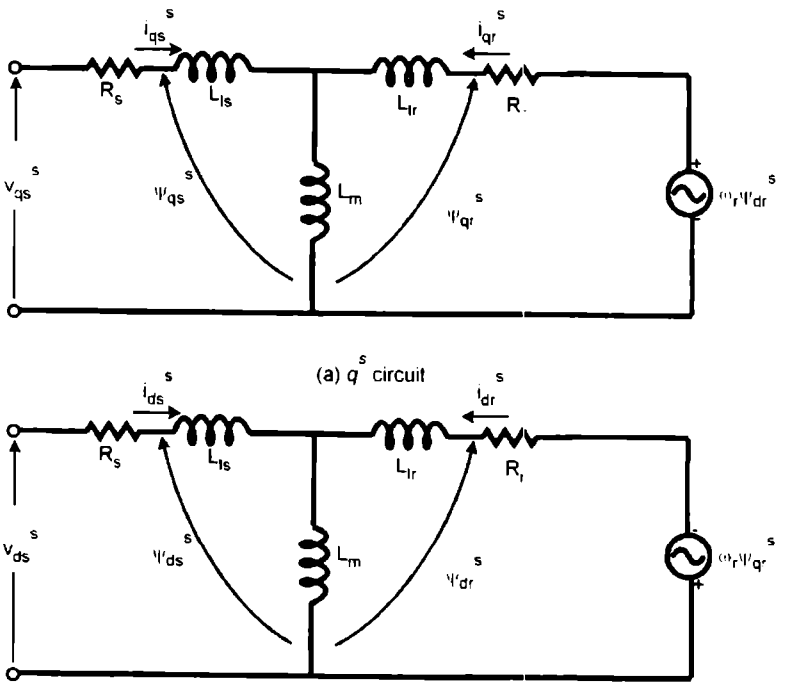

Figure 30. d^s-q^s equivalent circuit, (Bose 2002)

From the squirrel-cage equivalent circuit of Figure 30.

$$\frac{d\psi_{dr}^s}{dt} + R_r i_{dr}^s + \omega_r \psi_{qr}^s = 0 \quad (2.51)$$

$$\frac{d\psi_{qr}^s}{dt} + R_r i_{qr}^s - \omega_r \psi_{dr}^s = 0 \quad (2.52)$$

Adding $\frac{L_m R_r}{L_r} i_{ds}^s$ and $\frac{L_m R_r}{L_r} i_{qs}^s$ in equations (2.51) and (2.52) respectively, it is obtained

$$\frac{d\psi_{dr}^s}{dt} + \frac{R_r}{L_r}(L_m i_{ds}^s + L_r i_{dr}^s) + \omega_r \psi_{qr}^s = \frac{L_m R_r}{L_r} i_{ds}^s \quad (2.53)$$

$$\frac{d\psi_{qr}^s}{dt} + \frac{R_r}{L_r}(L_m i_{qs}^s + L_r i_{qr}^s) + \omega_r \psi_{dr}^s = \frac{L_m R_r}{L_r} i_{qs}^s \quad (2.54)$$

Substituting (2.46) and (2.47).

$$\frac{d\psi_{dr}^s}{dt} = \frac{L_m}{\tau_r} i_{ds}^s - \omega_r \psi_{qr}^s - \frac{\psi_{dr}^s}{\tau_r} \quad (2.55)$$

$$\frac{d\psi_{qr}^s}{dt} = \frac{L_m}{\tau_r} i_{qs}^s - \omega_r \psi_{dr}^s - \frac{\psi_{qr}^s}{\tau_r} \quad (2.56)$$

Where $\tau_r = L_r/R_r$

Equations (2.51) and (2.56) are known as the Blaschke equations. It is possible to note that this model requires speed estimation or sensing. The advantage is that this model can be extended down to speed zero. However, the speed sensing can affect the control accuracy and alternative solution could be the implementation of a speed estimator, but speed estimation implies machine parameters variations by temperature.

The direct vector control technique has two models for rotor flux calculation. The voltage model works well at higher speed ranges, whereas the current model can work at any speed. Therefore, a good solution is a hybrid model, using voltage model for high speed and current model for low speed.

2.1.2.3.2 Indirect Vector Control

This technique was developed by Karl Hasse (Hasse 1968) in his PhD thesis. It is also known as feedforward vector control because it uses feedforward signals for unit vector calculation. The following phasor diagram explains the indirect vector control. From Figure 31 the synchronous speed and angle is calculated as follows:

$$\theta_e = \theta_r + \theta_{sl} = \int(\omega_r + \omega_{sl})dt \quad (2.57)$$

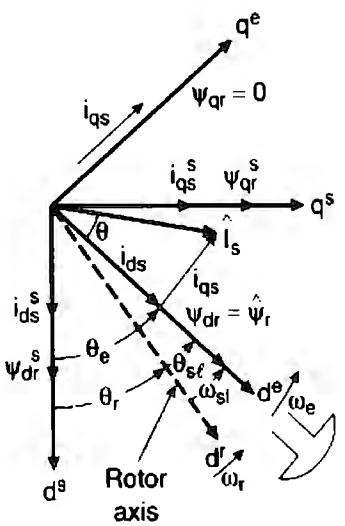

Figure 31. Phasor Diagram of Indirect Vector Control, (Bose 2002)

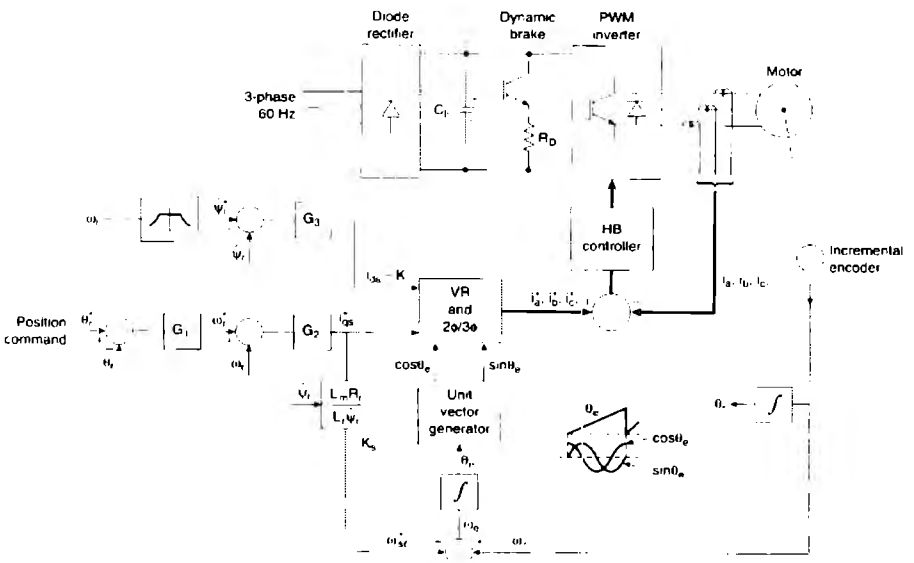

Figure 32. Indirect Vector Control Scheme, (Bose 2002)

From Figure 32 is possible to note how co-ordinates transformation and variables calculation interact into the vector control scheme. In this section will be explained step by step how this calculations are performed (Ponce and Sampé 2008) .

Rewriting the expression (2.35) with the constant K, it is possible to obtain the analogous expression of the DC motor (2.26).

$$T = K\psi_r i_{qs} \quad (2.58)$$

Where $K = \frac{3}{2}\frac{M}{1+\sigma_r}$, M is the mutual inductance and σ_r is the rotor dispersion coefficient. The equation (2.58) is expressed in terms of the rotor magnetic flux and stator current, similar as equation (2.26) for the DC motor. However, to be able to implement the expression (2.58) for an AC motor, it is needed to first achieve the motor decoupled. In the previous section was explained how DTC achieves the motor decoupled by means of the power electronics, now for the vector control this is achieved by means of algebraic manipulation.

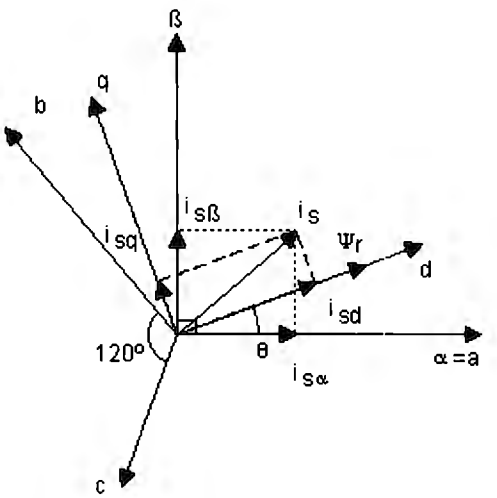

Figure 33. Co-ordinates Transformation

Figure 33 depicts the co-ordinates transformation between three phases to two phases and vice versa, which is possible to achieve with the implementation of Clarke and Park transformations. From this figure is possible to note how the components ψ_r-i_{qs} and i_α-i_β are related to the angle θ, which implies that θ (magnetization angle) needs to be calculate in order to achieve the co-ordinates transformation and variables calculation.

$$\frac{d\theta}{dt} = \omega_{mr} = \omega_r + \frac{i_{qs}}{\tau_r \psi_r} \quad (2.59)$$

Where $\tau_r = L_r/R_r$ and is known as the rotor time constant and ω_{mr} is magnetic flux angular speed. Later will be analyzed that this constant (τ_r) is not such a thing and adds uncertainty to the control. For now, τ_r will be treated as a constant in order to explain the complete vector control model. The second term of equation (2.59) corresponds to the slip angular speed, thus can be calculated like:

$$\theta = \int (\omega_r + \omega_{sl})\, dt \quad (2.60)$$

Reminding that the vector control goal is to control the stator current vector is possible to infer from Figure 33 that i_s is related to i_{qs} and i_{ds}, the latter is directly related to ψ_r thus i_{ds} can be calculated as:

$$i_{ds} = \tau_r \frac{d\psi_r}{dt} + \psi_r \quad (2.61)$$

With the equations defined is possible understand better Figure 32

1. The desire motor speed is set
2. The block Speed Controller receives an error and computes the desire torque
3. With the stator currents measured from the inverter output is calculated i_{ds} and i_{qs}.
4. With i_{ds} and implementing equation (2.61) is computed in the block Rotor Flux Calculation the value of ψ_r.

5. With the desire torque (T_e*) and ψ_r is calculated i_{qs} * using (2.58)

6. The rotor speed or motor speed is measured with a sensor. In the block θ Calculation uses ω_r, ψ_r and i_{qs} to compute (2.59) to later integration in order to obtain the value of θ.

7. The block i_{ds} * Calculation implements (2.61) with a constant value of ψ_r in order to compute the desire value of i_{ds} *.

8. The variables i_{ds} * and i_{qs} *are transformed from a time invariant to time variant framework and then from 2-3phases.

9. The block Current Controller has the PWM logic, which controls the inverter switching.

10. Finally, the inverter sends the current signals to the motor with the correct amplitude and frequency in order to reach the desire torque and speed values.

Vector control is a useful tool that uses the mathematic to achieve the motor decoupled. However, it requires powerful embedded devices for its implementation. This control technique has some variations in its scheme and each one adds some improvement to the control performance. The scheme studied in this subsection is the indirect vector control technique which implements a motor speed sensor instead a rotor flux model or a flux sensor to measure ψ_r also for this technique is considered the slip equation. The direct vector control technique implements a flux model to calculate ψ_r.

Some important remarks about the control vector implementation are:

- The rotor time coefficient τ_r depends on the rotor resistance and inductance. The latter has some variations under operation because the heat generated, however these variations can be neglected. Unlikely for R_r the variations generated by the heat produced by the motor under operation cannot be neglected. This is possible to see from the resistance equation

$$R_T = R_0(1 + \alpha(T - T_0))$$

where:
R_0 is the reference resistance at the reference temperature T_0
α is the temperature coefficient, depends on the material

Therefore R_r needs to be calculated online in order to have accurate motor results. Some research works (Zorgani et al. 2010; Karanayil, Fazlur Rahman, and Grantham 2007; Akatsu, Kawamura, and Member 2000; Ibtiouen 2003) propose observer models like the Kalman filter in order to solve this issue.

- The second commentary is related to the motor speed implementation, because this sensor can suffer negative effects produced by the heat generated inside the motor (similar like R_r). Therefore some research works (K. H. Park et al. 2011; Ghanes, Leon, and Glumineau 2006; Ghanes, Leon, and Glumineau 2007; Zorgani et al. 2010; Karanayil, Fazlur Rahman, and Grantham 2007) propose speed estimator methods, observer models and artificial intelligence methods.

The three main control techniques implemented for AC motors were explained in detail. However, in this thesis an intelligent vector control technique is developed to implement in an EV powertrain, but first will be analyzed the conventional vector control performance and further implementation in an induction motor.

The indirect vector control already explained is simulated by using Matlab/Simulink tools. The motor data are listed in the induction motor model section 2.1.1 and the vector control scheme developed in Simulink is presented in Figure 34.

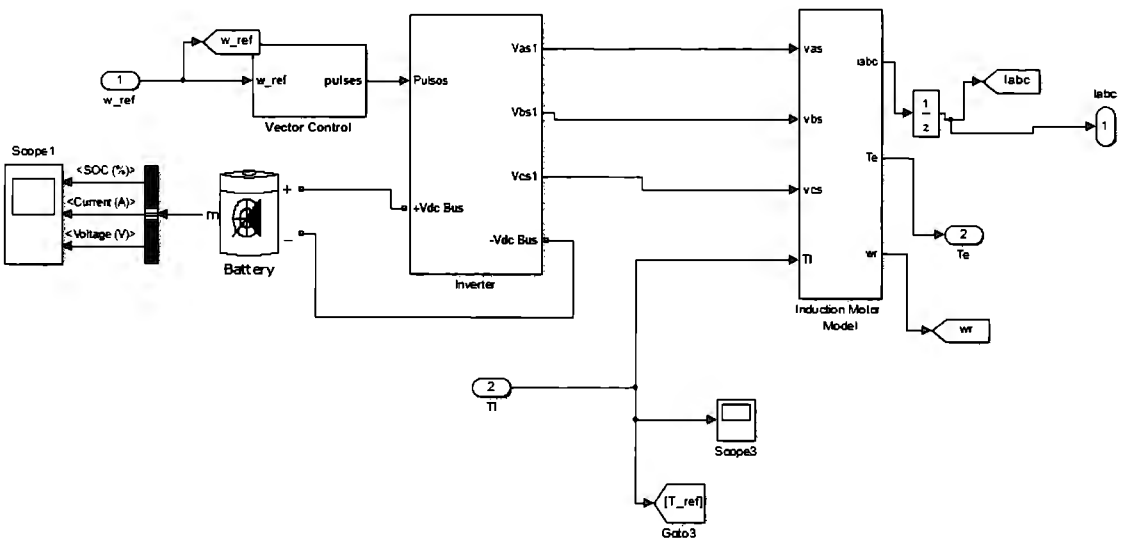

Figure 34. Indirect Vector Control Implementation

Two tests were carried out, the first was with no load torque and the desire motor speed was set to 80 rad/s. From Figure 35 to Figure 37 the results from the simulation are presented.

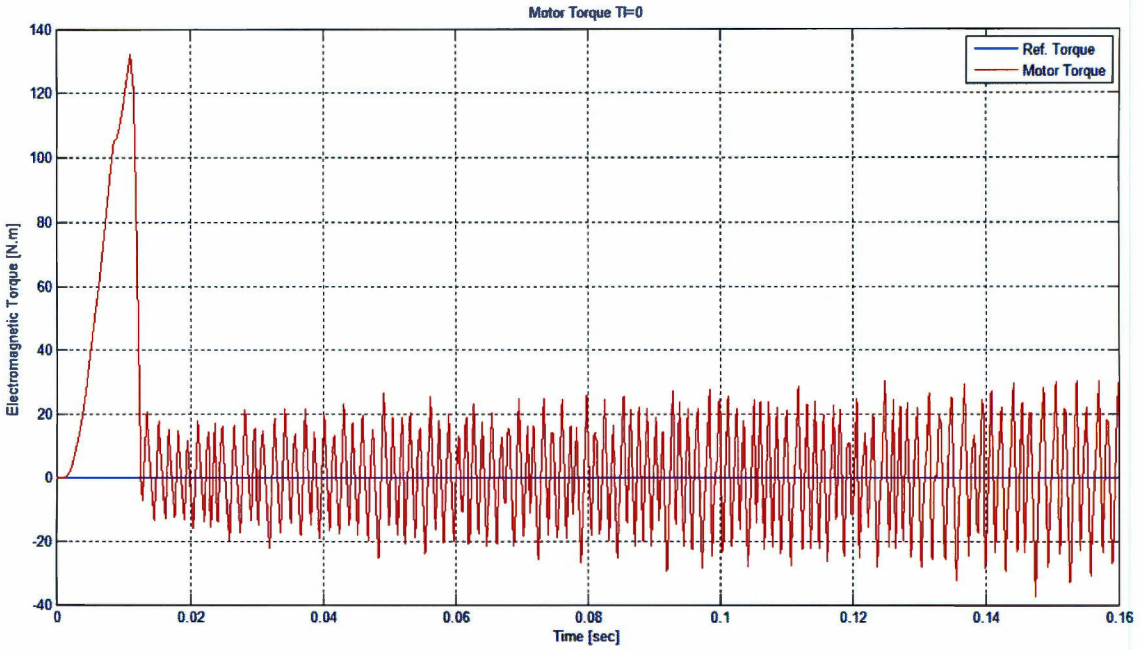

Figure 35. Motor Torque Response

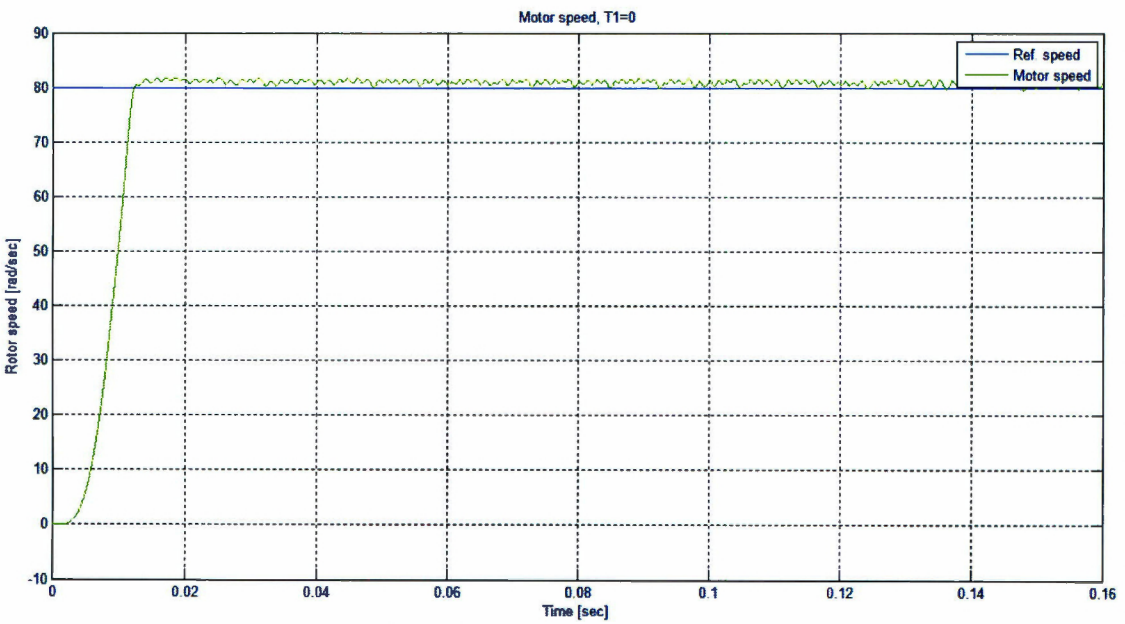

Figure 36. Motor Speed Response

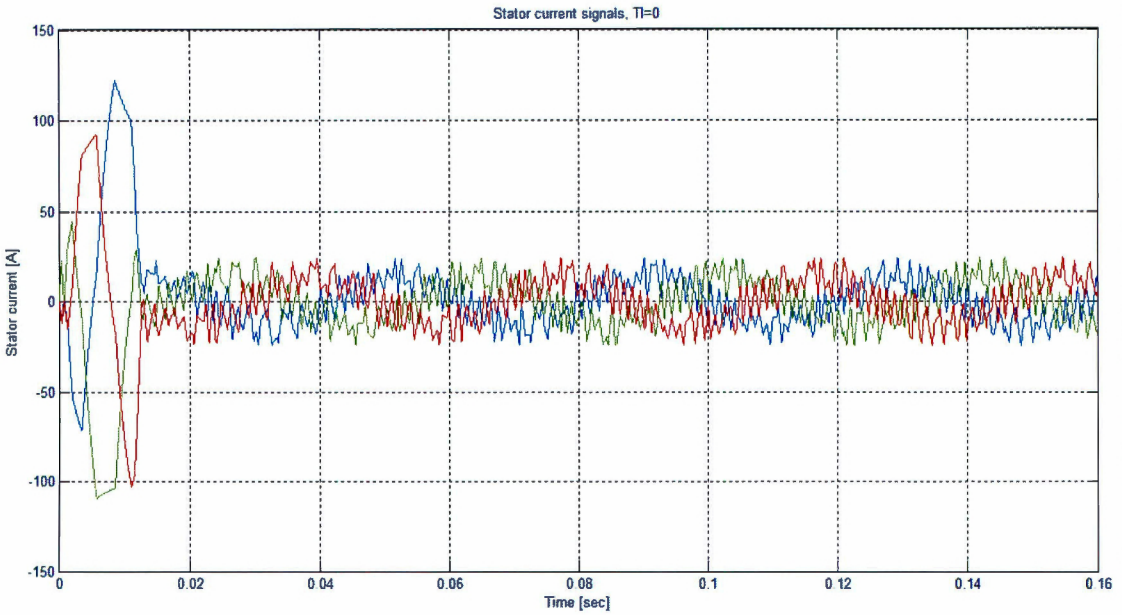

Figure 37. Stator Currents

The second test was for variable torque and speed. The torque step was set from 0 to 200Nm in t=0.3s and the speed step was set from 20 to 60 rad/s in t = 0.2s. The results are presented in from the Figure 38 to Figure 40.

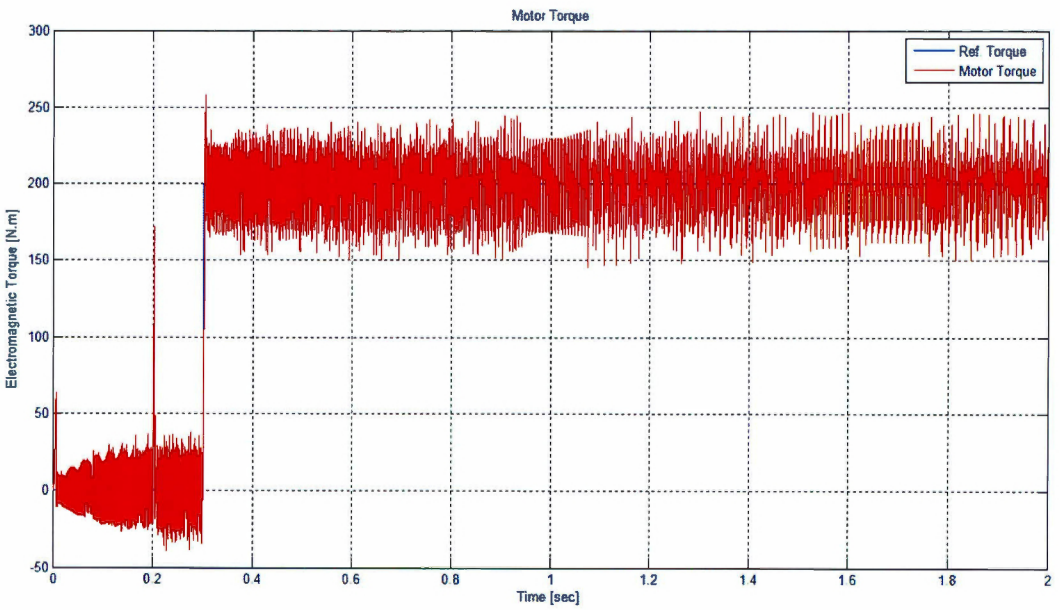

Figure 38. Motor Torque

Figure 38 shows a little variation in the motor torque at 0.2 due to the motor speed reference change and the 200Nm torque applied at 0.3 s.

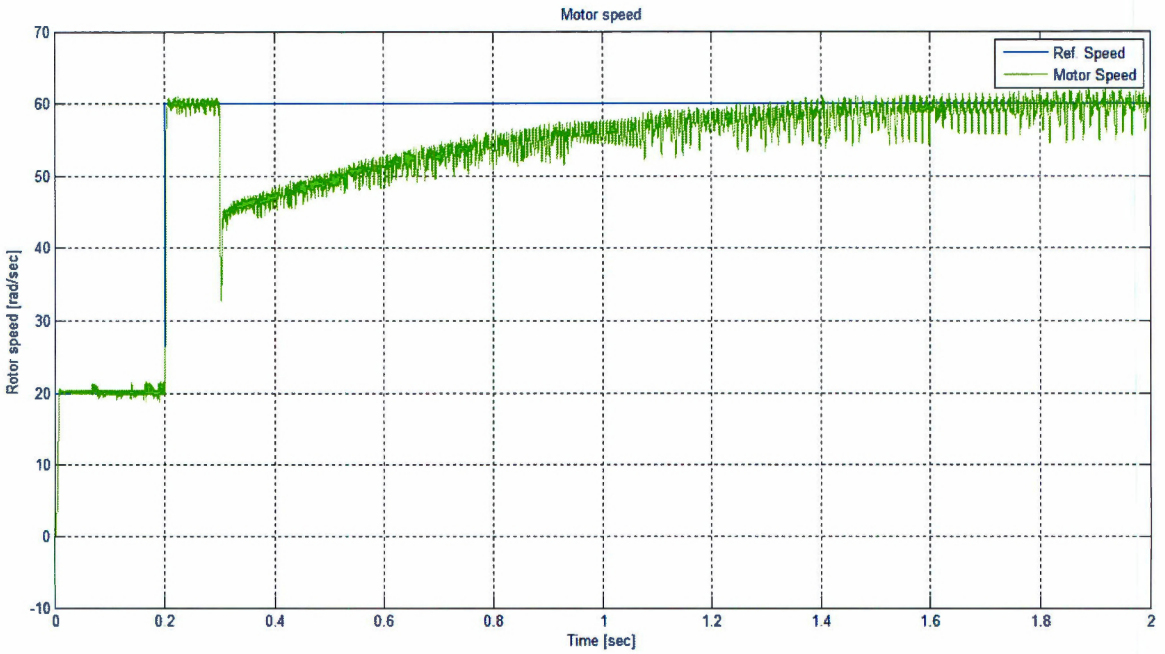

Figure 39. Motor Speed

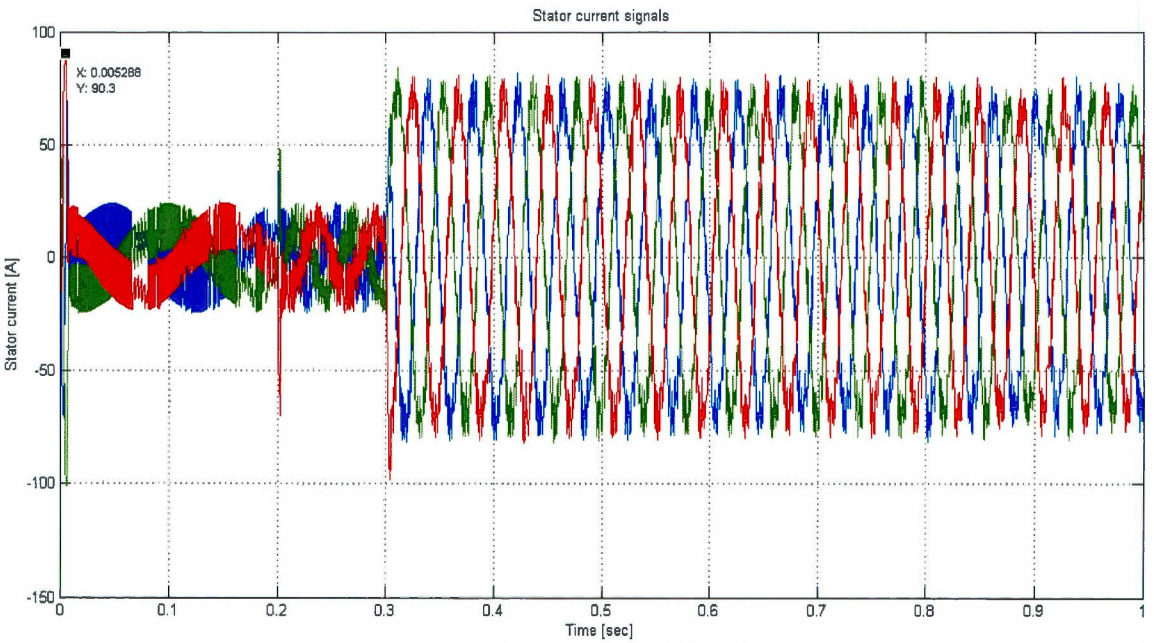

Figure 40. Stator Current Signals

From the results obtained is possible to note how the torque step at t=0.3s from 0 to 200 Nm generates in that the stator current amplitude increases. Also, from Figure 40 is important to mention that the starting current corresponds to the higher value achieved due to the static condition breaking. In general, the results obtained from this implementation are good and depicts the control response in transitory and steady states.

At this point three control techniques used for AC motor have been explained with their mathematical models. However, taking as an example the vector control scheme in Figure 32 is possible to note that

almost the 80% of the vector control scheme is related with the mathematical model explained above, but two important parts that were explained in chapter 1/section 1.2 Power Electronics, are the inverter and PWM techniques. These two are preponderant components for the control of an AC motor and in order to complete the AC motor control techniques explanation it will be introduced some important PWM models.

2.1.3 PWM Methods for Electric Motor Control

The control techniques explained in the subsection before are powerful tools to control AC motors, however for inspection of the DTC and Vector Control schemes (see Figure 26 and Figure 32) is possible to note that DTC uses the inverter as a voltage source (VSI) which means that the switching signals sent to the inverter generates 3 sinusoidal voltage signals to supply the AC motor. Unlikely, in this case for the vector control scheme the inverter is used as a current source (CSI), which means that currents signals are sent to supply the AC motor.

Hence to work with the inverter as VSI or CSI is necessary to define the inverter control or inverter logic, which is the PWM method. This was briefly presented in chapter 1, now will be presented some important PWM models used for AC motor control.

2.1.3.1 Sinusoidal PWM (Sine-PWM)

This PWM method is useful for implementation of the scalar control technique. This is a quite simple method that is based on the intersection of a carrier signal and the reference signal, the intersections among both signals generate the pulses and the resultant signal is defined by:

$$Vout = M \overset{M}{s} sen(\omega_1 t + \phi) + \sum harmonics \quad (2.62)$$

$\emptyset$ is the phase of the signal

ω_1 is the frequency of the output signal

The modulation index is defined by

$$M = \frac{V_{ref}}{V_{tri}} \quad (2.63)$$

Vref is the reference voltage

Vtri is the voltage of the carrier signal

The modulation index can change between 0 and 1

For this PWM method is obtained an efficiency around the 63%

The Sine-PWM was simulated in Labview. The simulation was carried out for a

$f_{Carrier}$= 9 Hz
f_{Ref}= 2.1 Hz
$V_{Carrier}$= 1 V

$V_{Carrier}$= 1.2 V

This PWM technique was implemented in National Instrument Labview and the block diagram is depicted in Figure 41.

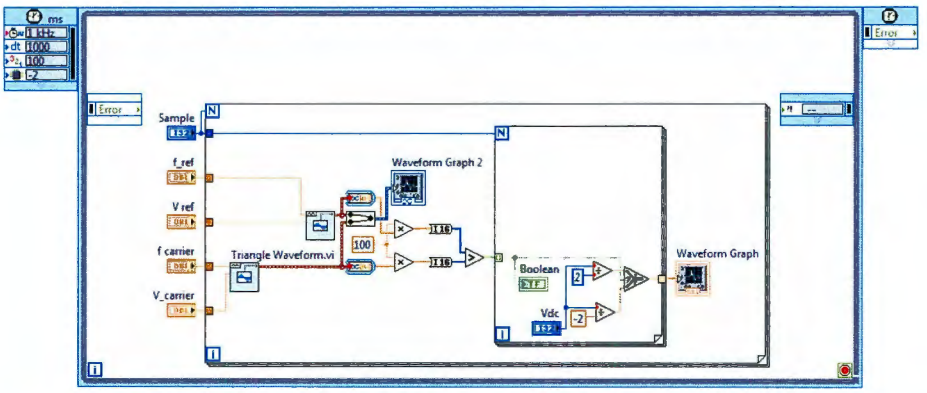

Figure 41. Sine-PWM Block Diagram

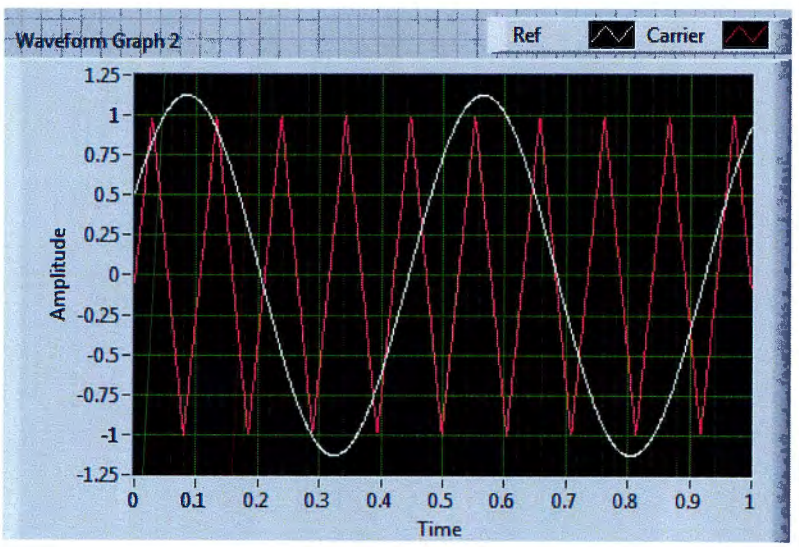

Figure 42. Sine-PWM

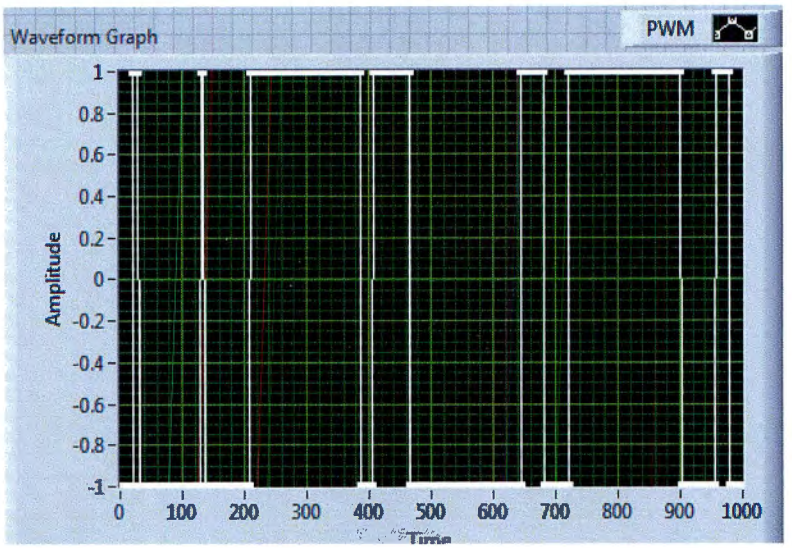

Figure 43. Sine-PWM pulse

The Sine-PWM does not filter all the harmonics of low order which is not a desire condition for the AC motor operation, this is one disadvantage of this PWM method.

2.1.3.2 Selective Harmonic Elimination (SHE-PWM)

The SHE-PWM is a technique that allows the elimination of harmonics depending on the selected harmonics to eliminate, that is, the control of the variable α_i, i_1,2,3,4, … ,n allows to eliminate the desire number of harmonics. Figure 44 shows a symmetric square wave with the first five components from the Fourier transfer (2.64), which allows to select the desire number of harmonics (in this case the first five even harmonics). This PWM method is based on the Fourier series (Enjeti, Ziogas, and Lindsay 1990) which is defined by:

$$v(t) = a_o + \sum_{n=1}^{\infty}[a_n cos(n\omega_o t) + b_n sen(n\omega_o t)] \quad (2.64)$$

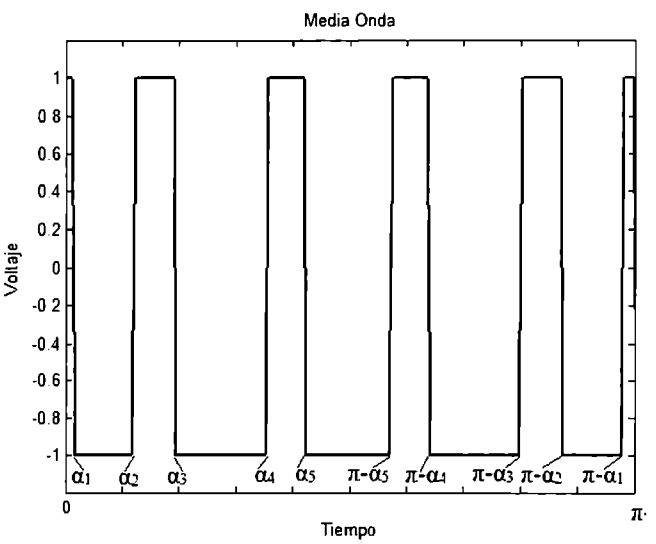

Figure 44. SHE-PWM

where

$$a_n = \frac{1}{\pi}\int_0^{2\pi} v(t)\cos(n\omega t)dt \quad (2.65)$$

$$b_n = \frac{1}{\pi}\int_0^{2\pi} v(t)sen(n\omega t)dt \quad (2.66)$$

Taking only into account the odd harmonic with sinusoidal components, it is obtained:

$$a_n = 0 \quad (2.67)$$

$$v(t) = \sum_{n=1}^{\infty} b_n sen(n\omega t) \quad (2.68)$$

$$b_n = \frac{4}{\pi}\int_0^{\frac{\pi}{2}} v(t)sen(n\omega t)d\omega t \quad (2.69)$$

Assuming an amplitude v(t)=1 and expanding for b_n.

$$\begin{aligned} b_n = \frac{4}{\pi}\Big[& \int_0^{\alpha_1}(+1)sen(n\omega t)d\omega t + \int_{\alpha_1}^{\alpha_2}(-1)sen(n\omega t)d\omega t \\ & + \int_{\alpha_2}^{\alpha_3}(+1)sen(n\omega t)d\omega t + \int_{\alpha_3}^{\alpha_4}(+1)sen(n\omega t)d\omega t + \ldots \\ & + \int_{\alpha_{K-1}}^{\alpha_K}(+1)sen(n\omega t)d\omega t + \int_{\alpha_K}^{\alpha_{\frac{\pi}{2}}}(+1)sen(n\omega t)d\omega t \Big] \end{aligned} \quad (2.70)$$

Integrating each part of (2.70)

$$\begin{aligned} \int_0^{\alpha_1} sen(n\omega t)d\omega t &= -\frac{1}{n}\cos(n\omega t)\Big|_0^{\alpha_1} \\ &= -\frac{1}{n}\left(\cos(n\alpha_1) - \cos(n0)\right) \\ &= \frac{1}{n}(1-\cos(n\alpha_1)) \end{aligned} \quad (2.71)$$

$$\int_{\alpha_1}^{\alpha_2} sen(n\omega t)d\omega t = -\frac{1}{n}\cos(n\omega t)\Big|_{\alpha_1}^{\alpha_2}$$
$$= -\frac{1}{n}\left(\cos(n\alpha_2) - \cos(n\alpha_1)\right)$$
$$= \frac{1}{n}(\cos(n\alpha_1) - \cos(n\alpha_2)) \quad (2.72)$$

Generalizing

$$\int_{\theta_1}^{\theta_2} sen(n\omega t)d\omega t = \frac{1}{n}(\cos(n\theta_1) - \cos(n\theta_2)) \quad (2.73)$$

For k

$$\int_{\alpha_k}^{\frac{\pi}{2}} (+1)sen(n\omega t)d\omega t = -\frac{1}{n}\cos(n\omega t)\Big|_{\alpha_k}^{\frac{\pi}{2}}$$
$$= -\frac{1}{n}\left(\cos(n\frac{\pi}{2}) - \cos(n\alpha_k)\right) = \frac{1}{n}\cos n\alpha_k \quad (2.74)$$

Finally, it is obtained for b_n

$$b_n = \frac{4}{n\pi}\left[1 + 2\left(-\cos n\alpha_1 + \cos n\alpha_2 - \ldots + \cos n\alpha_k\right)\right]$$
$$= \frac{4}{\pi}\left[1 + 2\sum_{k=1}^{k}(-1)^k \cos n\alpha_k\right] \quad (2.75)$$

Fort the equation (2.75) there are different solutions. Therefore, is selected the solution that satisfies the criterion

$$\alpha_1 < \alpha_2 < \alpha_3 < \cdots \alpha_N < \frac{\pi}{2} \quad (2.76)$$

Depending on the desire number of harmonics to eliminate is defined the order of *N*. It is important to remark that will be eliminated the odd harmonics not multiples of 3. For *N=5* the harmonics to eliminate are 5,7,11 y 13.

The system of equations will be:

$$\begin{bmatrix} 2\cos\alpha_1 & 2\cos\alpha_2 & 2(-1)^{N+1}\cos\alpha_N \\ 2\cos 5\alpha_1 & 2\cos 5\alpha_2 & 2(-1)^{N+1}\cos 5\alpha_N \\ \vdots & \vdots & \vdots \\ 2\cos(x_1)\alpha_1 & 2\cos(x1)\alpha_2 & 2(-1)^{N+1}(x_1)\cos\alpha_N \end{bmatrix} = \begin{bmatrix} \frac{\pi a_1}{4}+1 \\ 1 \\ \vdots \\ 1 \end{bmatrix} \quad (2.77)$$

where

$$x_1 = 3N - 2 \quad (2.78)$$

Programming the system of equation (2.77) in Matlab and thanks to the *fsolve* command for nonlinear systems was possible to obtain a solution depicted in Figure 45

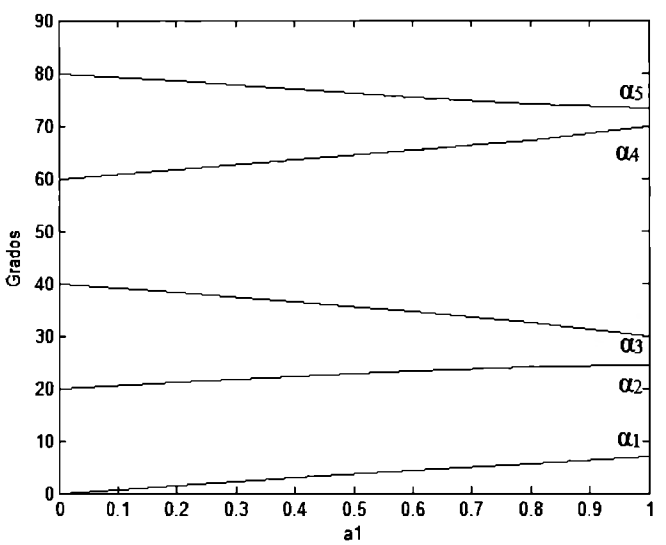

Figure 45. Solution for N=5

The block diagram of the implementation in Matlab/Simulink is presented in Figure 46. The Matlab function 1,2 and 3 are used for the programs that give the pulses, the universal bridge block is an inverter for the asynchronous motor used in this simulation.

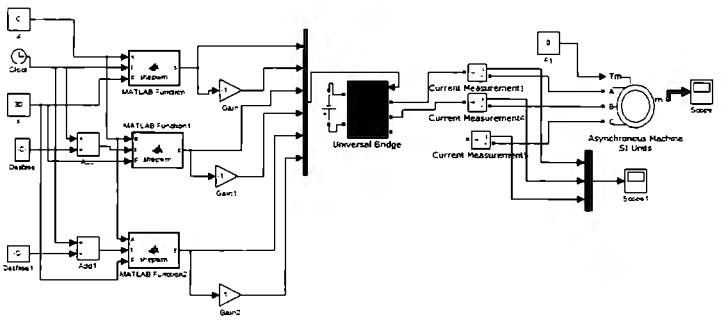

Figure 46. SHE-PWM Block Diagram

The simulation was carried out with the following set of parameters: frequency 30Hz, a1=0.4 and N=5.

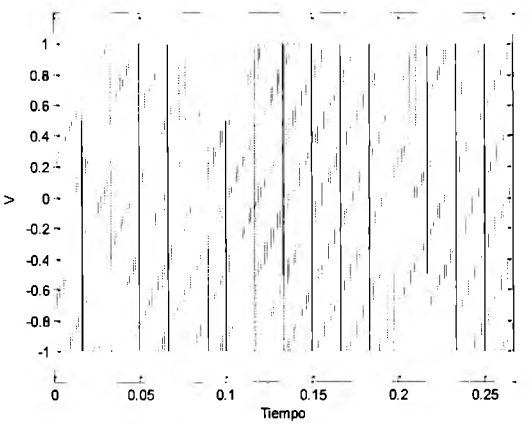

Figure 47. SHE PWM Pulses, f=30Hz and a1=0.4

In order to validate the harmonics elimination is presented the frequency spectrum

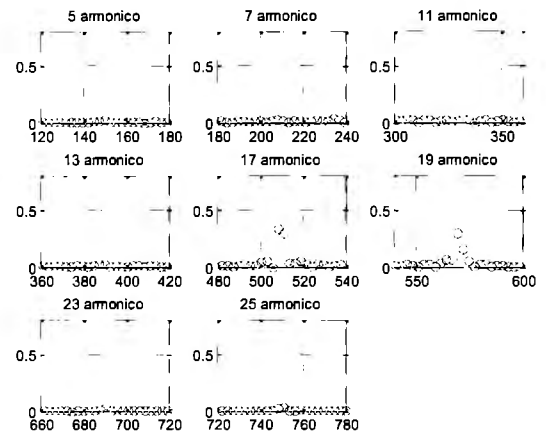

Figure 48. Frequency Spectrum

It is possible to note from Figure 48 how the harmonics 5,7,11 y 13 were eliminated with the implementation of SHE-PWM

2.1.3.3 Space Vector PWM

The SVPWM is a technique implemented to control electric motor; specifically, this technique uses the inverter (i.e. the inverter is the component that sends the current signals to the motor) as a voltage source (VSI).

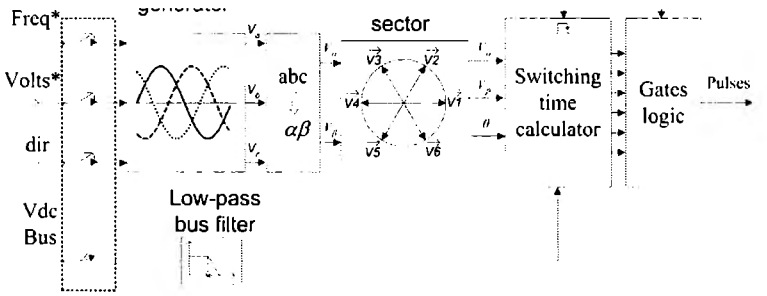

Figure 49. SVPWM Scheme

Figure 49 shows how the SVPWM works and the operations carried out. It is possible to note that the main inputs are: reference voltage (V_{ref}), frequency (f_{ref}) and DC bus voltage (V_{dc}). Then with the frequency and amplitude three signals of voltage with 120° phase between each other are generated, these are Va, Vb and Vc. After, the Park's transform is executed in order to obtain the voltage signals in an orthogonal framework. The Park's transform is achieved with:

$$T_{Park} = \sqrt{\frac{2}{3}}\begin{bmatrix} 1 & -\frac{1}{2} & -\frac{1}{2} \\ 0 & \frac{\sqrt{3}}{2} & -\frac{\sqrt{3}}{2} \end{bmatrix}$$

$$\begin{bmatrix} V_\alpha \\ V_\beta \end{bmatrix} = \sqrt{\frac{2}{3}}\begin{bmatrix} 1 & -\frac{1}{2} & -\frac{1}{2} \\ 0 & \frac{\sqrt{3}}{2} & -\frac{\sqrt{3}}{2} \end{bmatrix}\begin{bmatrix} V_a \\ V_b \\ V_c \end{bmatrix} \quad (2.79)$$

With the voltage in an orthogonal framework is possible to identify the components of the reference voltage into the following sectors.

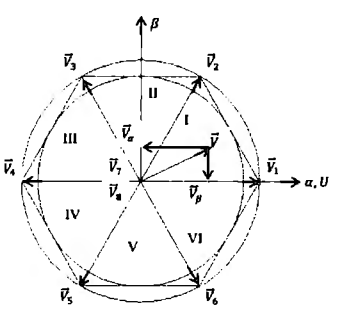

Figure 50. Inverter states representation

Figure 50 depicts the inverter states that are presented in Table 4 with their values, that is for each row corresponds an inverter state.

Table 4. Inverter state

a	b	c	v_a	v_b	v_c	v_{ab}	v_{bc}	v_{ca}
0	0	0	0	0	0	0	0	0
1	0	0	2/3	−1/3	−1/3	1	0	−1
1	1	0	1/3	1/3	−2/3	0	1	−1
0	1	0	−1/3	2/3	−1/3	−1	1	0
0	1	1	−2/3	1/3	1/3	−1	0	1
0	0	1	−1/3	−1/3	2/3	0	−1	1
1	0	1	1/3	−2/3	1/3	1	−1	0
1	1	1	0	0	0	0	0	0

The SVPWM is the control logic of the inverter, that is, it defines the on or off states (i.e. 1 or 0 digital signals) and the times for each state. Therefore, the SVPWM calculates the switching time with:

$$T_1 = 0.5\, T_{pwm} m\, \sin(60 - \alpha) \qquad (2.80)$$

$$T_2 = 0.5\, T_{pwm} m\, \sin(\alpha)$$

where $m = \sqrt{(V_\alpha{}^2 + V_\beta{}^2)}/\,(2/3)V_{DC}$ and $\alpha = \tan^{-1} V_\beta / V_\alpha$

The time T_{pwm} defines the SVPWM period, that means the time in which is execute each sector of the SVPWM. However, T_1 and T_2 are the times for the active vectors (V_1 to V_6), but from Figure 50 is possible to note that V_7 and V_8 are in the origin, and for these vector there is a component of time that defines the symmetry of the pulses, this is:

$$T_0 = 0.5\, T_{pwm} - T_1 - T_2 \quad (2.81)$$

This SVPWM that will be implemented for this work is an alternating-reverse sequence. This means that during the pulse sequence, the active vector (V_7) and null vector (V_0) are introduced. Figure 51 presents the vectors and times alternation for this kind of SVPWM (Raed H. Ahmad, George G. Karady, Tracy D. Blake 1997).

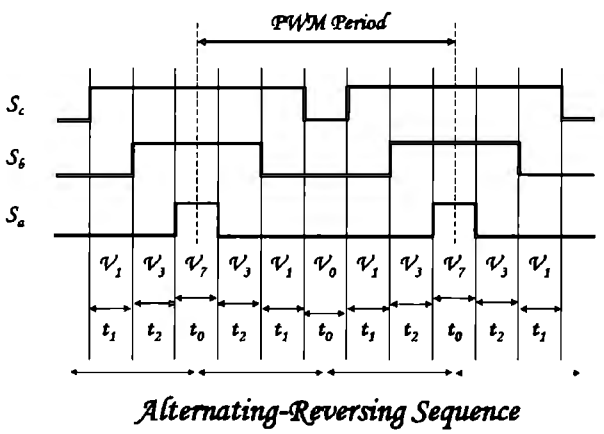

Figure 51. Times and pulses for each phase

However, the calculations presented are for linear modulation mode, that is, modulation under the circle defined within the hexagon of Figure 50. There are two other modulation modes that can occur during operation:

- Linear modulation: $\frac{|V_{ref}|}{V_{dc}} \leq \frac{1}{\sqrt{3}}$, within the hexagon.
- Overmodulation mode I: $\frac{1}{\sqrt{3}} < \frac{|V_{ref}|}{V_{dc}} \leq \frac{2}{3}$, in boundary of the circle.
- Overmodulation mode II: $\frac{2}{3} < \frac{|V_{ref}|}{V_{dc}}$, beyond the circle.

It is important to note that for the linear modulation part the peak reference voltage magnitude is $|V_{ref}| = \frac{V_{dc}}{\sqrt{3}}$ and if the modulation coefficient defined before as $m = |V_{ref}|/(2/3)V_{DC}$, then $m = 0.866$. This result means that the space vector PWM in the linear modulation zone can use 86.6 % of the DC bus voltage.

LabVIEW was used to simulate the SVPWM, the initial values used for this simulation were V_{ref} of 400 and 300 V to a 70Hz frequency. The block diagram and result are presented in Figure 52 and Figure 53, respectively.

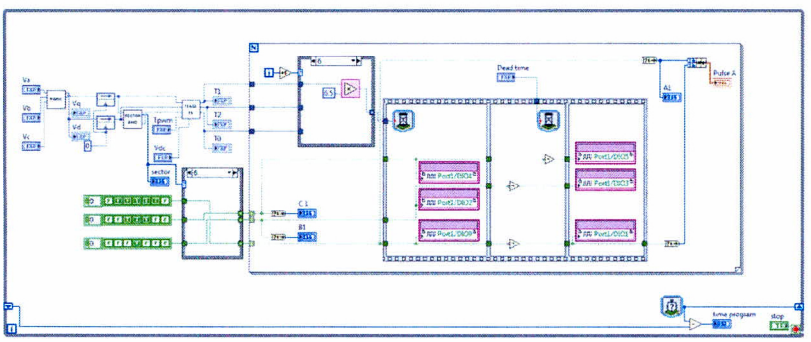

Figure 52. SVPWM Block Diagram

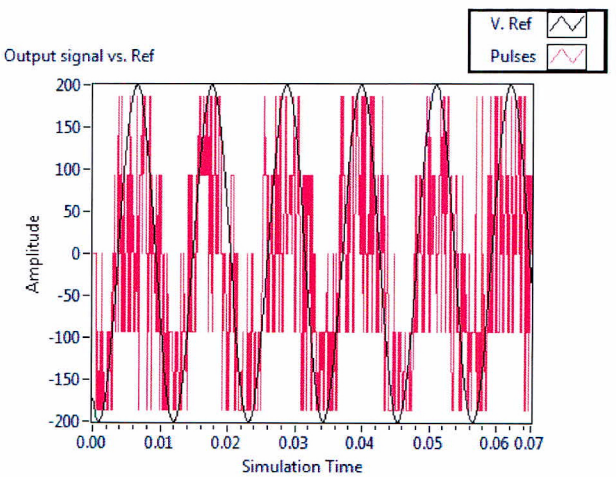

Figure 53. SVPWM Result

This PWM method has a better dc supply power use than the methods explained before. Also, it has a good filtering for harmonics of low order.

2.2 EV Powertrain Model and Control Implementation

The EV powertrain has three main parts: the electric motor, storage unit and transmission. These parts concentrate the EV success in terms of performance. Figure 54 depicts the EV configuration where is depicted the three components just mentioned.

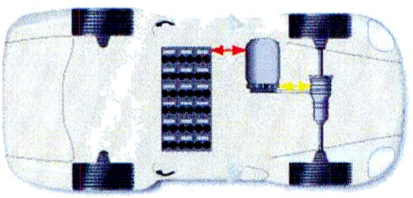

Figure 54. Electric Vehicle Configuration

An important tool used in automotive industry is called ADVISOR (Markel et al. 2002) a powertrain simulation tool developed by the National Renewable Energy Laboratory (NREL). Several research works (Hou and Guo 2008; Wishart 2008; Hoekstra 2005; K. Wipke et al. 1998; K. B. Wipke, Cuddy, and Burch 1999) related to alternative energy sources implementation for vehicles implement ADVISOR for design, simulation and validation of their models. However, in this work ADVISOR will be used as reference in order to implement an accuracy vehicle model. Hence the following section will explain the electric vehicle model and its powertrain control.

2.2.1 Conventional Vector Control Implementation to the EV

The relation power/mass (i.e. horse power per kg) for internal combustion engine vehicles is quite important to achieve a good vehicle performance. This condition is equally important to achieve for EVs. Therefore, for the design and evaluation of a control model for the EV powertrain the tractive effort must be calculated first in order to define the motor size, energy storage unit type and all the components of the powertrain system.

2.2.1.1 Tractive Effort

This is the force propelling the vehicle forward transmitted to the ground through the drive wheels. The total tractive effort is defined below.

$$F_{TE} = F_{rr} + F_{ad} + F_{hc} + F_{la} + F_{\omega a} \quad (2.82)$$

These forces are represented in Figure 55, where F_{rr} is the rolling resistance force, F_{ad} is the aerodynamic drag, F_{hc} is the hill climbing force, F_{la} is the acceleration force and F_{wa} is the angular acceleration force (Larminie and Lowry 2003)

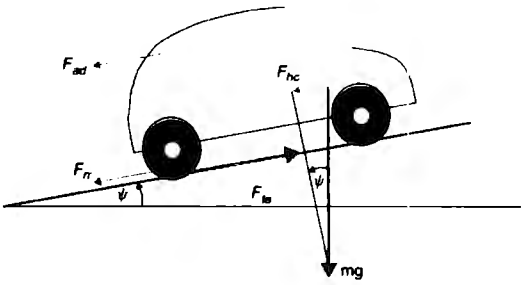

Figure 55. Forces Acting on a Vehicle

The rolling resistance force is calculated is caused by the tire deformation on the road, this force is defined by:

$$F_{rr} = \mu_{rr} mg \quad (2.83)$$

where μ_{rr} is the rolling resistance coefficient, m is the vehicle mass and g is the gravity acceleration. The aerodynamic drag is the viscous resistance of the air acting upon the vehicle, it is defined by:

$$F_{ad} = \frac{1}{2}\rho A C_d v^2 \quad (2.84)$$

where ρ is the air density [kq/m^3], A is the vehicle front area [m^2], v is the vehicle's speed [m/s] and C_d is the drag coefficient. Since EVs offer more flexibility in the location of components, then EVs have a C_d value around 0.19.

The hill climbing force (with positive operational sign) and the downgrade force (with negative operational sign) are given by

$$F_{hc} = mgsin(\psi) \quad (2.85)$$

The acceleration effort is defined by the Newton's second law

$$F_{la} = ma \quad (2.86)$$

Where a is the vehicle acceleration [m/s^2]. Also for a more real modeling, it is important to consider the force needed to make the rotating part achieve the desire speed and torque requirements. Therefore, the angular acceleration is defined by

$$F_{wa} = I\frac{G^2}{\eta_g r^2}a \quad (2.87)$$

Where I is the moment of inertia of the rotor of the motor [kg/m^2], G is the gear ratio, r is the radius of the tyre [m] and the η_g is the gear efficiency, The latter depends on the gear box configuration, however for a EV is not necessary to have a complex gear box then η_g has values around 0.85-0.95.

2.2.1.2 Energy Flow

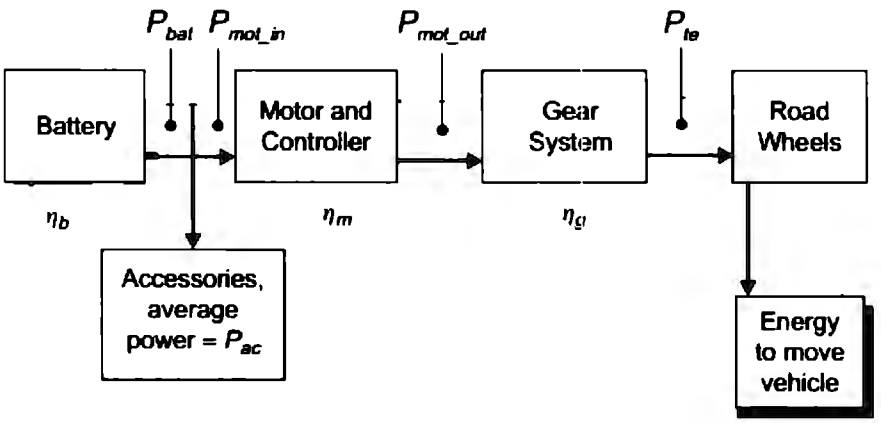

Figure 56. Energy Flow of the Electric Vehicle

The energy flow for an EV is depicted in Figure 56. To predict the range, the energy required to move the vehicle for each second of the driving cycle is calculated. The process is repeated until the battery is flat. Therefore, the power requirements depicted in Figure 56 need to be calculated.

The energy required to move the vehicle is given by

$$P_{TE} = F_{TE} * v \quad (2.88)$$

The equation above requires the previous calculation of the tractive effort (2.82). From Figure 56 is possible to note that the efficiency of the gear, motor and battery are considered.

The motor and controller efficiency are considered as one for convenient. The motor efficiency varies considerably with power, torque, and also motor size. The efficiency is quite well modelled by the equation

$$\eta_m = \frac{P_{out}}{P_{in}} = \frac{P_{out}}{P_{out}+P_{Losses}} \quad (2.89)$$

$$\eta_m = \frac{T\omega}{T\omega+k_c T^2+k_i\omega+k_w\omega^3+C} \quad (2.90)$$

k_c: copper losses coefficient

k_i: iron losses coefficient

k_w: windage losses coefficient

C: constant losses that apply to any speed

With the motor/controller efficiency is possible to calculate the motor power_ in and power_out with the expressions given by

$$P_{mot\_in} = \frac{P_{mot\_out}}{\eta_m} \quad (2.91)$$

$$P_{mot\_out} = \frac{P_{TE}}{\eta_g} \quad (2.92)$$

The equations above are for the case when the vehicle is being driven. For the opposite case, when the motor is being used to slow the vehicle is defined by

$$P_{mot\_in} = P_{mot\_out} * \eta_m \quad (2.3)$$

$$P_{mot\_out} = P_{TE} * \eta_g \quad (2.94)$$

Power required from the battery is given by

$$P_{bat} = P_{mot\_in} + P_{ac} \quad (2.95)$$

For regenerative breaking operation the P_{mot_in} will be negative, and so this will reduce the magnitude of P_{bat}. The simulation algorithm is depicted in Figure 57

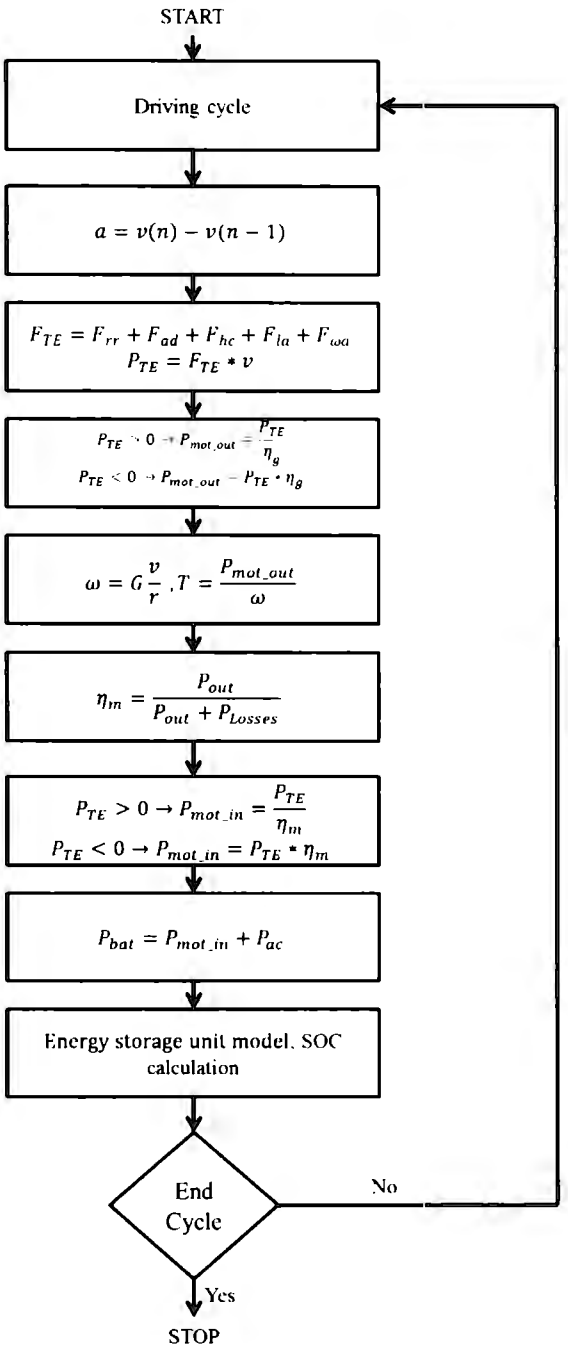

Figure 57. Flowchart for the EV Simulation

The algorithm depicted above is simulated with Matlab/Simulink for different driving cycles and vehicle specifications.

2.2.1.3 *Simulations*

The block diagram for the vehicle model is shown in Figure 58

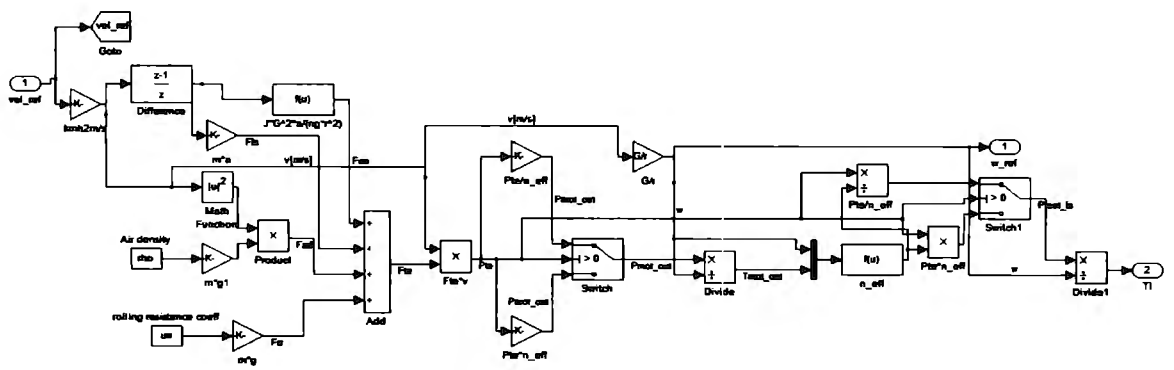

Figure 58. EV Model with Matlab

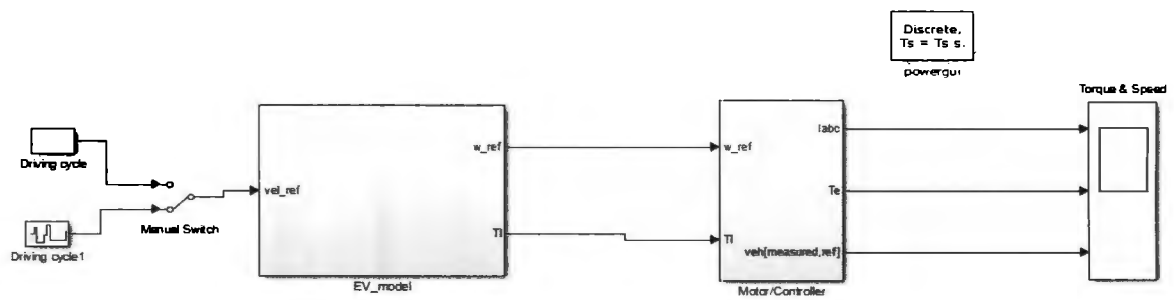

Figure 59. EV with Control model

First is simulated a Peugout Scooter using the induction motor presented before, the parameters for the scooter are:

- m= *115kg*, m_{driver}=*70 kg*, m_{total}=*185kg*
- *Cd=0.75*
- A=*0.6* m^2
- μ_{rr}=0.007
- G=2
- r=0.21m
- ρ=1.25kg/m^3
- η_g=0.95

The parameters of the motor are

- P= 2 (Number of poles)
- Rs= 16.19 ohms (Stator resistance)
- Rr= 21.34 ohms (Rotor resistance)
- Lm= 1.3704 (Magnetizing impedance [H])
- Lls= 0.04994 (Stator side leakage impedance [H])
- Llr= 0.04994 (Rotor side leakage impedance [H])
- J= 0.000589448 (Rotor inertia)
- Power= 370W

The conventional vector control that is used for this test, and the one that will be implemented for experimental tests, has the same basic indirect vector control structure but it differs in the PWM technique implemented. Now a SVPWM will be used and therefore a voltage regulator is implemented. Further details will be shared in chapter 4 about the design of this voltage regulator. The indirect vector control scheme is depicted in Figure 60.

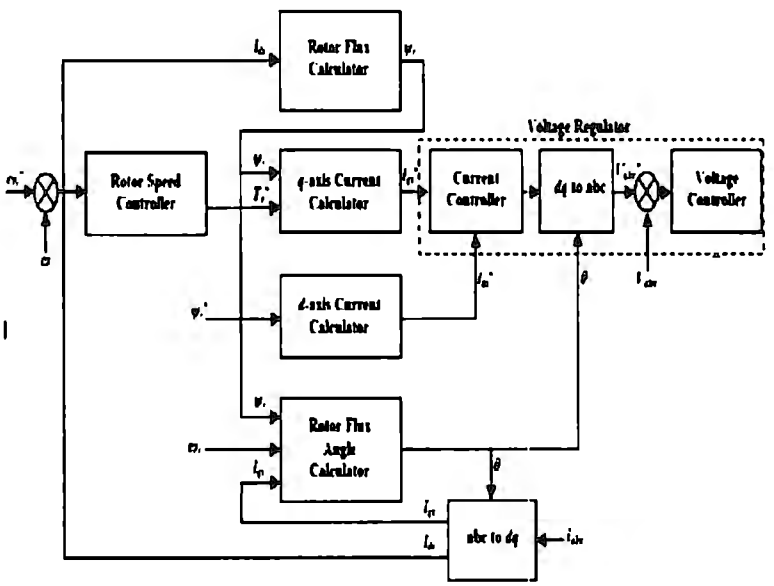

Figure 60. Indirect Vector Control Scheme

This vector controller has the following features:

- The desire flux reference is set to a constant value
- PI's controllers are used to define the torque and currents d-q reference
- A Space Vector PWM is implemented

FUDS (Federal Urban Driving Cycle) is implemented to test the electric vehicle model (for this first case the electric scooter) the vehicle speed profile, torque and power requirements are depicted in the following figures. The simulation time is 1.4 x10^3 seconds, for simplicity is scaled 1:1000.

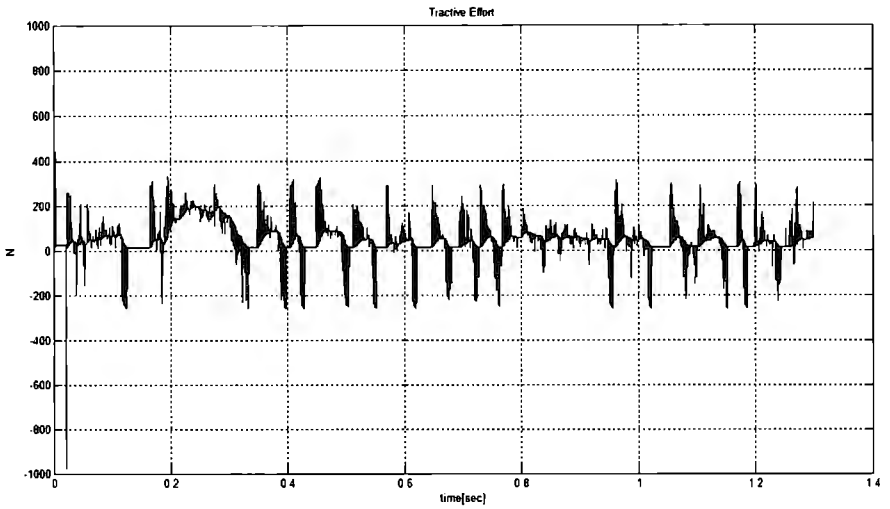

Figure 61. Tractive Effort, FUDS

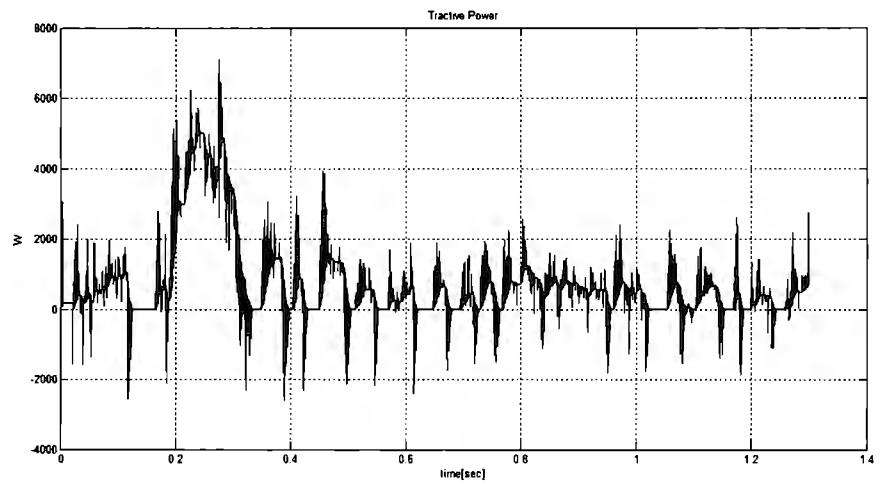

Figure 62. Tractive Power, FUDS

Figure 61 and

Figure 62 depict the force and power required to move the vehicle through the driving cycle. The energy storage unit for this electric scooter is a Lead-Acid battery with an initial SOC of 100%. In this simulation is analyzed the vehicle model performance and it is implemented the indirect vector control to the electric motor, the following results are obtained.

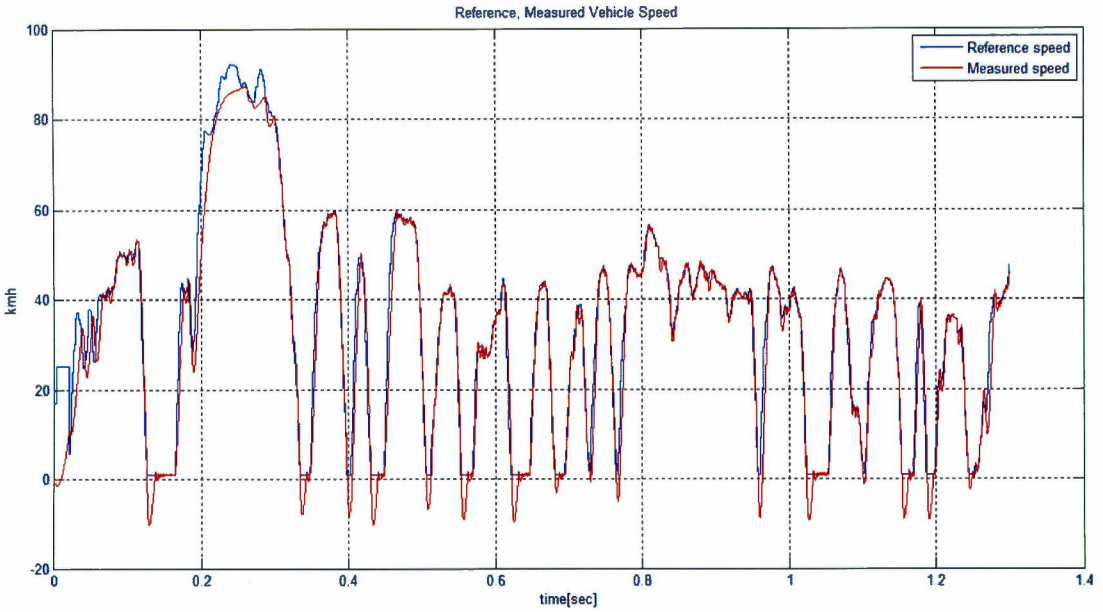

Figure 63. Reference and Measured speed, FUDS

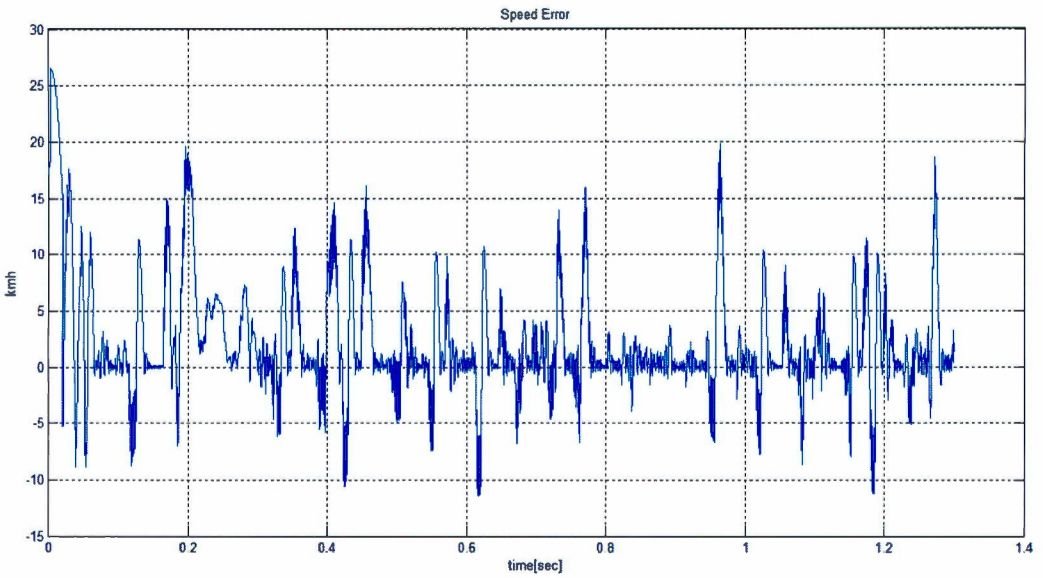

Figure 64. Vehicle Speed Error, FUDS

The error is evaluated based on the mean quadratic error which is computed following the next equation:

$$MSE = \frac{1}{n}\sum_{i=1}^{n}(Y_i - Y_i^*)^2$$

where Y_i is the measured vector with size n, and Y_i^* is the reference vector with the same dimension. The *MSE* obtained for the FUDS driving cycle is 8.4482 km/h

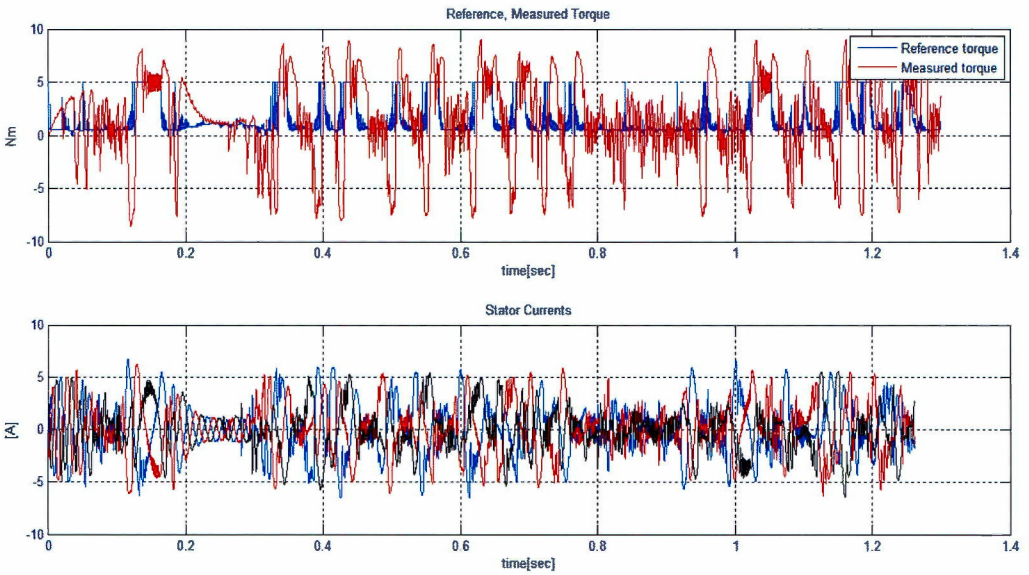

Figure 65. Torque and Stator Currents, FUDS

Satisfactory results were obtained from the simulation for a FUDS driving cycle. It is possible to note that the FUDS test requires several speed variations which also imply torque variations.

A second test is carried out with a speed variation pattern capable to reproduce in a simple testbed. The results obtained from this second test are presented in the following figures.

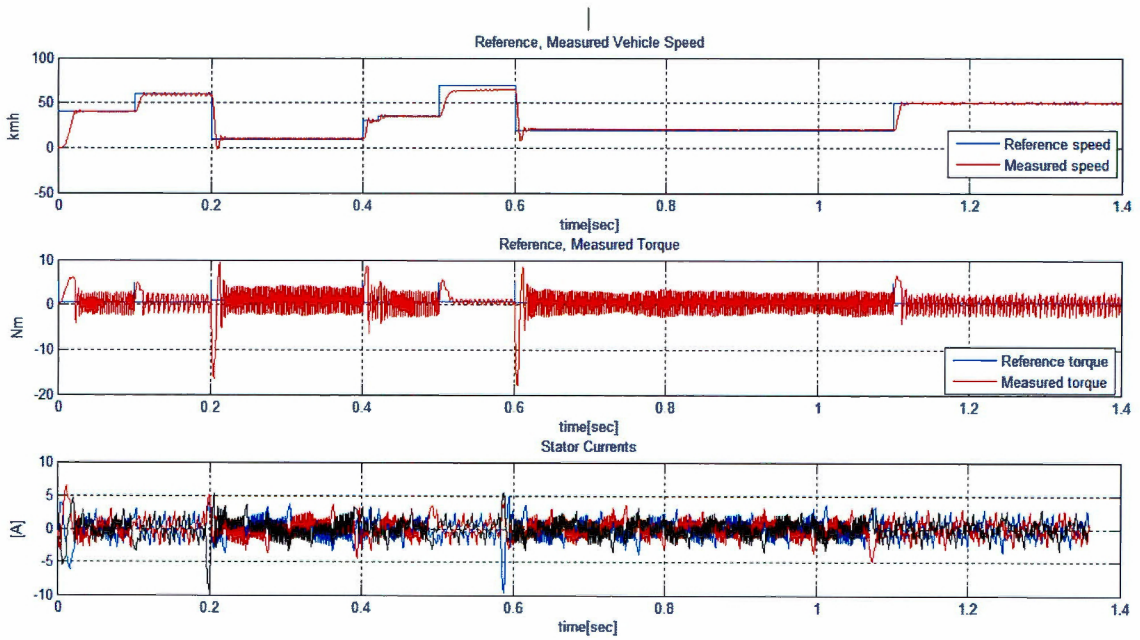

Figure 66. Vehicle speed, motor torque and currents results

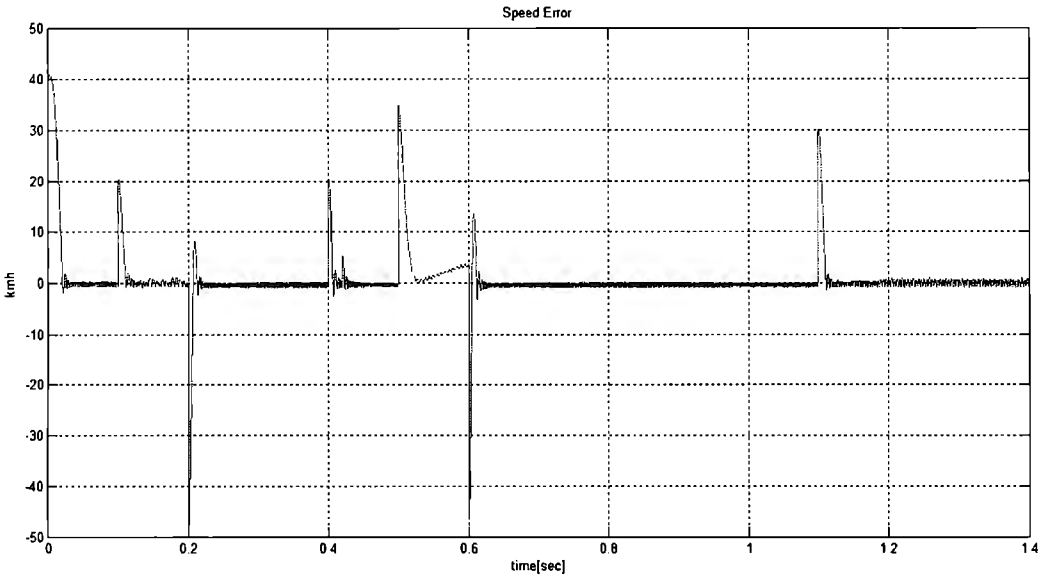

Figure 67. Vehicle speed error, motor torque and currents results

The MSE obtained for this test is 8.2934 km/h which is close to the error obtained with the implementation of a conventional indirect vector control for the FUDS. The main idea of this second test is to simulate the possible results that can be obtained from real experiments.

Later in this work this model will be programed in a Field Programmable Gate Array (FPGA) of National Instruments using LabVIEW, the bed test will be composed by the energy storage unit, electromagnetic break to simulate the load, a squirrel cage induction motor and a two level IGBTs inverter; the parameters will be set based on the motor size.

Chapter 3: Intelligent Vector Control for Electric Vehicle Powertrain

The indirect vector control technique can be implemented with the stator or rotor flux vector, in this thesis is implemented the indirect vector control with rotor flux orientation. Recalling the control scheme (Bose 2002) in Figure 68 is established the starting point for the intelligent vector control.

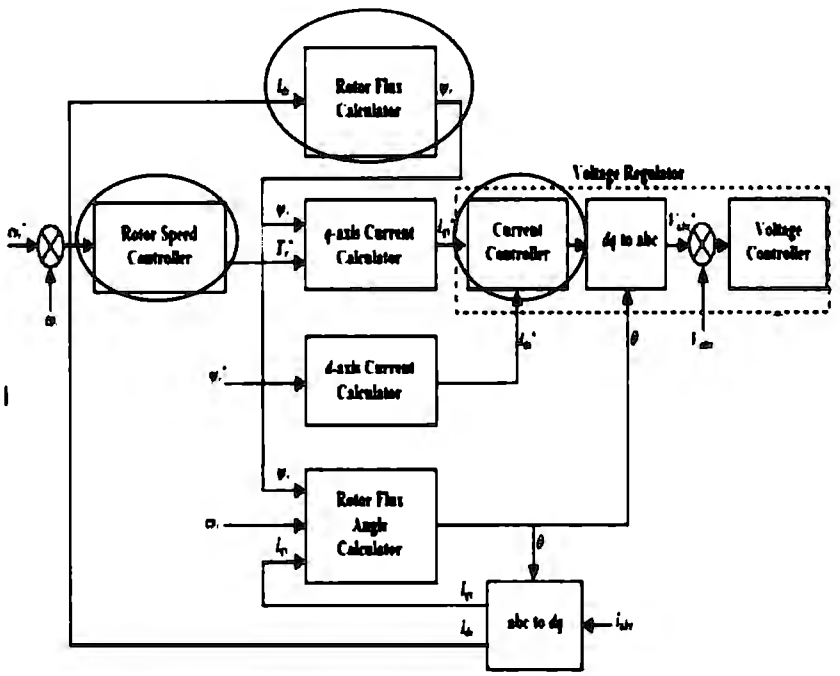

Figure 68. Conventional Indirect Vector Control with Rotor Flux Orientation

From Figure 68 is possible to list each part that will be improved with robust control techniques and artificial intelligence methods, these are listed as follows:

1. The PI control speed that was implemented for the conventional vector control will be changed by a sliding mode controller.
2. The rotor flux calculation will be made with a weakening rotor flux
3. Two fuzzy PI controller are implemented to calculate the quadrature-direct voltage components.

Each part listed above will be explained in the following sections. The basically idea is to explain the theory foundations of the improvement proposed in this thesis.

3.1 Sliding Mode Control

Sliding model control (SMC) is a nonlinear control technique that was proposed by Utkin a researcher of the old USSR (Utkin 1977). This control technique is quite useful for tracking applications where it is needed to follow a specific control command (e.g. speed, position, etc.). The sliding mode control designed in this section follows the approach proposed by Slotine (Slotine and Welping 1991). The main idea of the sliding mode control is to track the surface S=0, this is graphically explained in Figure 69, where $x, \dot{x}$ are the controllable state and its derivative.

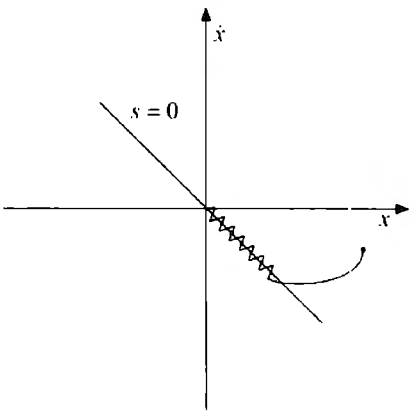

Figure 69. Sliding Mode Control

The surface s is defined by:

$$s = \dot{e} + \lambda e \quad (3.1)$$

where $e = \omega_r^* - \omega_r$ is the error. ω_r^* and ω_r correspond to the reference motor speed and measured rotor speed respectively.

Following the Soltine's approach and using the implementation of the sliding mode control in the research work of Dunnigan (Dunnigan et al. 1998) for indirect vector control, it is first defined the single component as follows:

$$i_{qs}^* = -ksat(s/\phi) \quad (3.2)$$

The equation (3.2) defines the torque command, k is the control gain and the function *sat* is defined as:

$$sat\left(\frac{s}{\phi}\right) = \begin{cases} sgn(s) & |s| > \phi \\ \frac{s}{\phi} & |s| \leq \phi \end{cases} \quad (3.3)$$

k is normally defined to be the maximum value of control effort possible, however this could be unnecessary wasteful in terms of control energy. Therefore, Slotine proposed a method (Slotine 1984) k could be calculated and considered the control law to consist of two components, a continuous one reflecting knowledge of the system dynamics, and a discontinuous one to ensure the sliding occurs. In order to define the continuous component is defined the following second-order model of the induction motor (Dunnigan et al. 1998).

$$\dot{\omega}_r^* = f + bi_{qs}^* \quad (3.4)$$

Differentiating equation (3.1) and substituting (3.4) is obtained

$$\dot{s} = \ddot{\omega}_r^* - \ddot{\omega}_r + \lambda\dot{e} \quad (3.5)$$

Since SMC proposes a sliding surface S=0 then the condition $\dot{s} = 0$ allows the discontinuous component to ensure the sliding occurs. The dual-SMC is defined as:

$$i_{qs}^{*} = \frac{\hat{u}^{*} - ksat(s/\phi)}{\hat{b}} \quad (3.6)$$

The equations to calculate the variables are defined as:

$$\hat{u}^{*} = \hat{f} + \dot{\omega}_r^{*} - \lambda \dot{e} \quad (3.7)$$

$$\hat{f} = \frac{f_{min} + f_{max}}{2} \quad (3.8)$$

$$f_{min} = \frac{-B_1 \omega_r - B_2 sgn(\omega_r)}{J_{max}} \quad (3.9)$$

$$f_{max} = \frac{-B_1 \omega_r - B_2 sgn(\omega_r)}{J_{min}} \quad (3.10)$$

$$f = \frac{-B_1 \omega_r - B_2 sgn(\omega_r)}{J} \quad (3.11)$$

$$\hat{b} = \left(\frac{K_{Tmin}}{J_{max}} \frac{K_{Tmax}}{J_{min}}\right)^{1/2} \quad (3.12)$$

B_1 is the viscous friction constant, B_l is the coulomb friction constant, and J is the moment of inertia. Previously in chapter 2 K_T was defined, for SMC this constant is defined for a constant ψ_r (rotor flux), this is:

$$T_e = \frac{3}{2}\frac{P}{2}\frac{L_m}{L_r}\psi_r i_{qs}^{*} \quad (3.13)$$

Where ψ_r is defined as:

$$\psi_r = L_m i_{ds} \quad (3.14)$$

So K_T is defined as:

$$K_T = \frac{3}{2}\frac{P}{2}\frac{L_m^{2}}{L_r} i_{ds} \quad (3.15)$$

In order to define K_{Tmin} and K_{Tmax} it is defined a variation in the rotor inductance in order to include variations due temperature.

In order to have the control law completely defined, the gain k is calculated as follows

$$k \geq \beta(F + \eta) + (\beta - 1)|\hat{u}^{*}| \quad (3.16)$$

where

$$\beta = \left(\left(\frac{K_{Tmax}}{J_{min}} \right) / \left(\frac{K_{Tmin}}{J_{max}} \right) \right)^{1/2} \quad (3.17)$$

$$F = |f - \hat{f}| \quad (3.18)$$

The SMC defined in this section has three parameters that can be treated as constants; from equation (3.6) ϕ is a constant introduced in order to define the width of the switching line and in equation (3.16) η is a stricter positive constant which is introduced to define the sliding condition:

$$s\dot{s} \leq -\eta|s| \quad (3.18)$$

In equations (3.1), (3.5) and (3.7) λ is the third constant of this SMC model, however in this work was found more useful to calculate λ from equation (3.5) knowing that $\dot{s} = 0$, so λ is defined as

$$\lambda = \frac{\ddot{\omega}_r - \ddot{\omega}_r^*}{\dot{e}} \quad (3.19)$$

In order to improve the SMC performance and to reduce issues related to the chattering introduced by the SMC controller, it will be implemented fuzzy logic. The following section will explain how fuzzy logic work.

3.2 Fuzzy Logic

This is an artificial intelligence technique wide implemented for rapid problem solution based on knowledge. Fuzzy logic was proposed by Zadeh (Zadeh 1965) in his publication "fuzzy sets", the basic idea of the theory proposed by Zadeh is that fuzzy sets have elements with a grade of membership between 0 and 1 unlike binary sets that just have 0 or 1 values of membership (i.e. the grade of involvement with a set or another), the graphic form of the fuzzy sets proposed by Zadeh is depicted in the following figure.

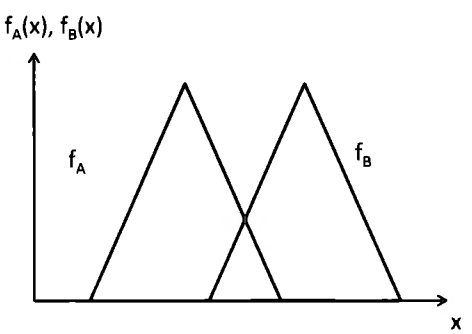

Figure 70. Union and interception of Fuzzy sets (Zadeh 1965)

From the Figure 70 above is possible to see that each set has its elements and also other elements in the x axis corresponds to the interception among sets, this is applicable to a number higher than 2 sets and it is dependent on the application requirements. The implementation of fuzzy logic in this thesis will be related to controllers which are composed by three main parts:

3.2.1 Fuzzification

Fuzzy logic processes crisp entries through fuzzy sets to finally obtain crisp outputs, thus the initial step is to assign fuzzy values (i.e. grade of membership) to the inputs, and this is called fuzzification. This is simpler to understand with the following figure.

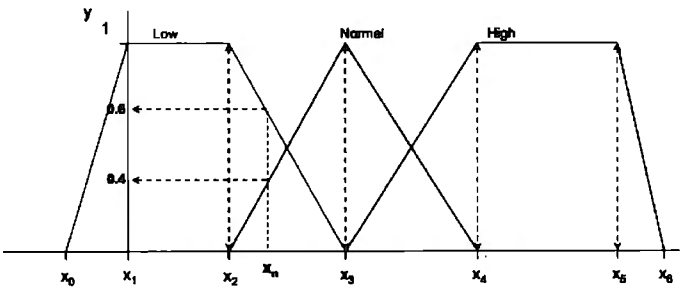

Figure 71. Three membership function, fuzzification

From the Figure 71 above the range between x_0 and x_6 defines the crisp or real values space, thus in the fuzzification step each crisp value has a grade of membership, for example x_n has a grade of membership of 0.4 in the Normal fuzzy set and 0.6 to the Low fuzzy set. Depending on the membership function shape it will be defined the grade of membership calculation.

3.2.2 Rule base definition

From the first step is possible to see that each membership function (MF) is defined with a linguistic label (e.g. low, normal, high, etc.). Therefore, fuzzy logic offers a simple method to define the control law, this is the rules based on linguistic labels. The rules implemented in fuzzy logic have the form:

$$if\ x\ is\ A_1\ \ AND\ y\ is\ B_1, then\ z\ is\ ...$$
$$if\ x\ is\ A_2\ \ AND\ y\ is\ B_2, then\ z\ is\ ...$$

x is the crisp value that belongs with a grade of membership to a MF. Depending on the inputs number AND operators will be used, for the example above x and y are inputs, and depending on the grade of membership of each input to a specific MF it will be defined the decision. However, it is possible to note that an input can have more than one grade of membership from different MFs, thus the third step defines the final decision.

3.2.3 Defuzzification

There are two types of defuzzification methods that are used depending on the fuzzy controller application:

3.2.3.1 Mamdani

The mamdani fuzzy controller uses MFs for the defuzzification part and the final output can be calculated

based on the centroid defuzzification theorem, it is calculated based on the following equation:

$$output = \frac{\sum \mu(x) * x}{\sum \mu(x)} \quad (3.20)$$

where $\mu(x)$ is the grade of membership of a crisp input. This method concentrates the center area where the output has the higher value and thus the controller send the signal. A mamdani fuzzy controller is useful for applications where the output or the controller response has a range of operation.

3.2.3.2 Sugeno

Takagi and Sugeno propose a mathematical approximation for the fuzzy model, this is synthesized in the following expression.

$$Z: If\ f(x_1\ is\ A_1, \dots, x_k\ is\ A_k)\ then\ y = g(x_1 \dots x_k) \quad (3.21)$$

The expression (3.21) depicts how the output is computed based on a mathematical function, this one has the form:

$$y = ax_1 + bx_2 \ (3.22)$$

where a and b are constants.

The SMC theory explained before is implemented for the design of the speed controller and fuzzy controllers are used for the V_d and V_q variables based on the flux and torque current components (i.e. i_d and i_q). The direct and quadrature voltage components are inputs for the SVPWM, therefore the correct performance of SVPWM depends on the good performance of the V_d and V_q fuzzy controllers.

3.3 Field-weakening technique

Normally the indirect vector control implements a constant rotor flux for simplicity. However, there are operation conditions where a constant rotor flux value can deteriorate the motor/controller performance. Thus, the implementation of a field-weakening technique allows the controller to change the rotor flux value based on the motor operation conditions.

The field weakening is defined by the boundary among the base speed (ω_b) which is defined based on the voltages and currents in the direct-quadrature coordinates. See Figure 72.

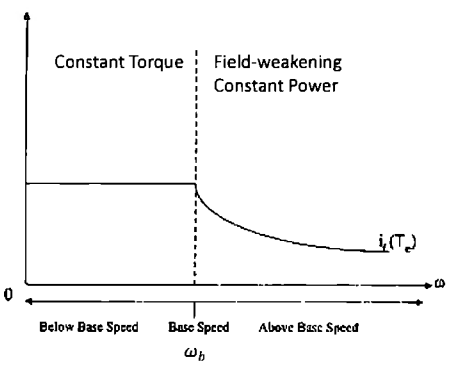

Figure 72. Field-weakening mode

The base speed is calculated with the following equation:

$$\psi_r^* = \frac{\omega_b \psi_b}{\omega_r} \quad (3.23)$$

Based on the motor speed measured (ω_r), it is defined the reference rotor flux constant. The rotor flux reference calculation is used to calculate the desired value for the flux current component, which is used as a reference for a PI that controls the rotor flux loop. The implementation of the field-weakening helps to improve the complete controller performance since the current flux component is estimated based on the motor speed operation and not assumed as a constant.

The theory related to the modifications implemented in the vector control was explained, now the controller is tested with the same speed variation used in chapter 2.

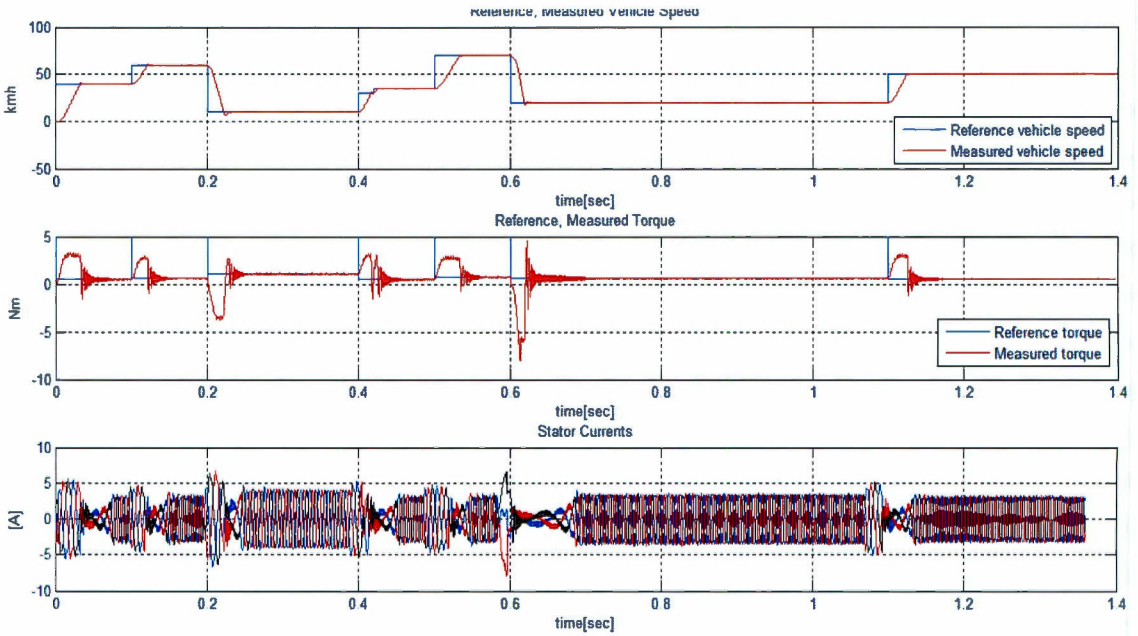

Figure 73. Speed , torque and current variations

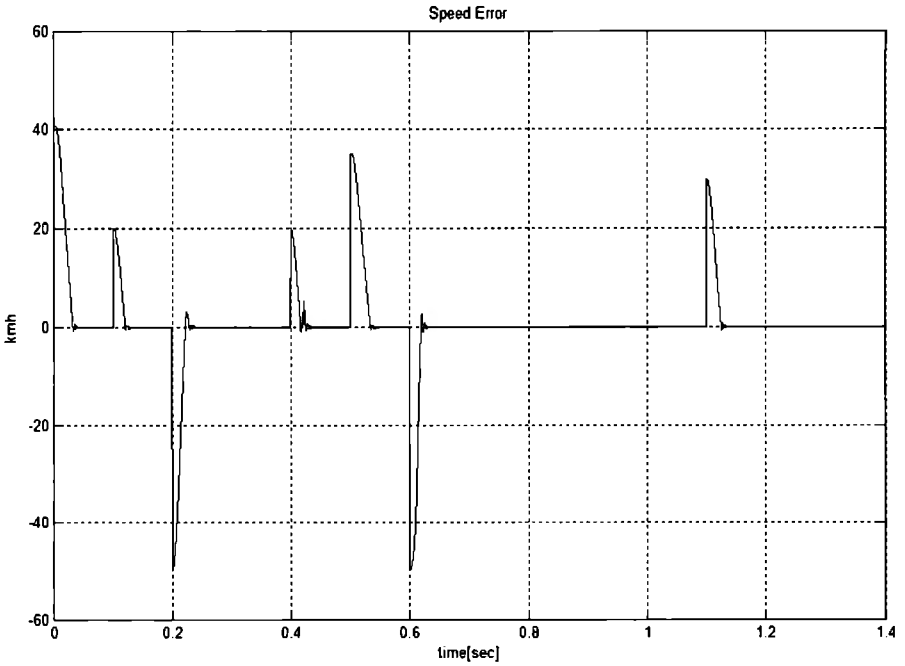

Figure 74. Vehicle speed error

Figure 74 depicts the vehicle speed error obtained from the test. The MSE obtained from this test is 5.9414 km/h which is significantly lower than the results obtained in chapter 2.

The final step of this thesis is to implement the controller designed in chapter 2 and 3 in order to carry out a real test with an induction motor with the same parameters used for the tests simulated in chapter 2 and chapter 3. Also, it will be depicted in the following chapter how is developed an intelligent vector control in the co-simulation environment.

Chapter 4: Validation and Results

The vector control that is proposed in this thesis work is implemented in a FPGA of National Instruments (NI) and a squirrel cage induction motor with its corresponding power electronic phase. Both controllers, the conventional and the proposal vector control are programmed in fixed point variable in a Compact RIO 9012, each stage of the control design is presented in detail in this chapter with the results obtained.

An FPGA is considered as an array of Configurable Logic Blocks (CLBs) that can be connected together through a vast interconnection matrix to form complex digital circuits, a normal configuration is depicted in Figure 75.

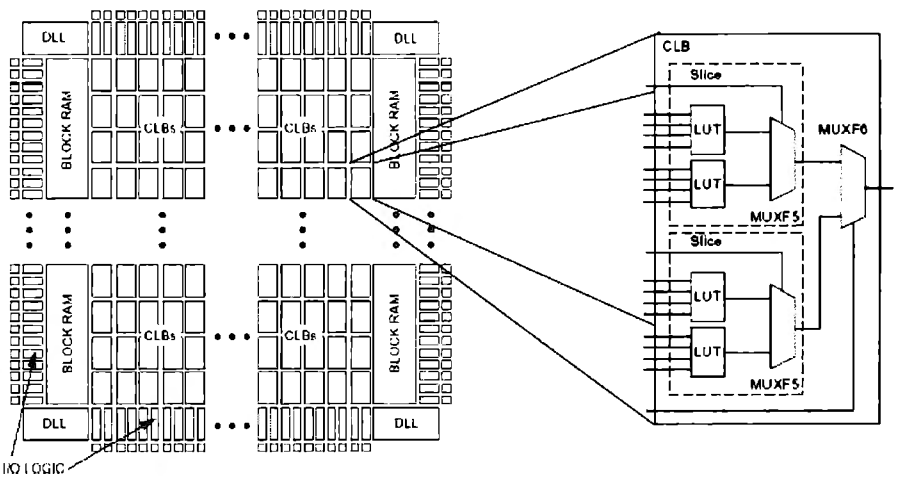

Figure 75. Structure of a typical FPGA

Usually, FPGA is programmed based on VHDL (VHSIC Hardware Description Language) and many software are used for this propose. This programming method can implement low-level (i.e. it provides little or no abstraction from a computer's instruction set architecture) and high level programming (i.e. strong abstraction from the details of the computer), since can be used components for a low level description of a circuit or large functional blocks to do a high level circuit description.

In this thesis work the conventional vector control is implemented in a NI FPGA which uses Labview for the programming phase, this is a high-level programming method. With Labview, the complexity related to the programming process of a FPGA is reduced and the hardware structure allows an easier control implementation for experimental proposes. The programs developed for the conventional and intelligent vector controls are explained in detail in the following subsections.

4.1 Programming of the Conventional and Intelligent Vector Control

The main parts of these controllers are listed below:

1. Speed and currents reading and processing
2. Mathematical calculation and processing
3. PWM signals generation

The programs used for each controller are explained in the following subsections.

4.1.1 Conventional Vector Control Program

The first step of the controller is depicted in the Figure 76, where is possible to see that the encoder pulses are counted, 5 rising edges represent one motor revolution and the counter is configured in milliseconds. Finally, the motor speed is obtained in rad/s units.

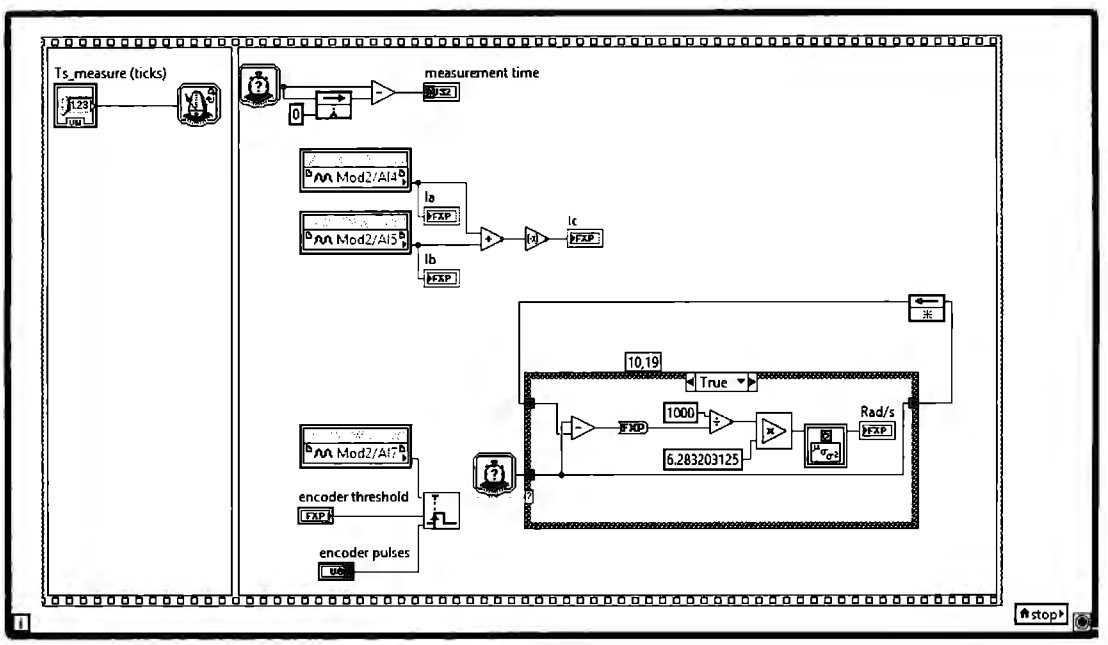

Figure 76. Speed and current reading

The motor currents are necessary for the vector control operation, therefore the currents I_A and I_B are measured and with the following equation, the third phase is calculated.

$$I_A + I_B + I_C = 0 \quad (4.1)$$

After the measuring the variables of speed and currents, the control calculation is made in order to compute the output that will be reflected on the SVPWM. The following figure shows the main calculation stage.

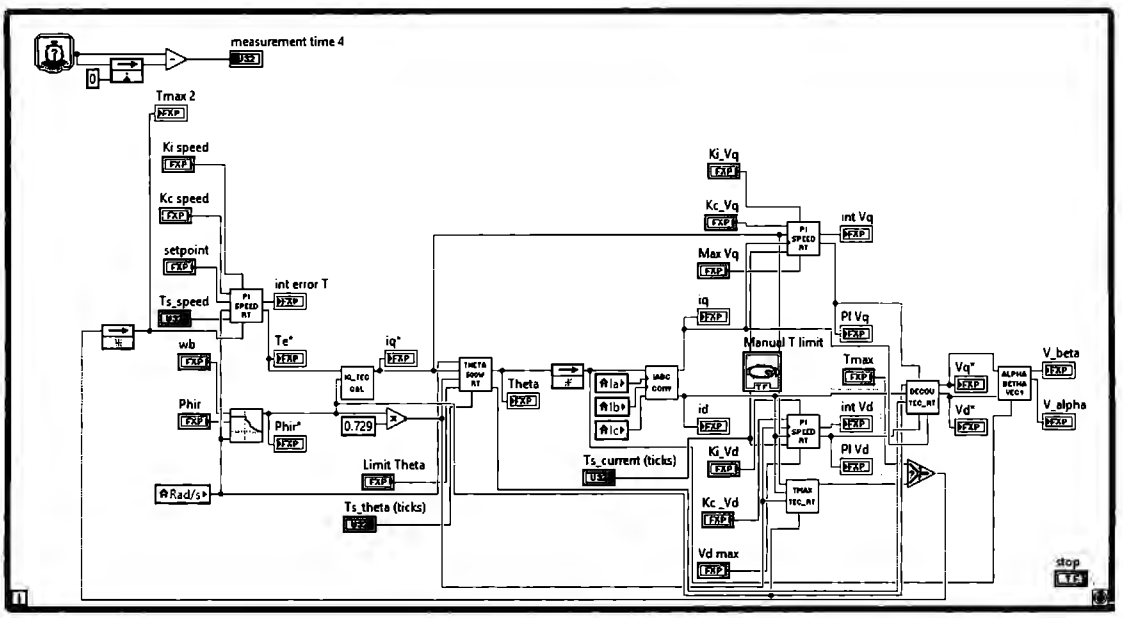

Figure 77. Main control calculation stage

Each block presented in Figure 77 will be explained in the following paraghraps. The "PI series RT" block receives the setpoint and measured motor speed value and it computes the reference torque signal. The calculation of this part is presented below.

A PI controller has the following equation in continuous time domain

$$u(t) = K_p * e(t) + K_I \int e(t)dt \quad (4.2)$$

From the equation above the part that introduces possible instability and programming issues is the error integral. Since the NI FPGA used fixed point variable the PIs are programmed in the discrete time domain, the equation is depicted below.

$$u(nT) = K_p * e(nT) + K_I[Ts * e(nT) + e(nT-1)] \quad (4.3)$$

The equation (4.3) uses the backward Euler integral method; the sample time used for the speed, V_d and V_q PI's, is $T_s = 1 * 10^{-6}s$.

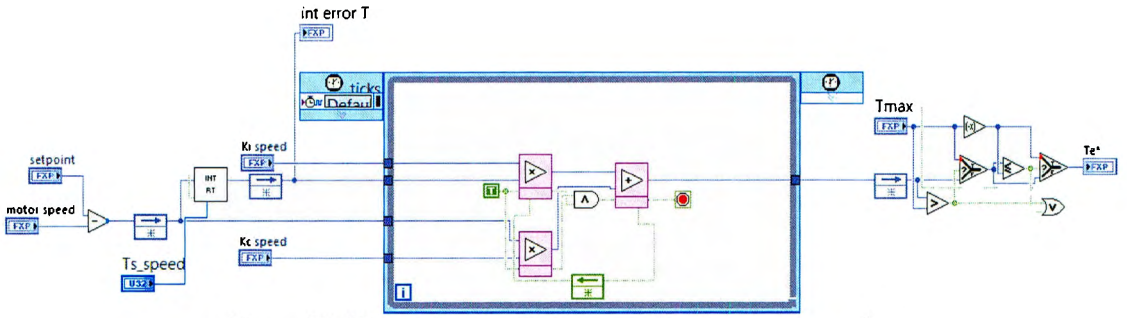

Figure 78. PI speed controller, conventional vector control

The Figure 78 shows a parallel PI controller program with NI Labview, an important thing to mention is that the PI's code implements a while timed loop which works with the FPGA clock (40 MHz). This programming method helps to improve code execution speed within the FPGA.

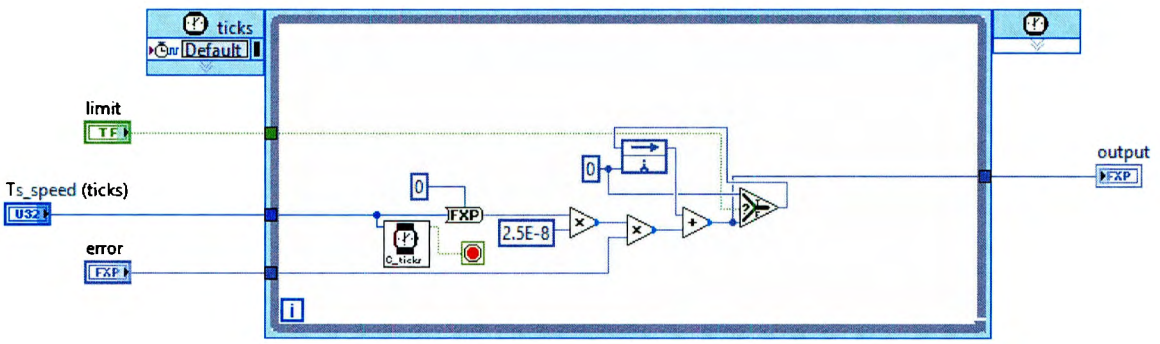

Figure 79. Backward Euler integral, conventional vector control

The backward Euler integral program is depicted in the Figure 79, a timed loop is usesd in order to execute one cycle in exactly one tick equivalent to one FPGA top clock (1tick=40 MHz= 25ns). Therefore the Ts is defined in ticks, for this application was set to 40 ticks = 1μs.

The same structure showed for the speed PI controller was used for the current regulators in the rotatory reference (i.e. iq and id stator current components on d-q rotatory frame). This is the reason why in Figure 77 the PI's under the label "PI series RT" corresponds to speed, iq and id regulators. It is the same code but for different variables size, this is known in NI Labview as a "Preallocated clone reentrant execution" allowing parallel execution of simultaneous calls while minimizing jitter and each VI keeps its own state and control values.

The field weakening VI depicted in Figure 80 by the weakening behavior helps to maintain the constant flux value for motor speed below or equal the nominal value. The program and equation for this VI are depicted as follows.

$$\psi_r^* = \frac{\omega_b * \psi_b}{\omega_r} \quad (4.4)$$

Where $\omega_b = 2\pi f_n$, f_n is the nominal motor frequency; $\psi_b = \frac{V_n}{\omega_b}$ and ω_r is the measured motor speed.

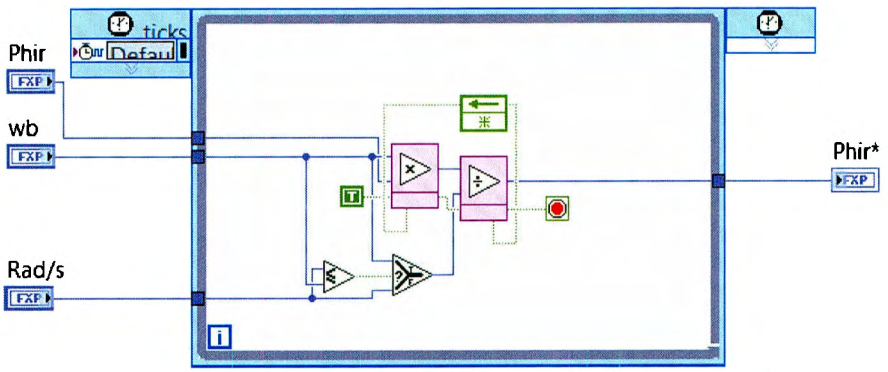

Figure 80. Rotor flux defnition , conventional vector control

The program above shows that while the measured motor speed (Rad/s) is equal or below the nominal motor speed, then the rotor flux will keep its nominal value. Otherwise, if the measured motor speed is higher than its nominal value, the flux will decrease based on the expression (4.4).

From the speed PI is obtained the reference torque command. With the reference torque value calculated and with the rotor flux value is obtained the reference quadrature current components (torque component) based on the following equation.

$$i_q^* = (2/3)(P/2)(L_r/L_m)(T_e/\psi_r) \quad (4.5)$$

In the Figure 81 is depicted that for the rotor flux is added a constant which is used to avoid divisions by zero. This is just to avoid a wrong induction motor operation at the start phase.

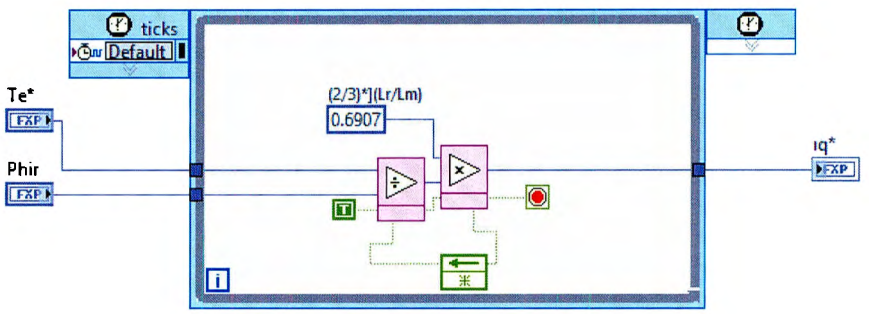

Figure 81. i_q calculation, conventional vector control

The calculation of the rotor flux angle (θ_r) is a key part for the correct performance of the whole vector control. This angle is computed based on the equation.

$$\frac{d\theta_r}{dt} = \omega_{mr} = \omega_r + \frac{R_r i_{qs}^*}{L_r i_{ds}^*} \quad (4.6)$$

The integral of the equation above gives the rotor flux position. The block "Theta cal RT" is depicted in Figure 82.

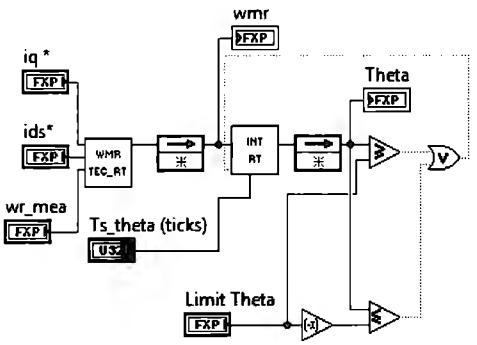

Figure 82. θ_r calculation, conventional vector control

With the rotor flux angle and the measurement of the stator currents is possible to compute the Clark´s and Park´s transformation. The equations for this part are:

- Clarke´s transformation

$$\begin{bmatrix} i_\alpha \\ i_\beta \end{bmatrix} = \sqrt{\frac{2}{3}} \begin{bmatrix} 1 & -\frac{1}{2} & -\frac{1}{2} \\ 0 & \frac{\sqrt{3}}{2} & -\frac{\sqrt{3}}{2} \end{bmatrix} \begin{bmatrix} i_A \\ i_B \\ i_C \end{bmatrix} \quad (4.7)$$

- Park's transformation

$$\begin{bmatrix} i_{ds} \\ i_{qs} \end{bmatrix} = \begin{bmatrix} cos\theta & sin\theta \\ -sin\theta & cos\theta \end{bmatrix} \begin{bmatrix} i_\alpha \\ i_\beta \end{bmatrix} \quad (4.8)$$

The programming for the block "Iabc conv" is depicted in the Figure 83.

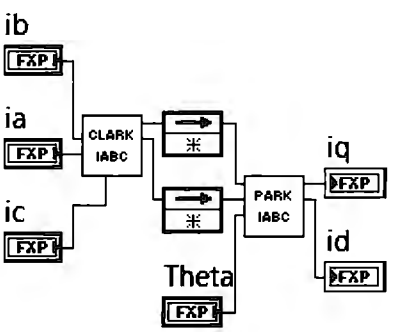

Figure 83. Clarke's and Park's transformation, conventional vector control

In order to limit the speed PI torque reference value, it is implemented the following program which takes into account the current components calculated from frame transformations and reference values. The equations involved are:

$$i_{max} = \sqrt{i_{sd}^2 + i_{sq}^2} \quad (4.9)$$

$$i_{q\,max} = \sqrt{i_{max}^2 + i_{sd}^{*2}} \quad (4.10)$$

$$T_{max} = (3/2)(P/2)(L_m/L_r)(i_{q\,max}\psi_r) \quad (4.11)$$

The program related to the equations below

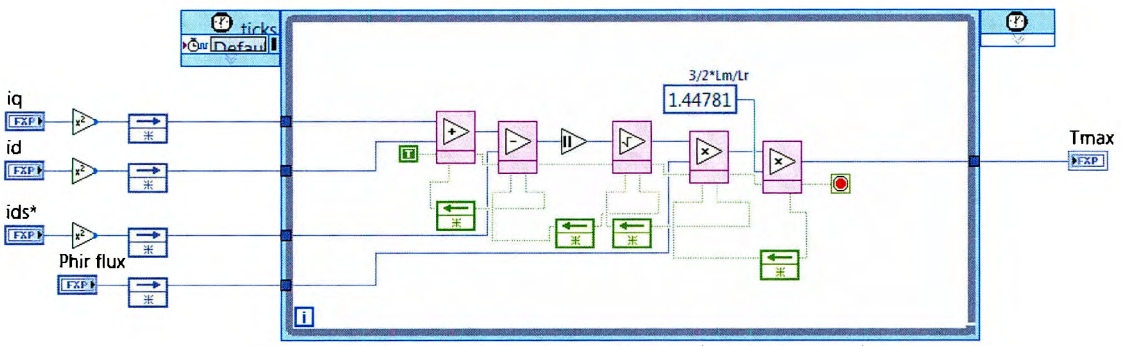

Figure 84.Torque limiter, conventional vector control

The equations that describe the voltage response are:

$$i_{ds}(R_s + DL_s\sigma) + \frac{L_m}{L_r} D\lambda_{rd} = V_d + \omega_e L_s \sigma i_q \quad (4.12)$$

$$i_{qs}(R_s + DL_s\sigma) + \omega_e \frac{L_m}{L_r} D\lambda_{rd} = V_q - \omega_e L_s \sigma i_d \quad (4.13)$$

where R_s is the stator resistance, L_s is the stator inductance, L_m the magnetizing inductance, σ is the leakage factor defined as $\sigma = 1 - \frac{L_m^2}{L_r}$, D is the differential operator.

From the right side of equations (4.12) and (4.13), is possible to notice that the quadrature and direct voltages components, V_q and V_d, are affected by opposite current components. (i.e. the terms adding and sustracting the voltage variables). Therefore a coupling effect is produced by these terms in the voltages response, which produce a lack of response in the vector control performance. For this reason a decouplig circuit is designed to extract $\omega_e L_s \sigma i_q$ and $\omega_e L_s \sigma i_d$ from V_d and V_q, correspondingly. In the Figure 85 is presented the program under the label "DECOU TEC_RT" in Figure 77.

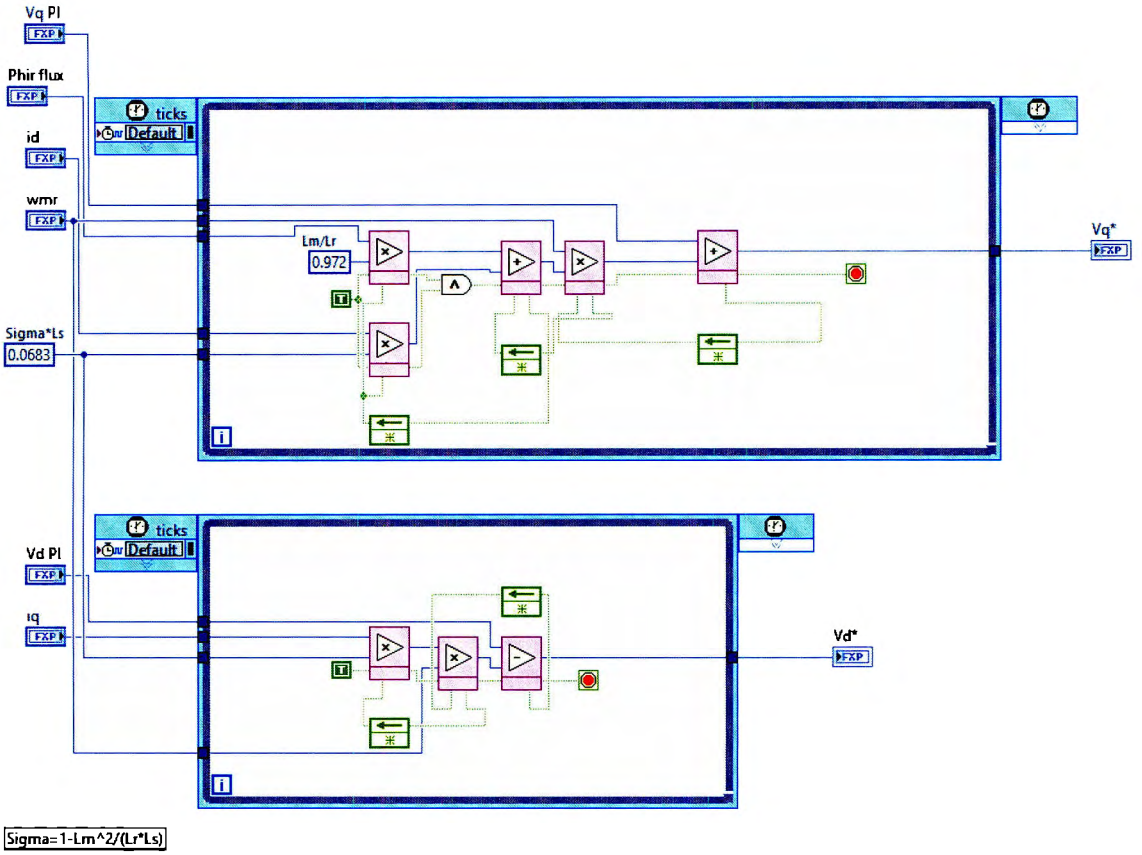

Figure 85.Decoupling voltage circuit, conventional vector control

An inverse Park's transformation is implemented to calculate the voltage components that are used for the SVPWM. The following figure shows the "Alpha Betha" block.

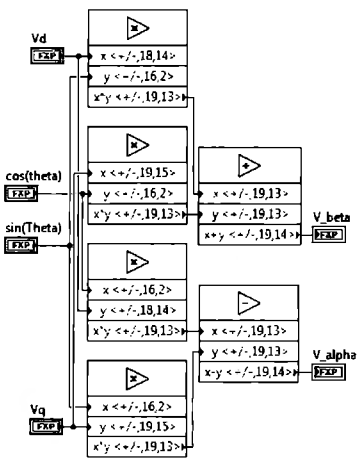

Figure 86.Voltage components calculation for SVPWM, conventional vector control

The final step of the main calculation stage is the time vector calculation that is used for the space vector PWM. The final stage takes those times in order to send the PWM signals for each motor phase.

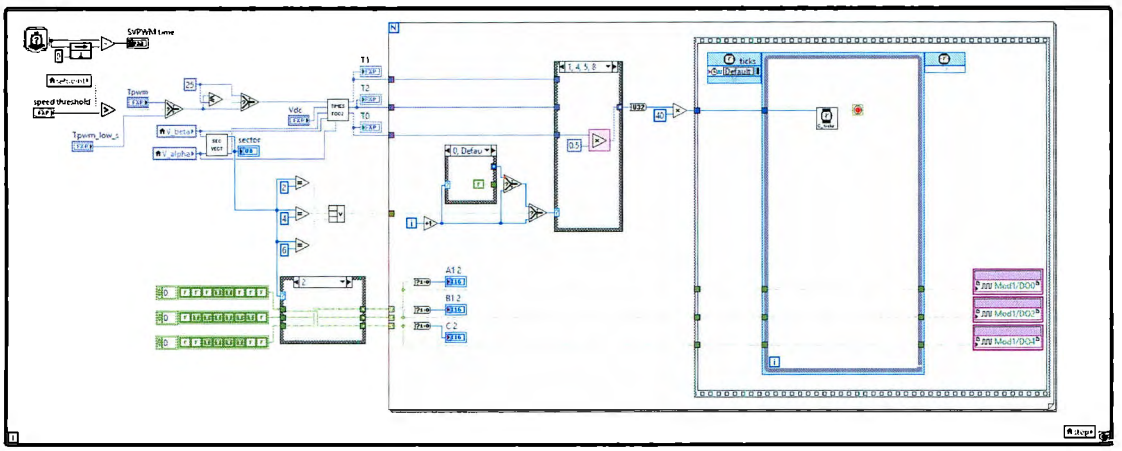

Figure 87. PWM signal generation

The PWM signals are generated for each phase in order to generate the three currents signals that fed the induction motor at the desired frequency in order to reach the desired motor speed commanded. These three parts conform the complete vector control that was explained in chapter 2 and the SVPWM that was presented in the same chapter.

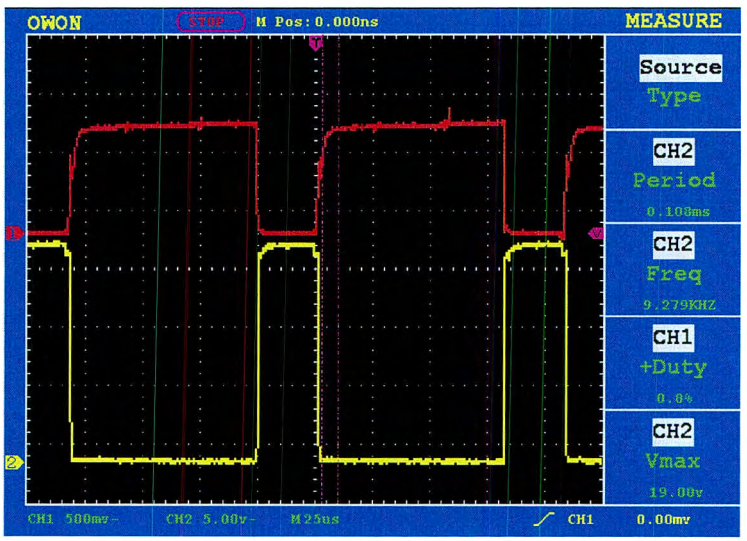

Figure 88. SVPWM pulses for one inverter leg

The switching period defined for the SVPWM is 10kHz, the pulses generated for one phase are presented in the Figure 88.

4.1.2 Intelligent Vector Control Program

The proposed vector controller used the same platform, but with the changes on the speed and voltages components (in direct and quadrature coordinates) sub-controllers. As it was mentioned in chapter 3 the PI controllers are replaced by fuzzy Mamdani type controllers and the speed controller uses the sliding mode technique.

The sliding mode controller implements the theory that was explained in chapter 3, the Figure 89 depicts the block diagram of the program in the NI FPGA.

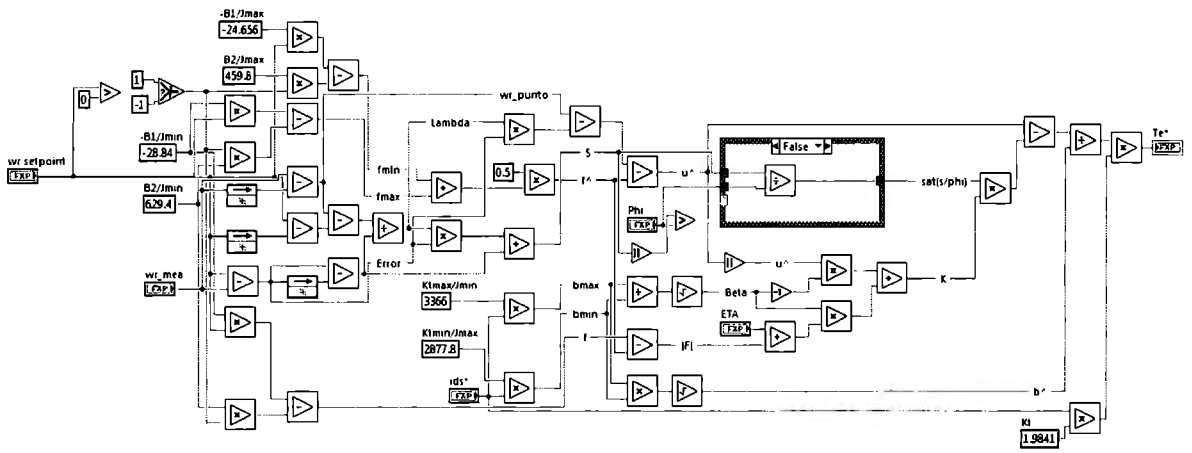

Figure 89. SMC controller in the NI FPGA

The calculation procedure was presented in chapter 3 and it is possible to note that the SMC technique is implemented with an extended mathematical calculation in order to achieve the desired control/motor performance.

One challenging part is related to the implementation of fuzzy controllers in fixed point variable, since normally several arrays are used in order to transfer crisp, membership and outputs values. The general block diagram for fuzzification and defuzzification is depicted in the Figure 90.

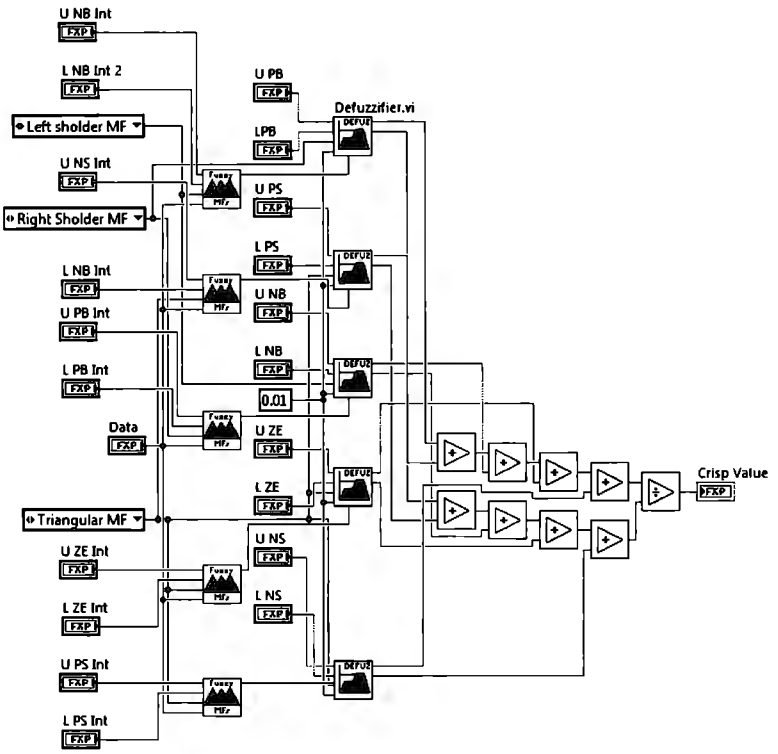

Figure 90. Fuzzification and defuzzification

Five triangle functions are used for the error and error derivative as inputs for the fuzzy PI controller. For the fuzzification process is implemented the following equation (the membership grades are obtained)

$$\mu^A(x,a,b,c) = max\left\{min\left[\frac{x-a}{b-a} \quad , \quad \frac{c-x}{c-b}\right], 0\right\} \quad (4.14)$$

Where x is the crisp input, a, b and c represent the triangle membership function points. Moreover, the defuzzification part is evaluated based on the equation

$$Z = \frac{\sum_{k=1}^{n} z_k \, \mu_{(z_k)}}{\sum_{k=1}^{n} \mu_{(z_k)}} \quad (4.15)$$

Where Z represents the crisp output of the fuzzy Mamdani type controller. This final part is presented in the following figure.

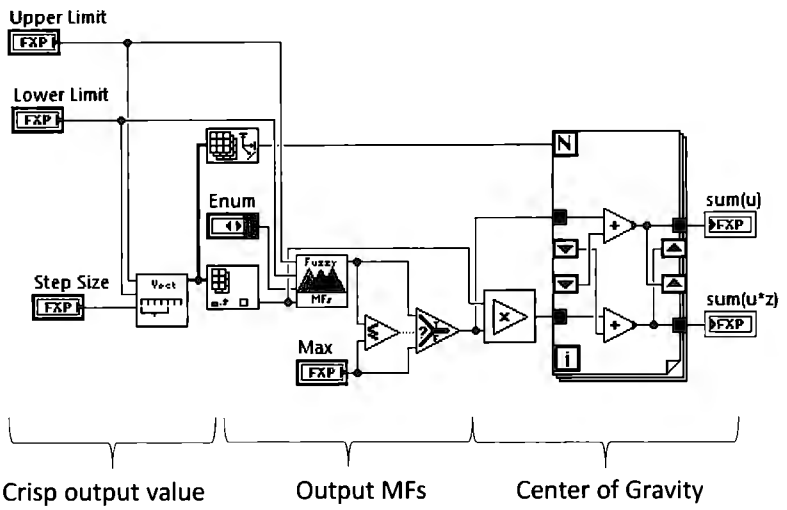

Figure 91. Defuzzification block diagram

The set of rules for the fuzzy logic controller are presented in Table 5.

Table 5. Fuzzy logic controller rules

$e\backslash\dot{e}$	Negative	Zero	Small_positive	Medium_positive	Big_positive
Negative	BN	BP	SP	SP	PB
Zero	BN	Zero	SN	SP	SP
Small_positive	BN	SN	SP	SP	SP
Medium_positive	BN	SN	SP	MP	BN
Big_positive	BN	SP	SP	SP	BP

The current controllers are configured with 25 rules and the inputs are error and error derivative with 5 memebership triangular functions (labels in Table 5). The Output has 5 membership triangular functions (Big_negative, Small Negative, Zero, Small Positive and Big Positive).

The SMC is used to control speed and the Fuzzy controllers are implemented to control *Id* and *Iq*. In the following section is explained how experiment is configured and the co-simulation results with the intelligent vector control.

4.2 Experimental and Co-Simulation Results

The program code for experimental and co-simulation tests were explained in detail for conventional vector control and intelligent vector control. In the following subsections will be explained the hardware used for both tests.

4.2.1 Hardware Layout

The inverter used to develop the experimental control test is a DC-AC converter with MOSFET transistors which helps to generate the sinusoidal signals to drive the electric motor. The main characteristics of the inverter implemented are:

- Voltage supply 250 Vdc
- Current supported 25 A
- Minimum dead time between pulses is 900ns
- Transistors: MOSFET
- Circuit inverter protection of 10A

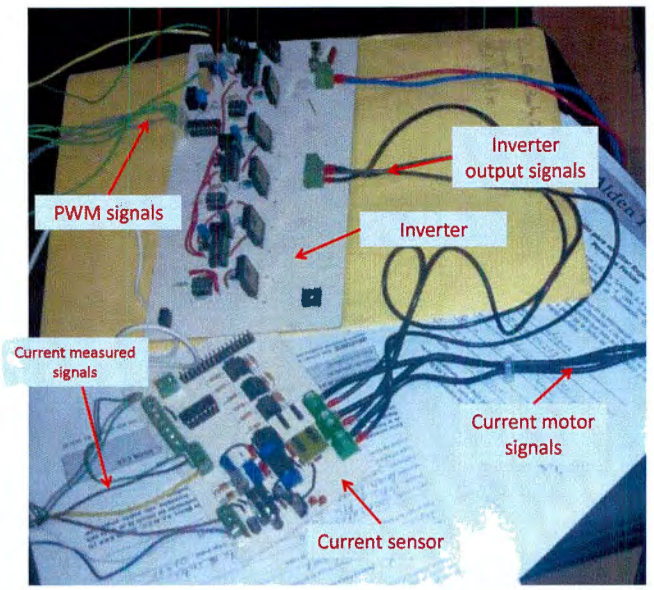

Figure 92. Inverter-current sensor layout

The layout depicted above represents the connections among the inverter and current sensor units. Also, it is possible to notice the inputs from the control unit labeled as PWM signals, these are generated from the Compact RIO 9612 hardware. The current sensor circuit is composed by hall sensors, which measured the current in two phases (i.e. It is assumed a balance system and therefore the three stator currents addition is equal to zero).

For the correct motor control is necessary to have the proper signal conditioning, which is possible by means of a first order analog filter after motor currents measurement. A simple RC circuit is implement to achieve the proper signal filtering with a cut frequency of 35Hz. The following figures show two examples at 1657 RPM with and without filtering.

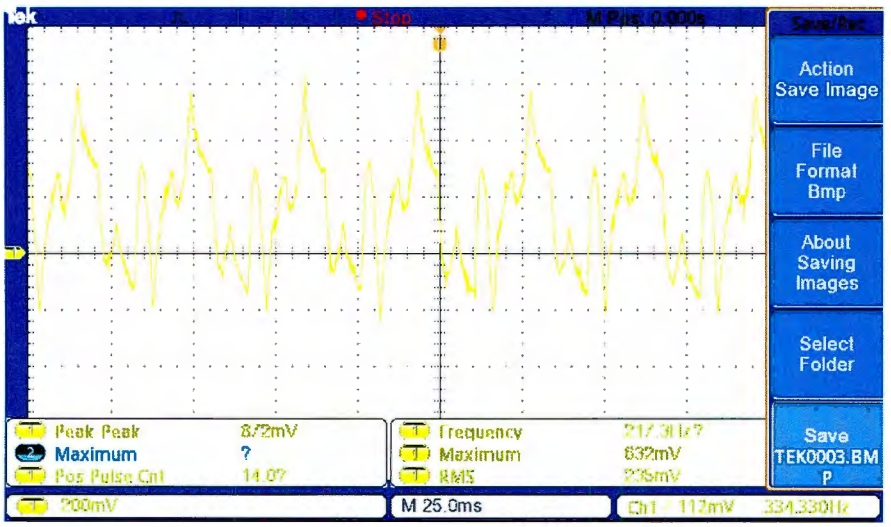

Figure 93. Current signal without filtering at 505 RPM

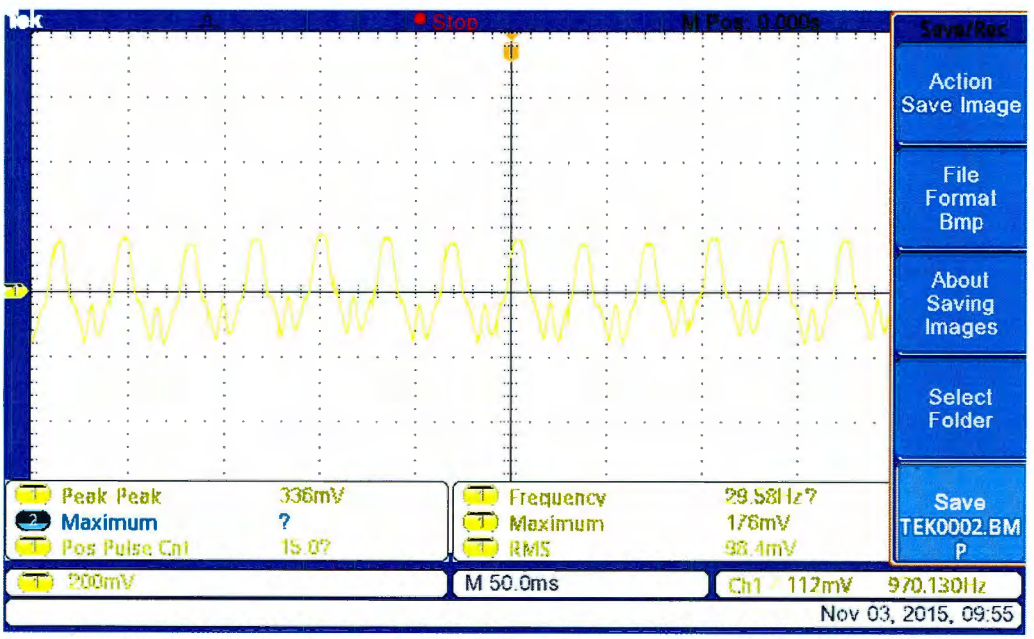

Figure 94. Current signal without filtering at 1657 RPM

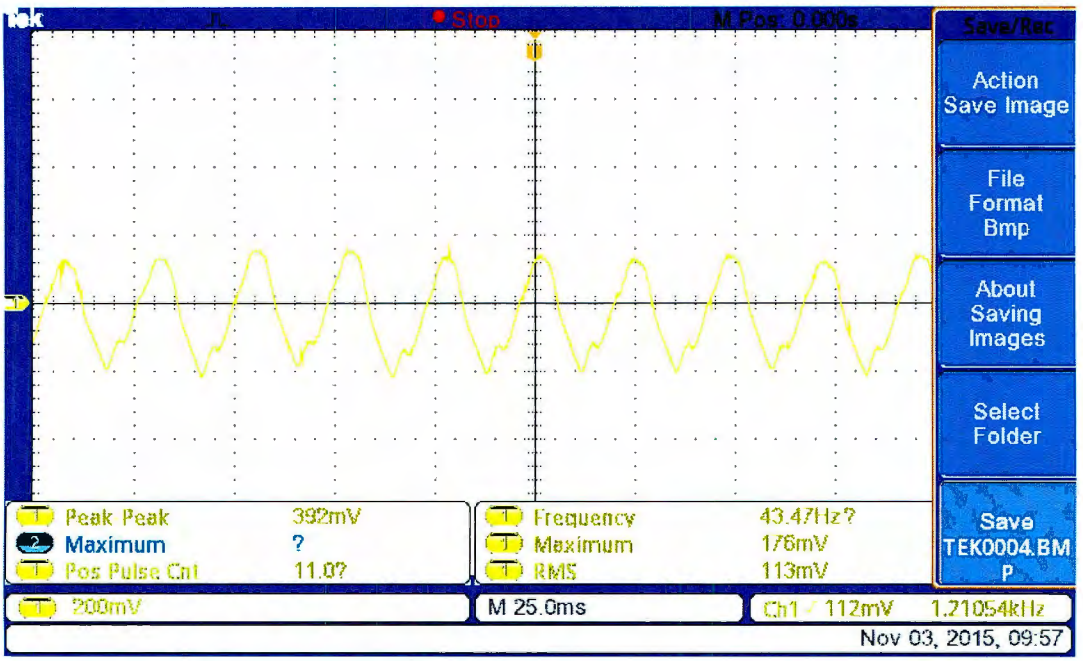

Figure 95. Current signal with filtering at 1657 RPM

The FPGA connections with sensors are inverter is depicted in Figure 96a. Figure 96b represents the connections depicted in Figure 96 a.

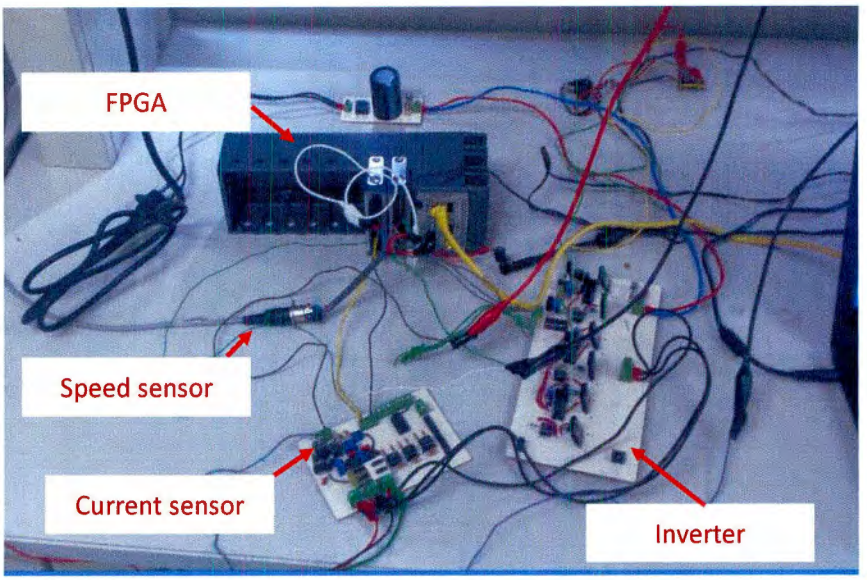

a)

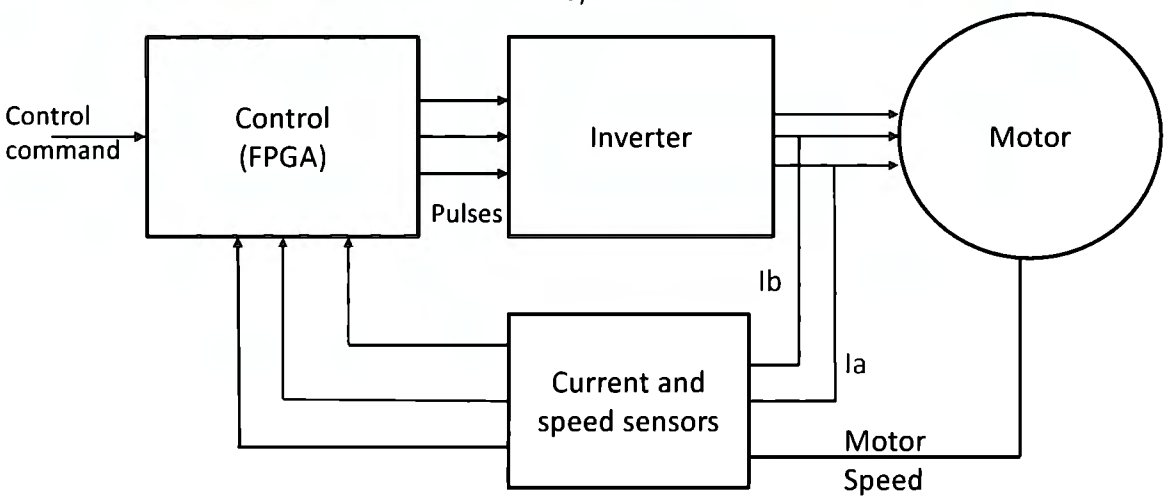

b)

Figure 96. a)FPGA with sensor and inverter connection b)Motor/control schematic

Now with the complete hardware set to perform the validation, it is presented in the following section the control experimentation.

4.2.2 Experimental Results

The vector control theory and design were explained in previous sections, now experimental results are presented for this controller. Tests were performed with setpoint variations similarly as was presented in chapter 3, the results are presented in the following figures.

The parameters of the motor are

- P= 2 (Number of poles)
- Rs= 16.19 ohms (Stator resistance)

- Rr= 21.34 ohms (Rotor resistance)
- Lm= 1.3704 (Magnetizing impedance [H])
- Lls= 0.04994 (Stator side leakage impedance [H])
- Llr= 0.04994 (Rotor side leakage impedance [Ohms])
- J= 0.000589448 (Rotor inertia)
- Power= 370W

The first sets of tests that will be with no load applied and for a low speed range conditions, from 100 to 900 rpm.

- 100 RPM

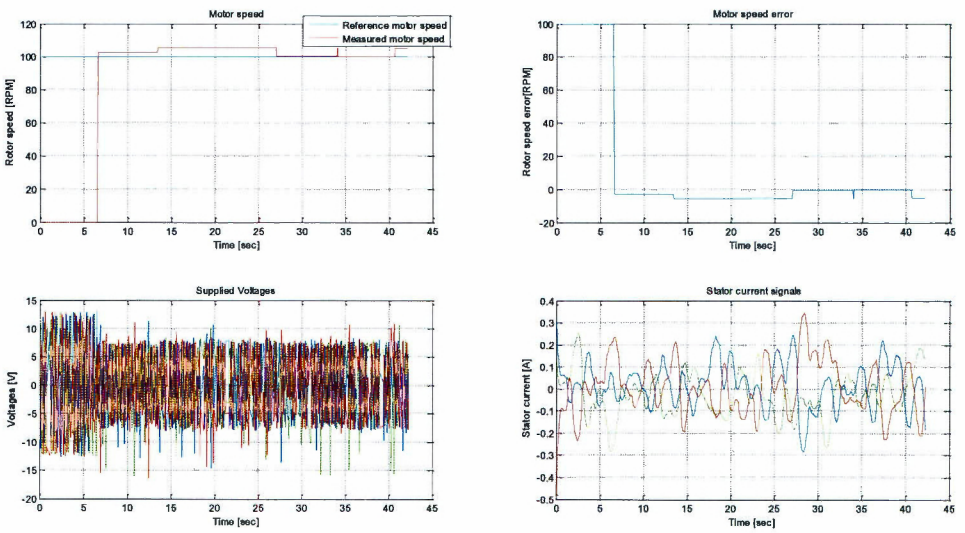

Figure 97. Low speed 100 RPM, without load

The MSE in steady state is 34.1672 RPM for a setpoint of 100 RPM

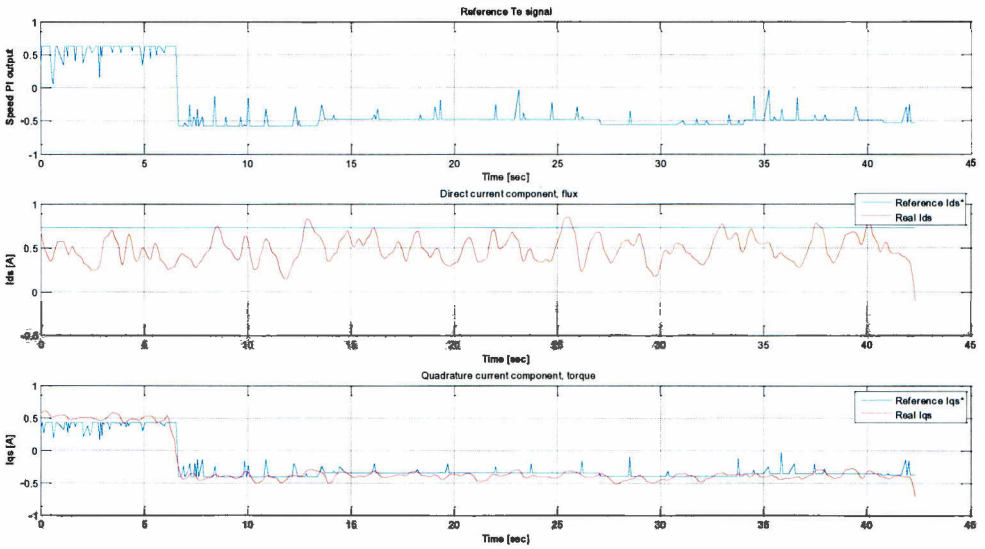

Figure 98. Speed PI output and curreent components Iq, Id. 100 RPM

➢ 200 RPM

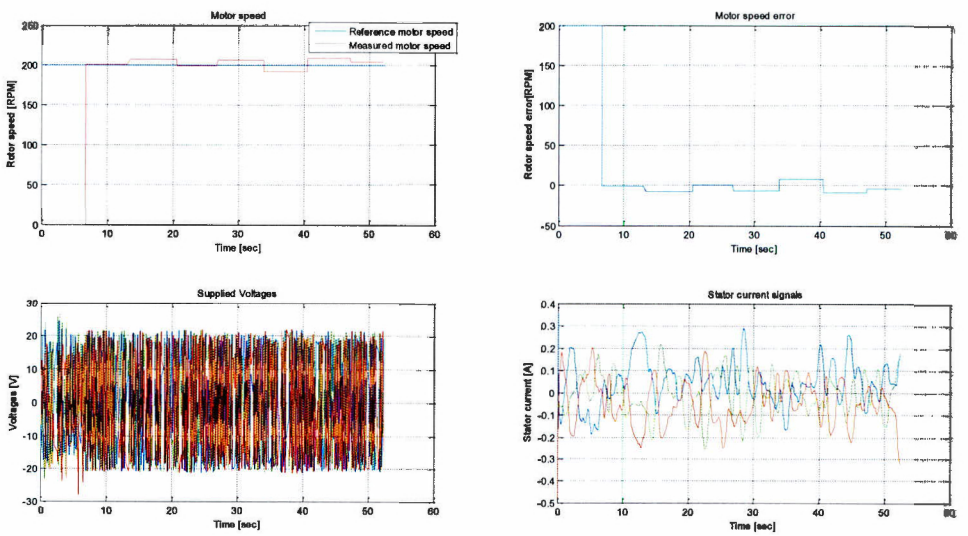

Figure 99. Low speed 200 RPM, without load

The MSE in steady state is 34.2013 RPM for a setpoint of 200 RPM.

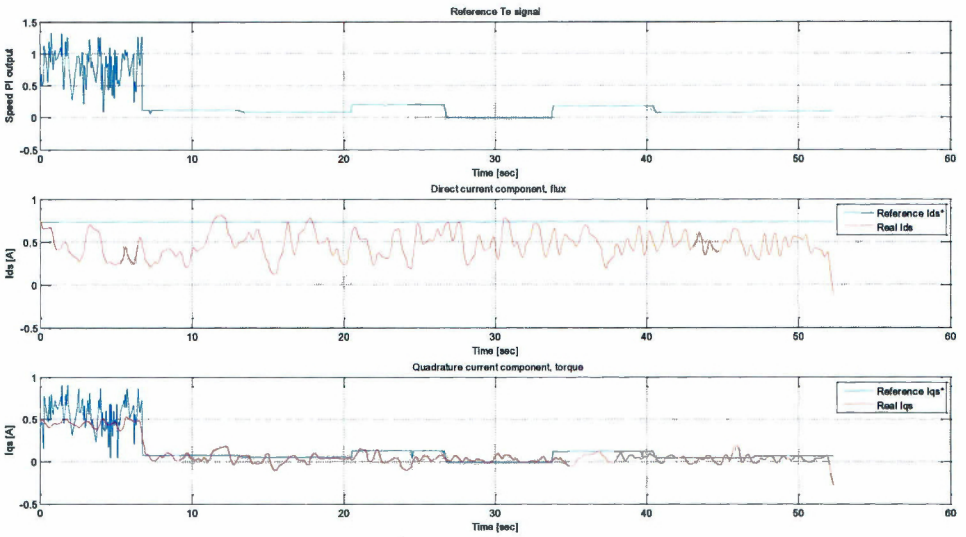

Figure 100. Speed PI output and curreent components Iq, Id. 200 RPM

➢ 300 RPM

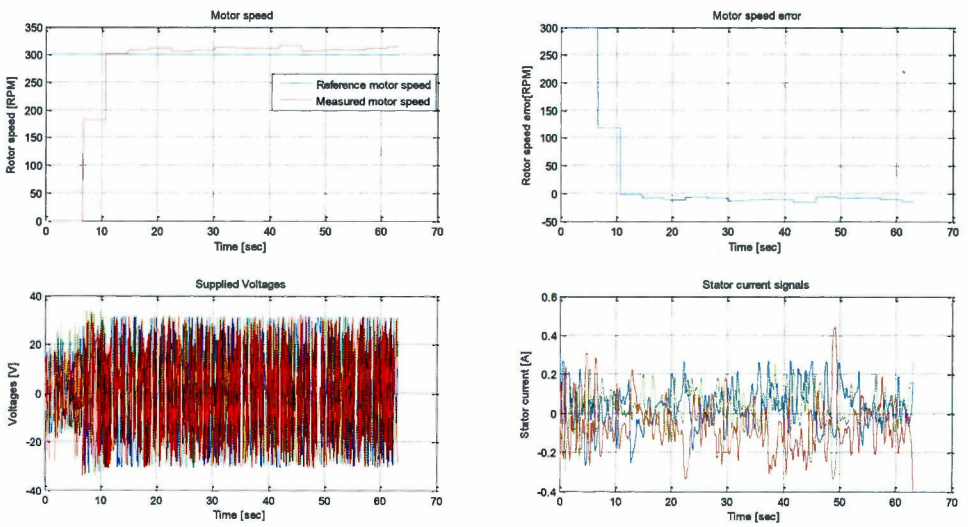

Figure 101. Low speed 300 RPM, without load

MSE in steady state is 20.9048 RPM

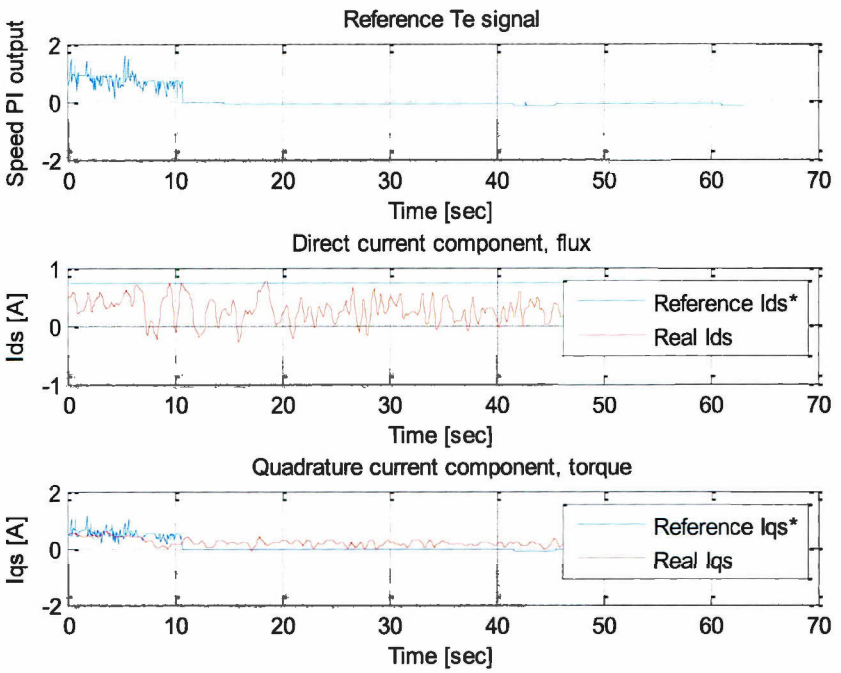

Figure 102. Speed PI output and curreent components Iq, Id. 300 RPM

➢ 400 RPM

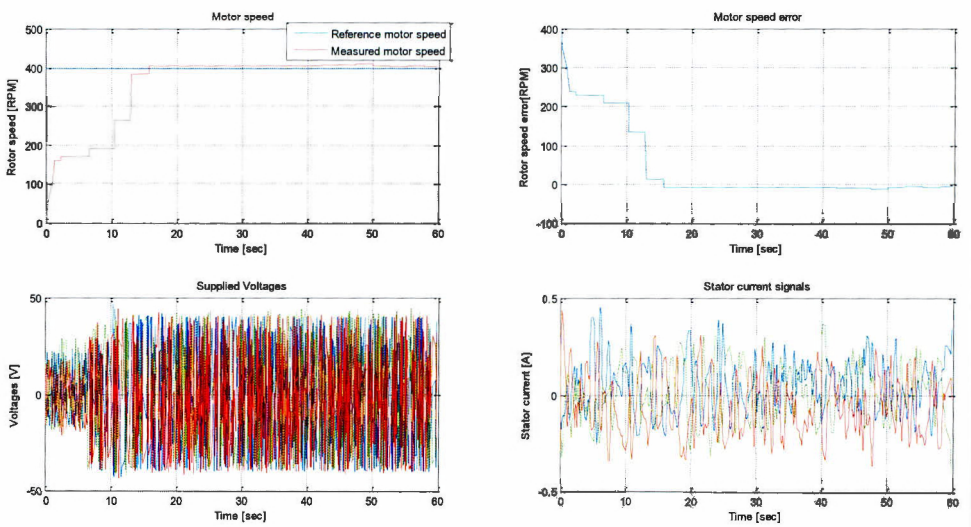

Figure 103. Low speed 400 RPM, without load

MSE in steady state is 7.55 RPM

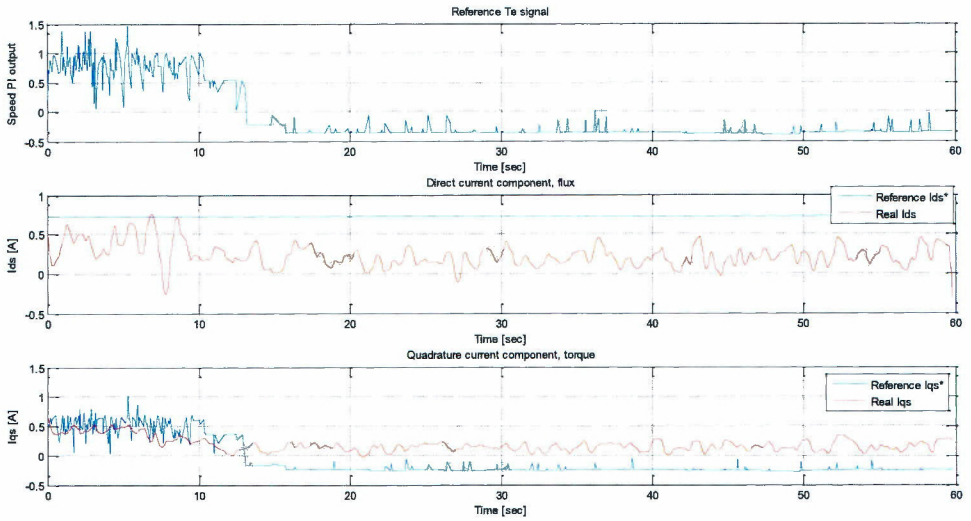

Figure 104. Speed PI output and curreent components Iq, Id. 400 RPM

- 500 RPM

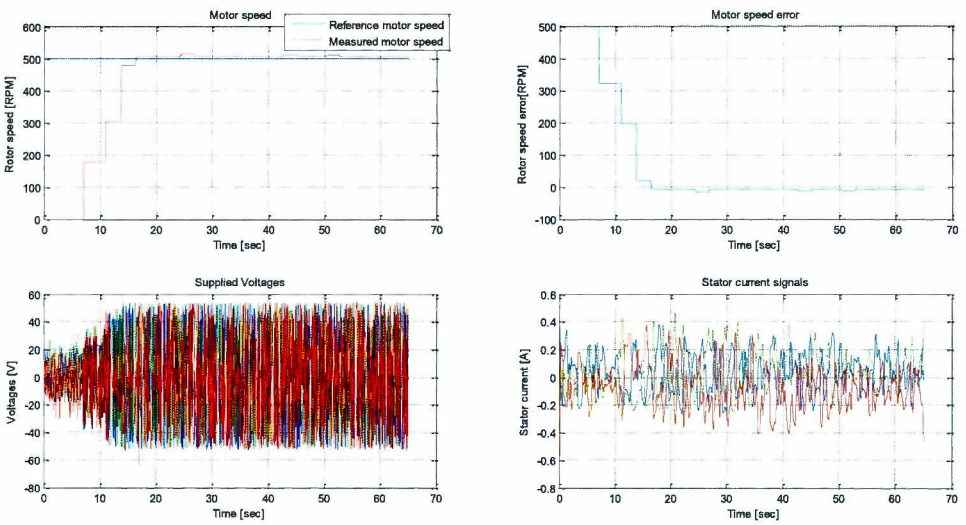

Figure 105. Low speed 500 RPM, without load

MSE in steady state is 8.0905 RPM

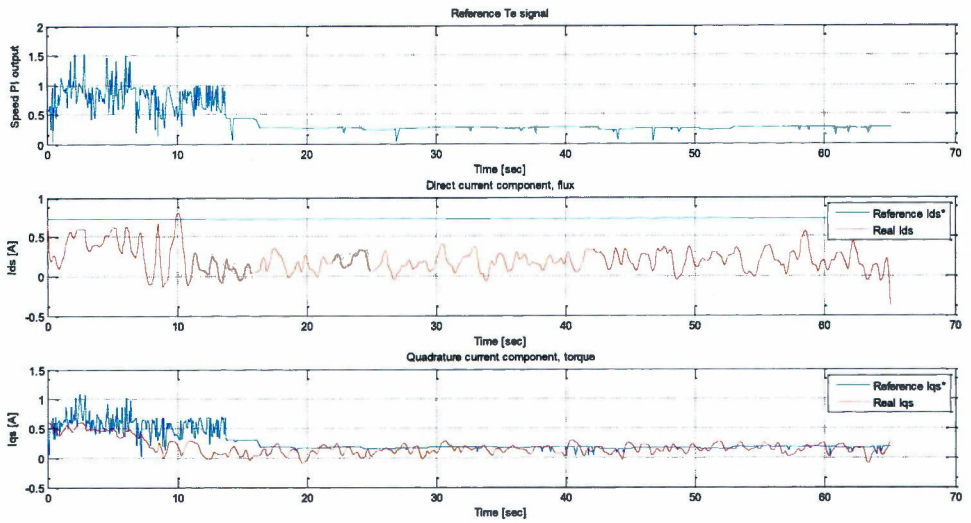

Figure 106. Speed PI output and curreent components Iq, Id. 500 RPM

➢ 600 RPM

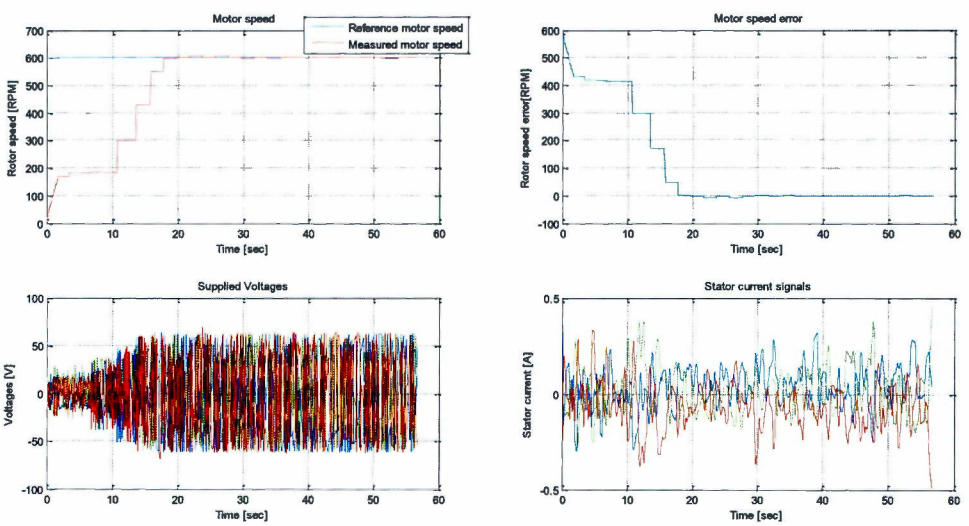

Figure 107. Low speed 600 RPM, without load

MSE in steady state is 9.5382 RPM

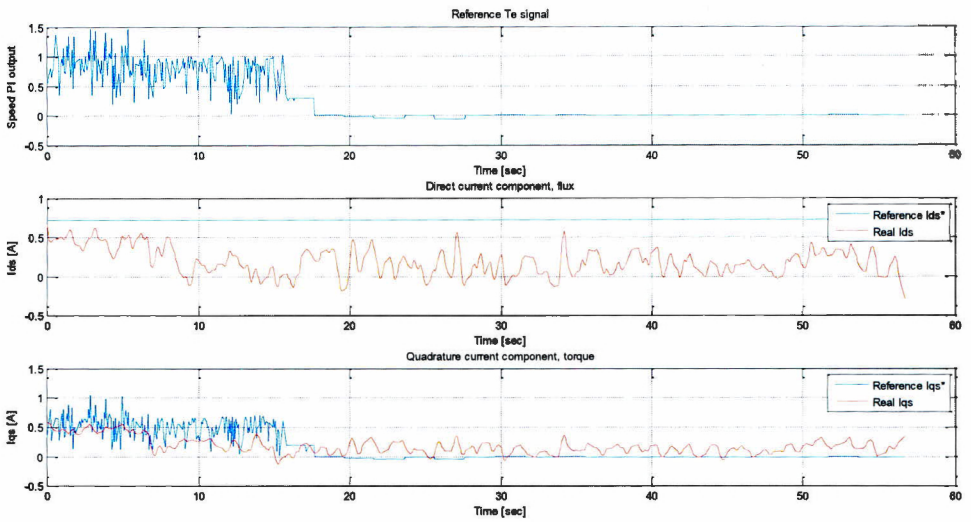

Figure 108. Speed PI output and curreent components Iq, Id. 600 RPM

➢ 700 RPM

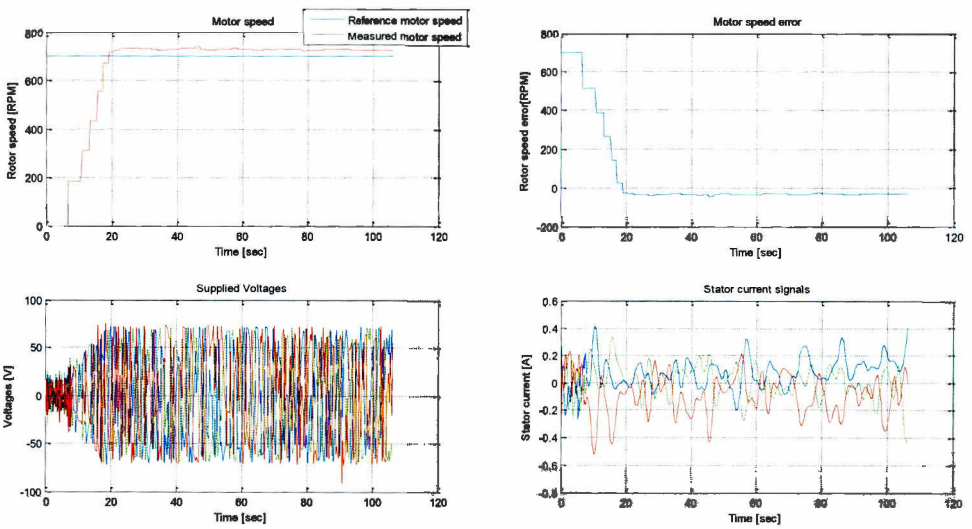

Figure 109. Low speed 700 RPM, without load

MSE in steady state is 20.1764 RPM

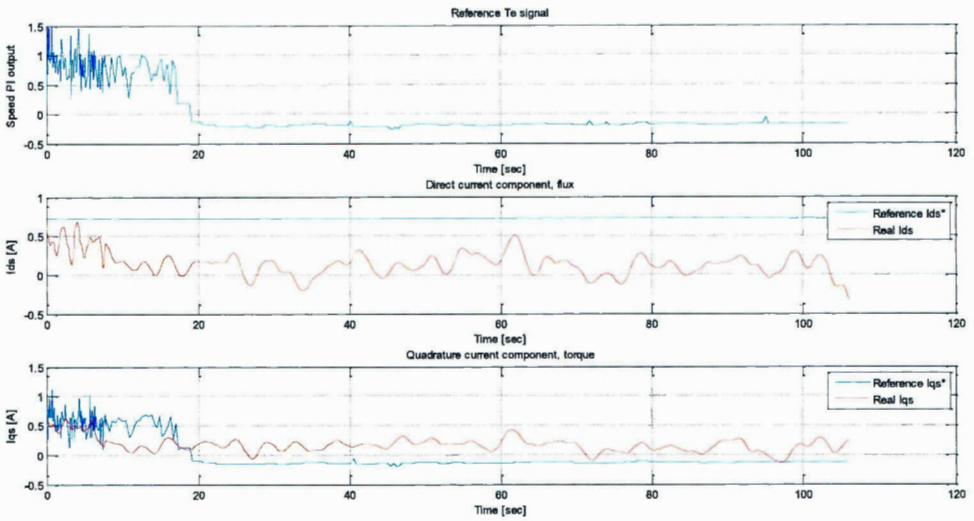

Figure 110. Speed PI output and curreent components Iq, Id. 700 RPM

➢ 800 RPM

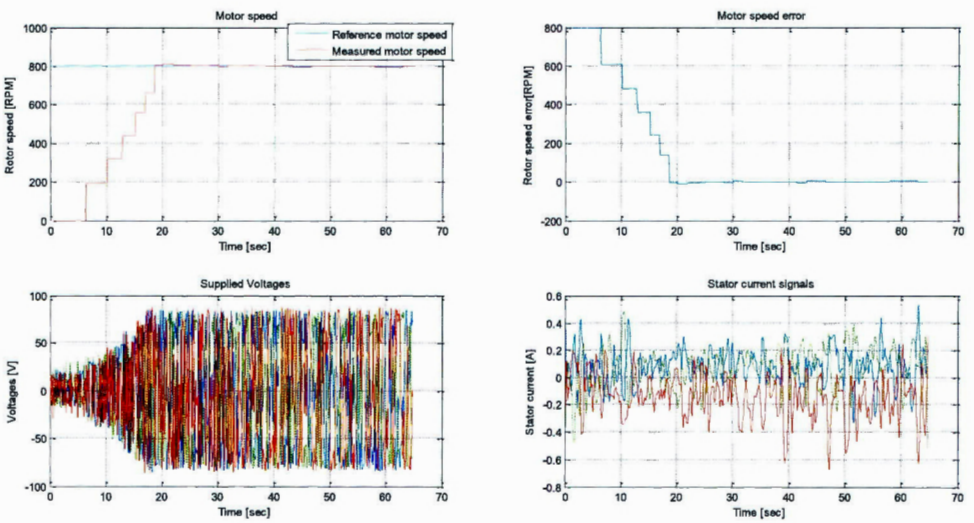

Figure 111. Low speed 800 RPM, without load

MSE in steady state is 2.6825 RPM

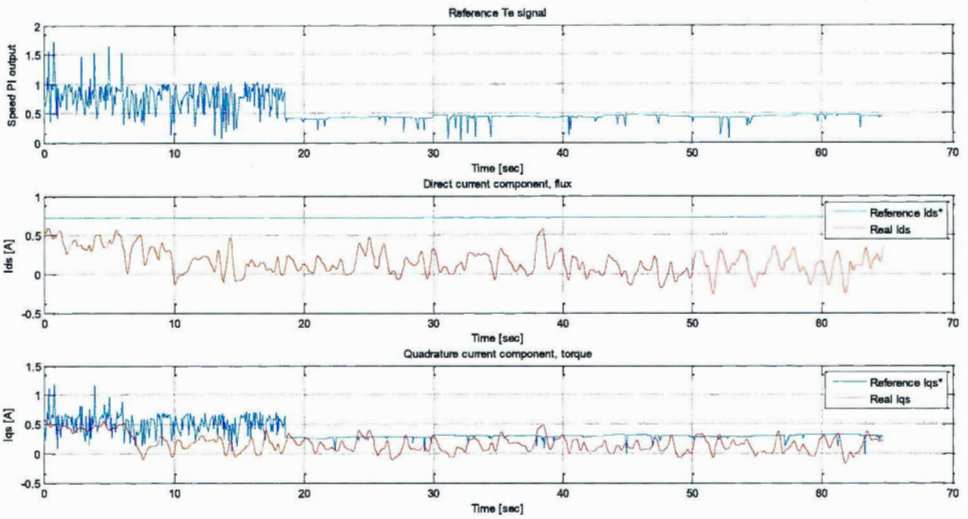

Figure 112. Speed PI output and curreent components Iq, Id. 800 RPM

➢ 900 RPM

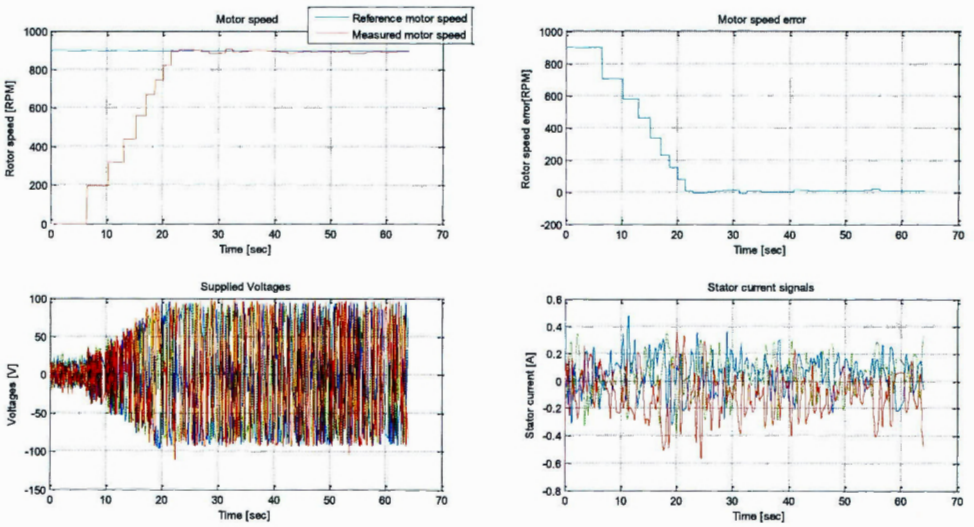

Figure 113. Low speed 900 RPM, without load

MSE in steady state is 13.7637RPM

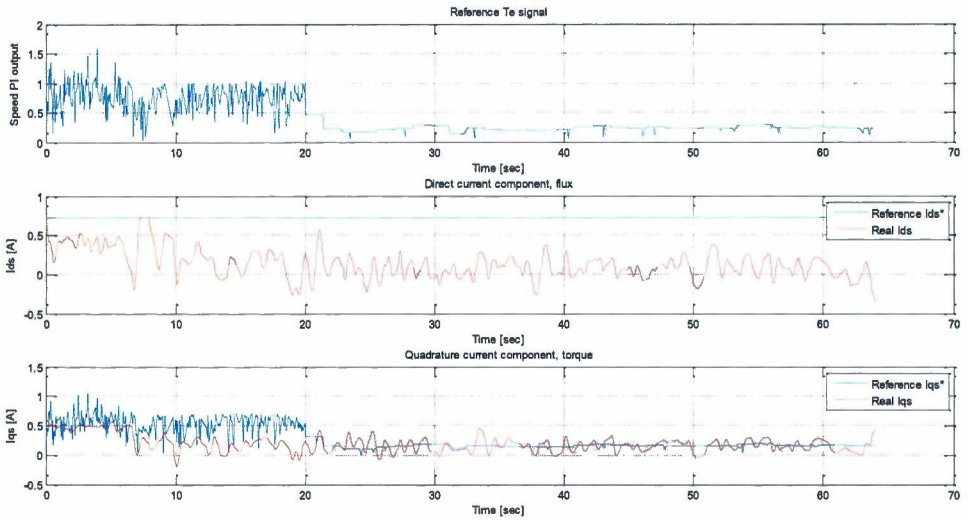

Figure 114. Speed PI output and curreent components Iq, Id. 900 RPM

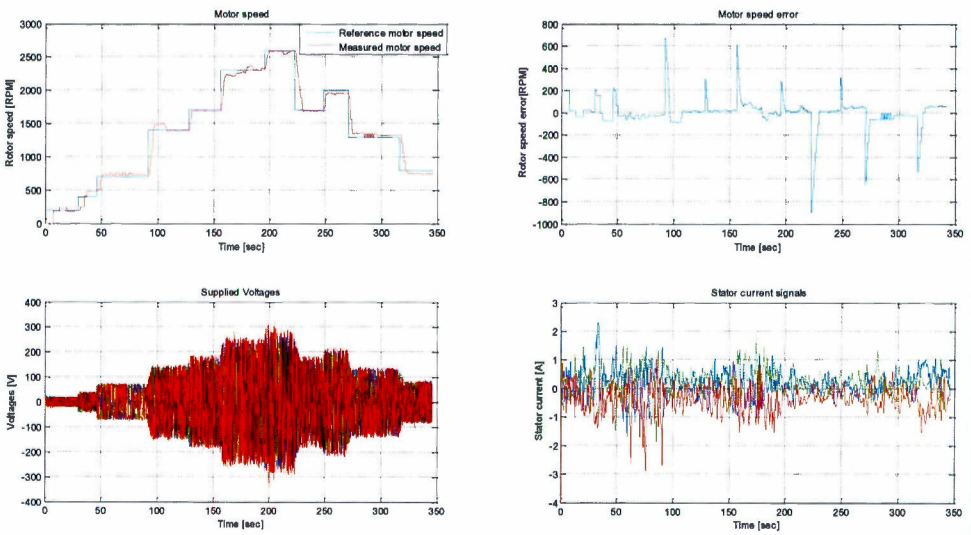

Figure 115. Speed reference variation, without load

MSE in steady state is 37.7991 RPM

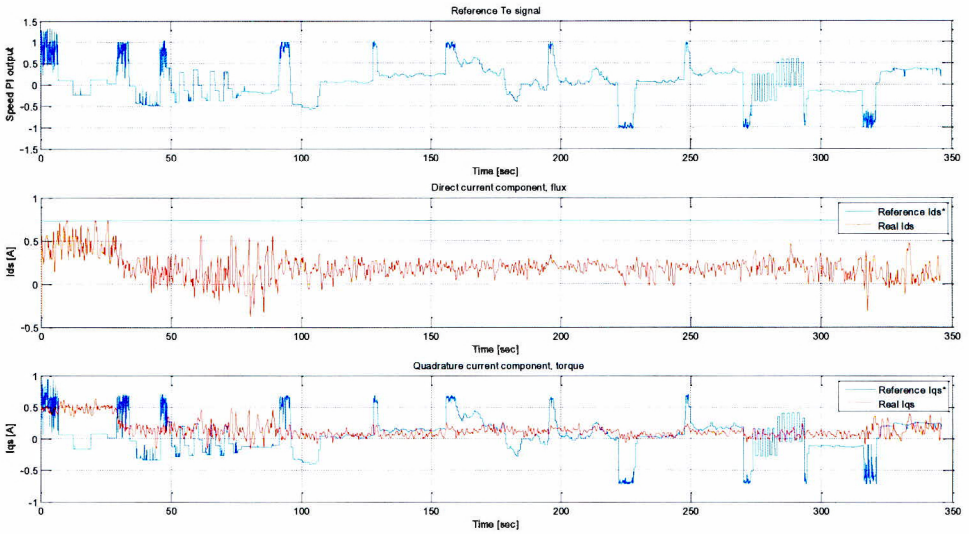

Figure 116. Speed PI output and curreent components Iq, Id.

Load applied during motor operation 1 Nm (100% of the nominal load).

- 100 RPM

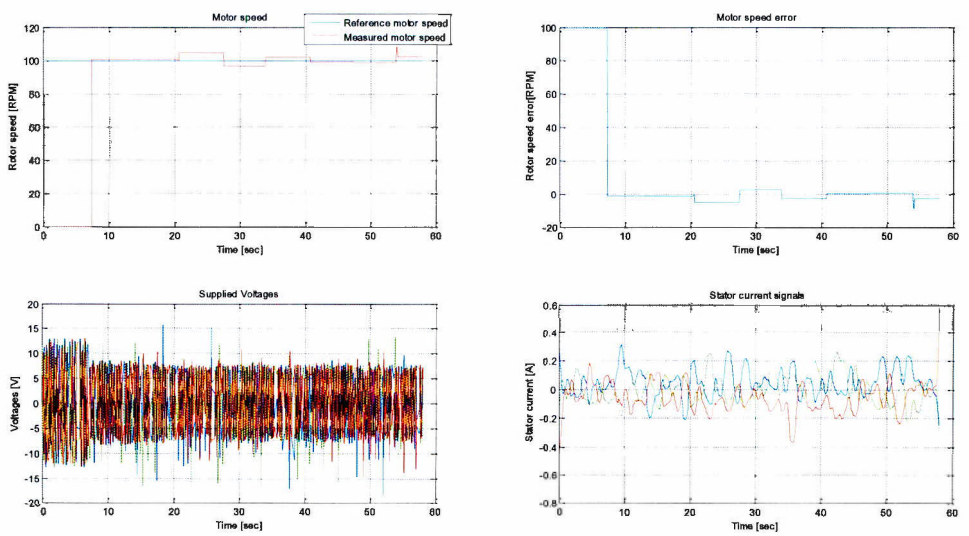

Figure 117. Low speed 100 RPM, with load

MSE in steady state is 34.0875 RPM

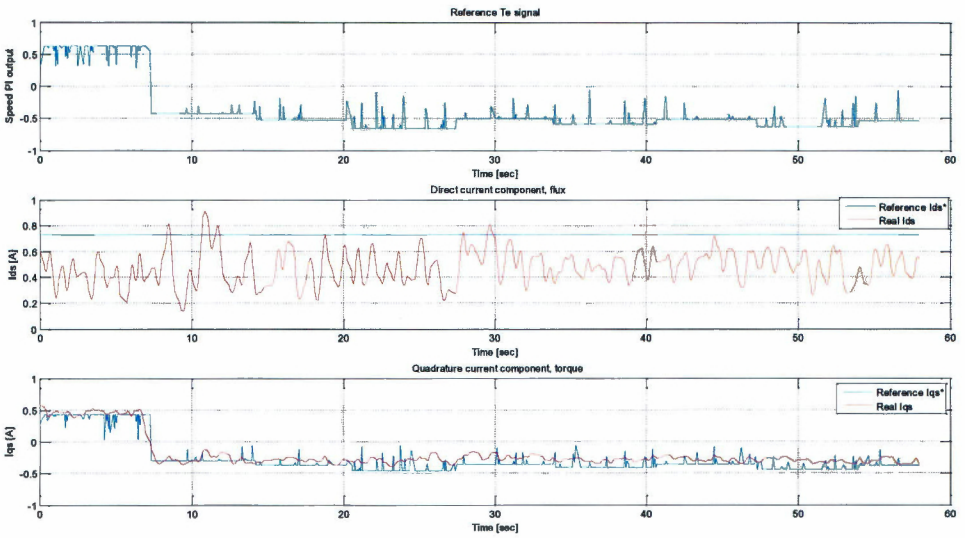

Figure 118. Speed PI output and curreent components Iq, Id. 100 RPM

➢ 200 RPM

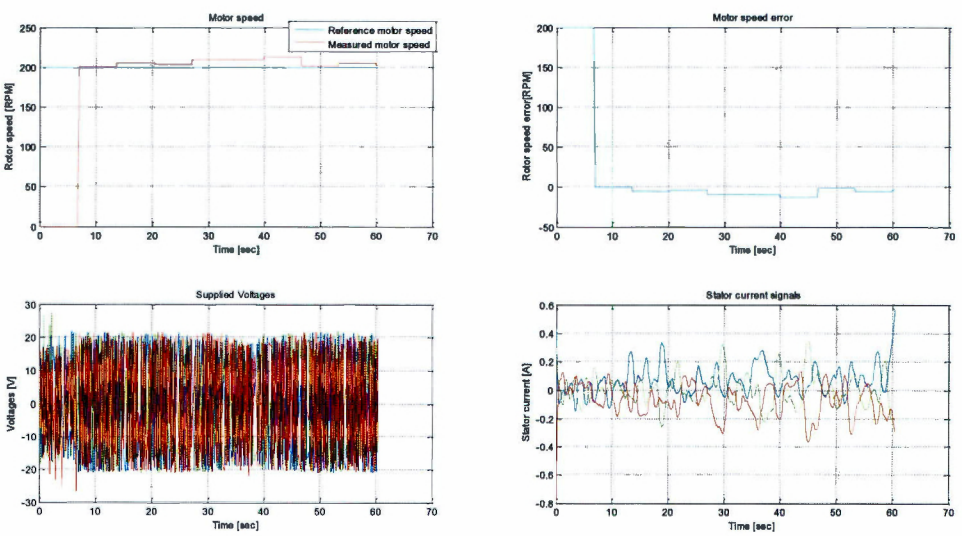

Figure 119. Low speed 200 RPM, with load

MSE in steady state is 34.1862 RPM

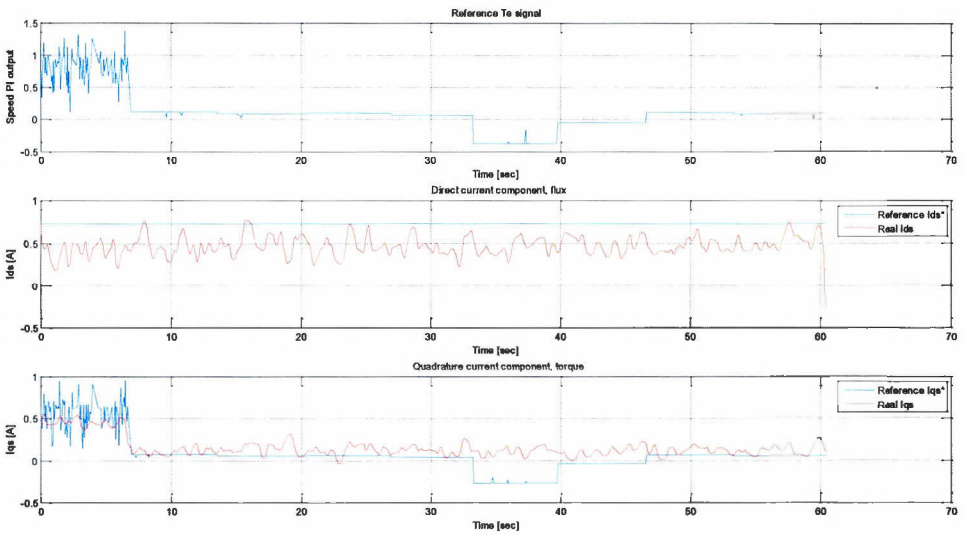

Figure 120. Speed PI output and curreent components Iq, Id. 200 RPM

➢ 300 RPM

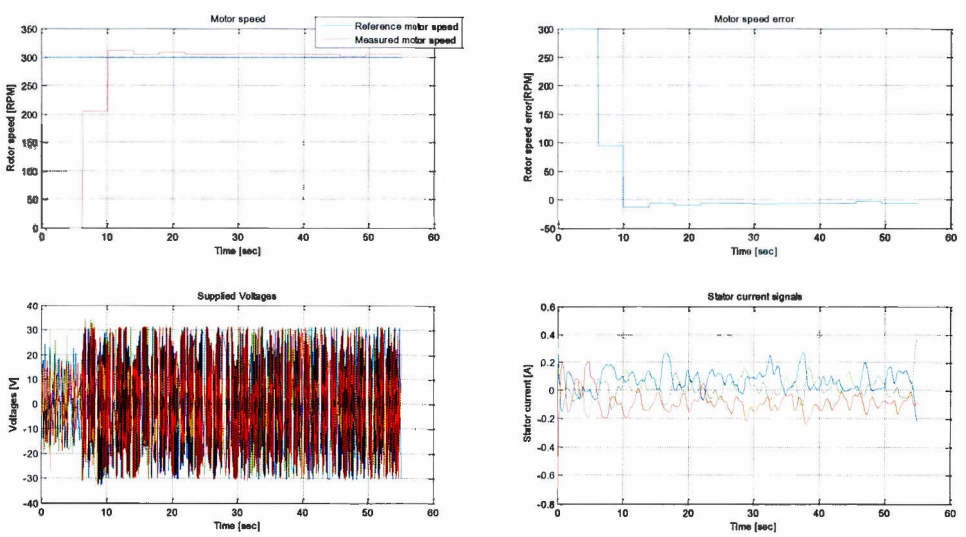

Figure 121. Low speed 300 RPM, with load

MSE in steady state is 14.4232 RPM

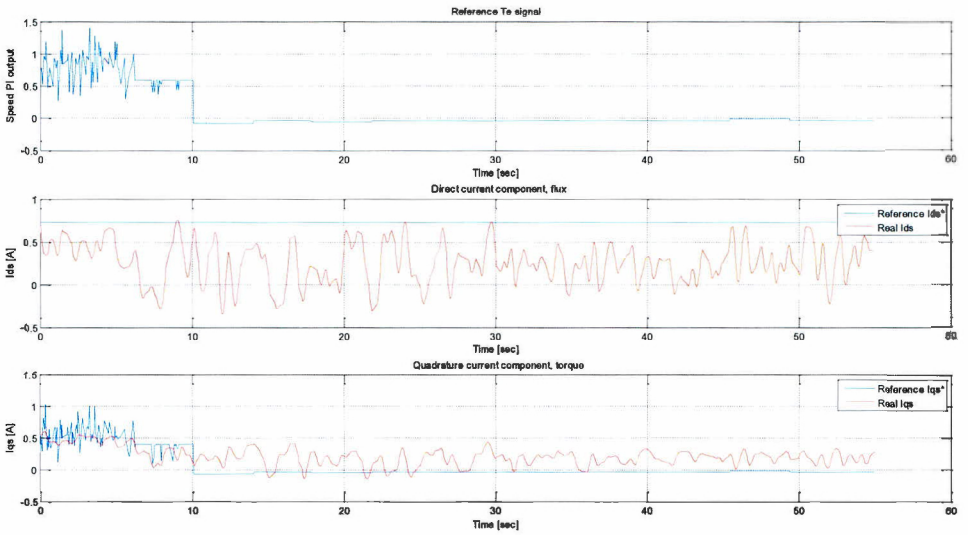

Figure 122. Speed PI output and curreent components Iq, Id. 300 RPM

- 400 RPM

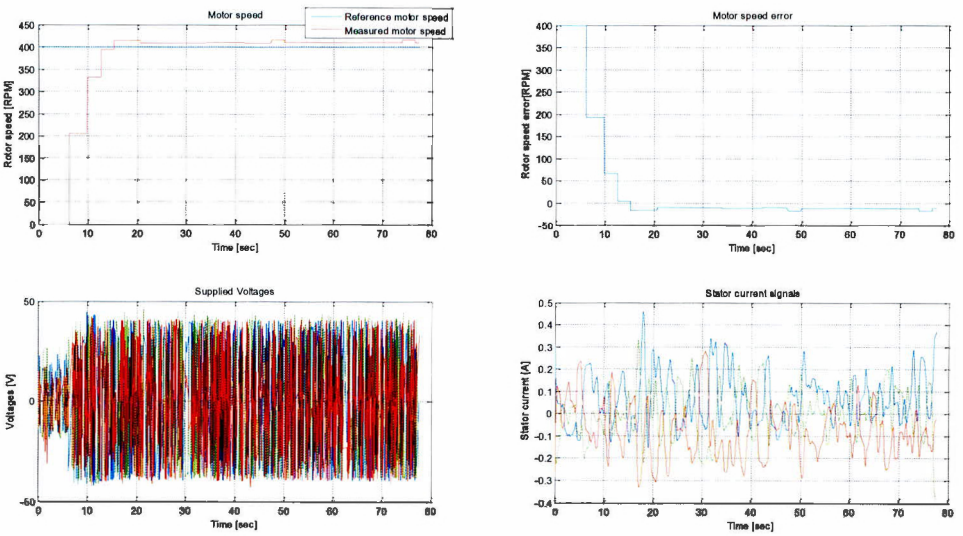

Figure 123. Low speed 400 RPM, with load

MSE in steady state is 33.9582 RPM

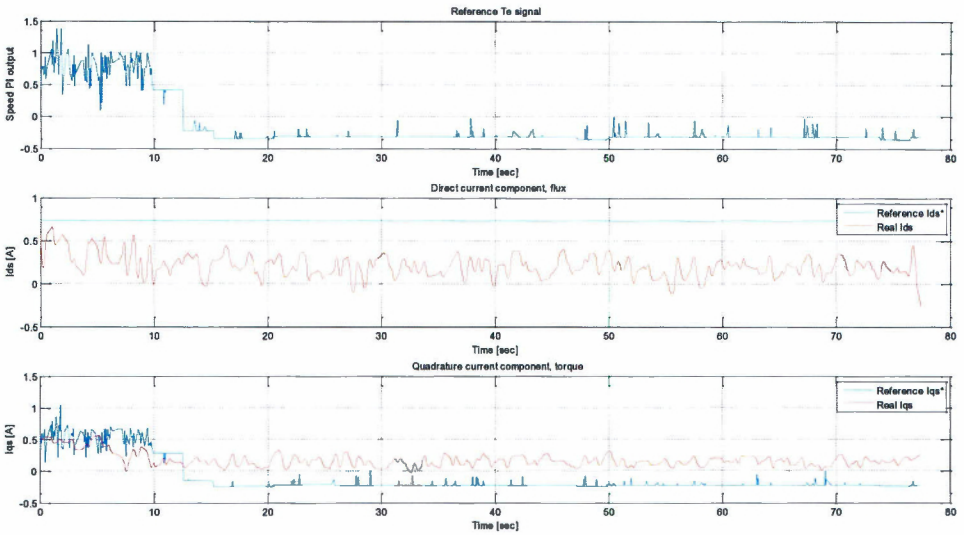

Figure 124. Speed PI output and curreent components Iq, Id. 400 RPM

➢ 500 RPM

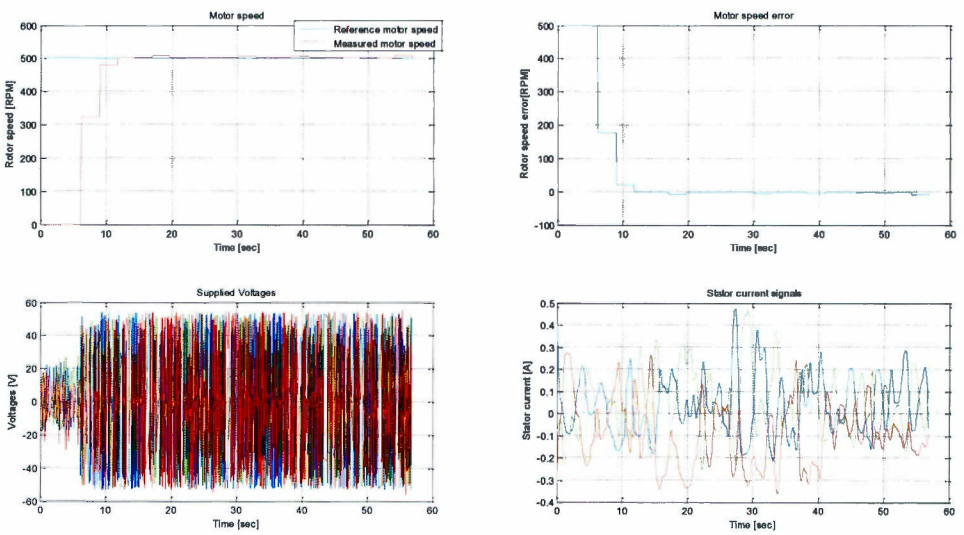

Figure 125. Low speed 500 RPM, with load

MSE in steady state is 33.1834 RPM

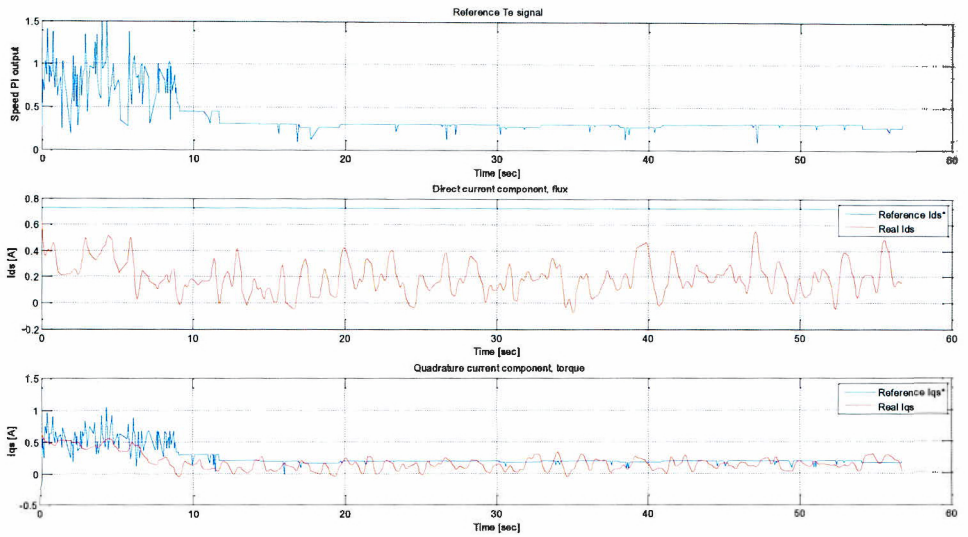

Figure 126. Speed PI output and curreent components Iq, Id. 500 RPM

➢ 600 RPM

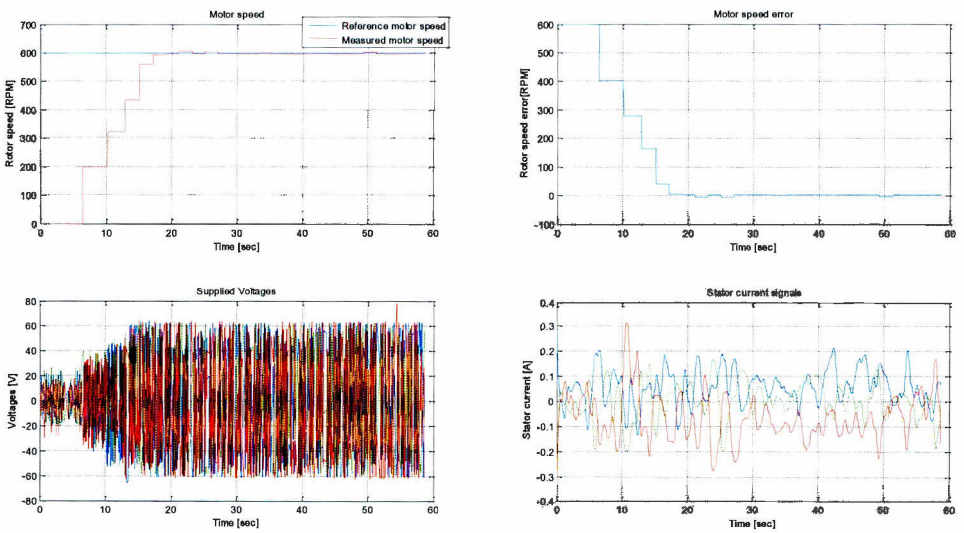

Figure 127. Low speed 600 RPM, with load

MSE in steady state is 33.3087 RPM

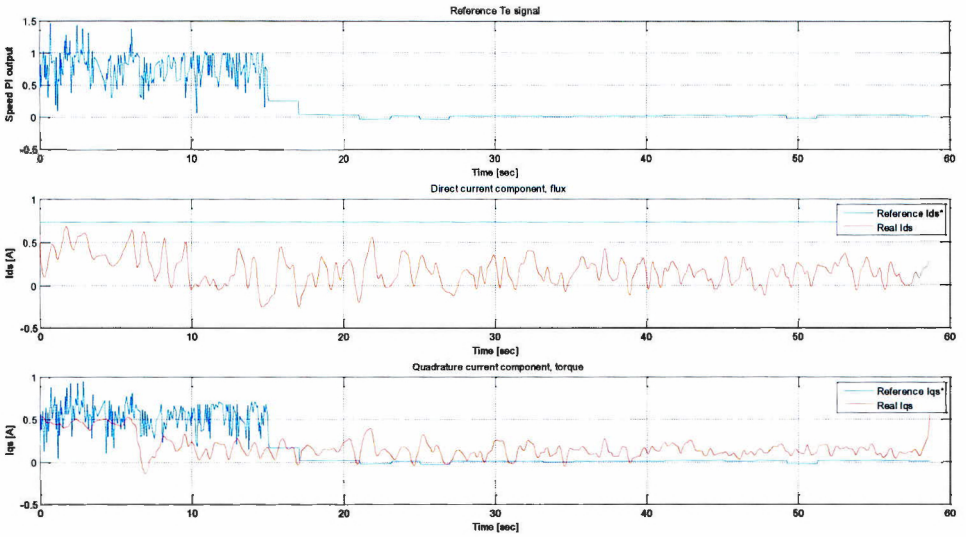

Figure 128. Speed PI output and current components Iq, Id. 600 RPM

➢ 700 RPM

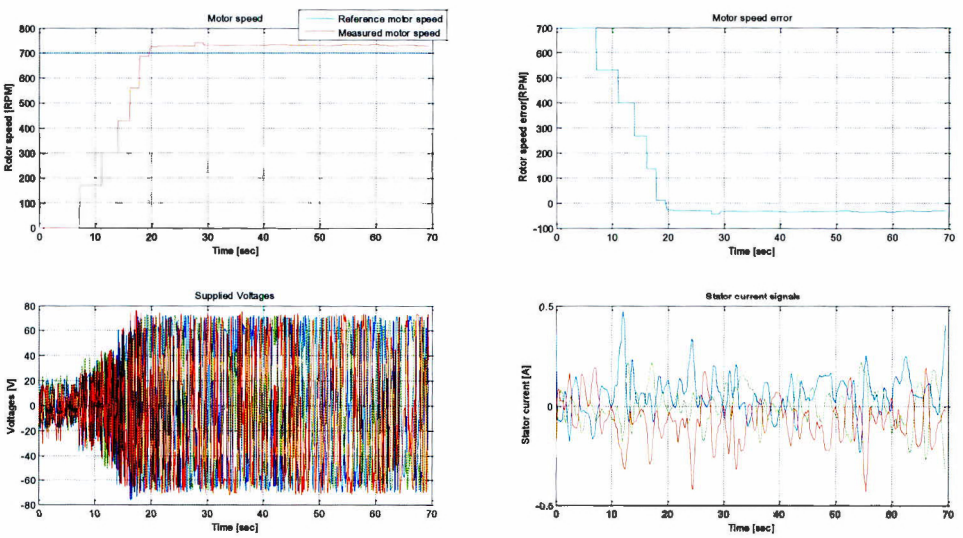

Figure 129. Low speed 700 RPM, with load

MSE in steady state is 35.3973 RPM

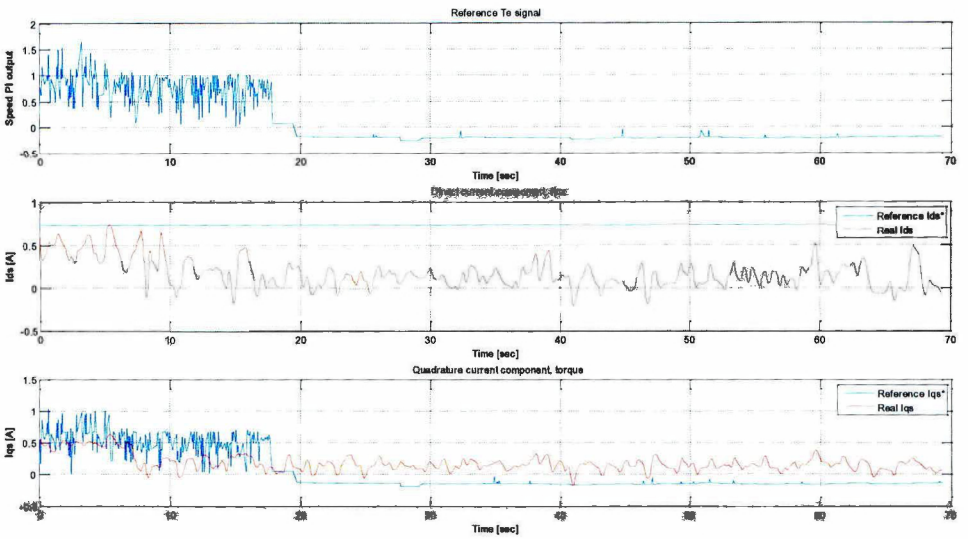

Figure 130. Speed PI output and curreent components Iq, Id. 700 RPM

➢ 800 RPM

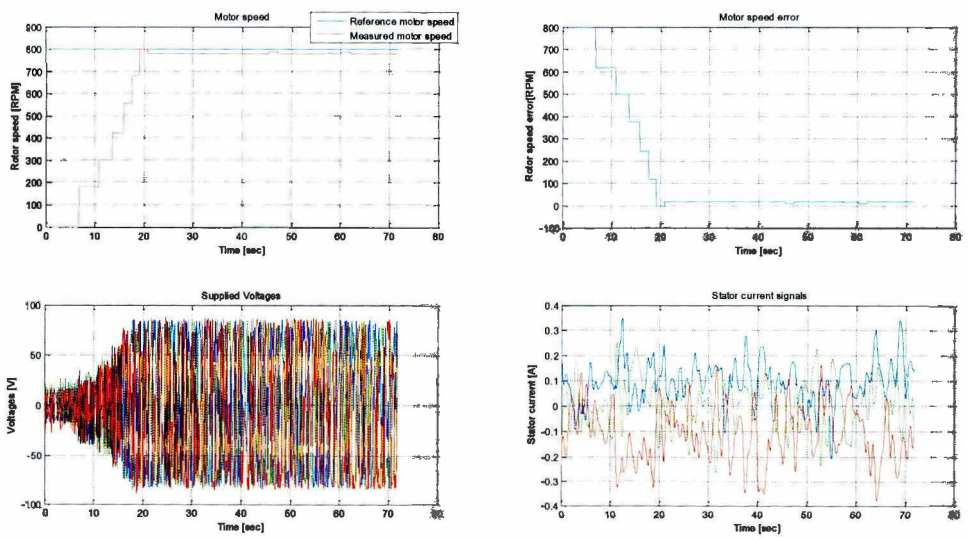

Figure 131. Low speed 800 RPM, with load

MSE in steady state is 33.9635 RPM

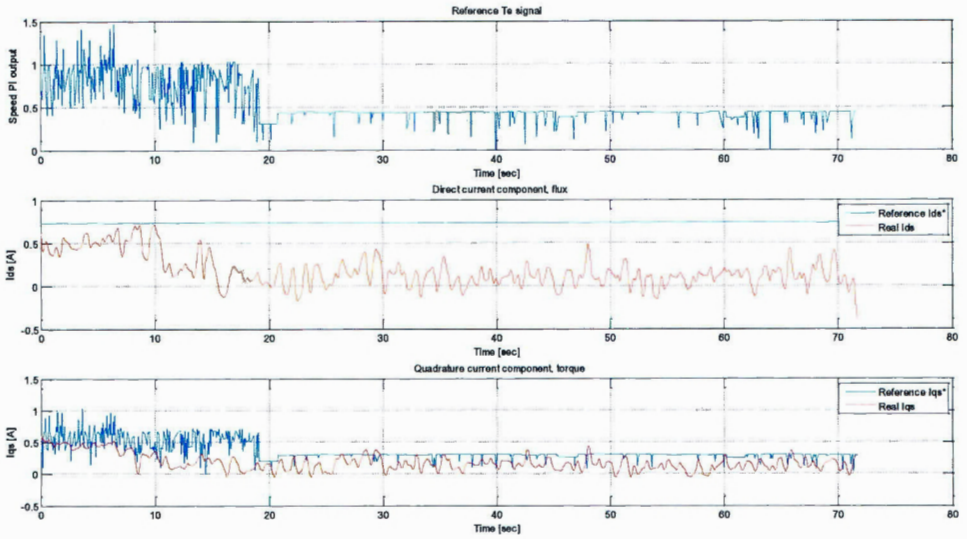

Figure 132. Speed PI output and curreent components Iq, Id. 800 RPM

➢ 900 RPM

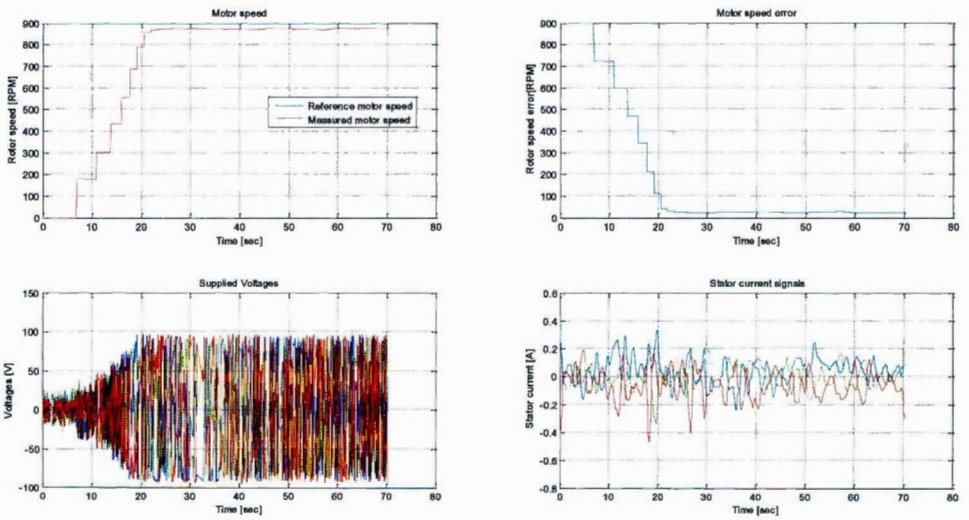

Figure 133. Low speed 900 RPM, with load

MSE in steady state is 34.7800 RPM

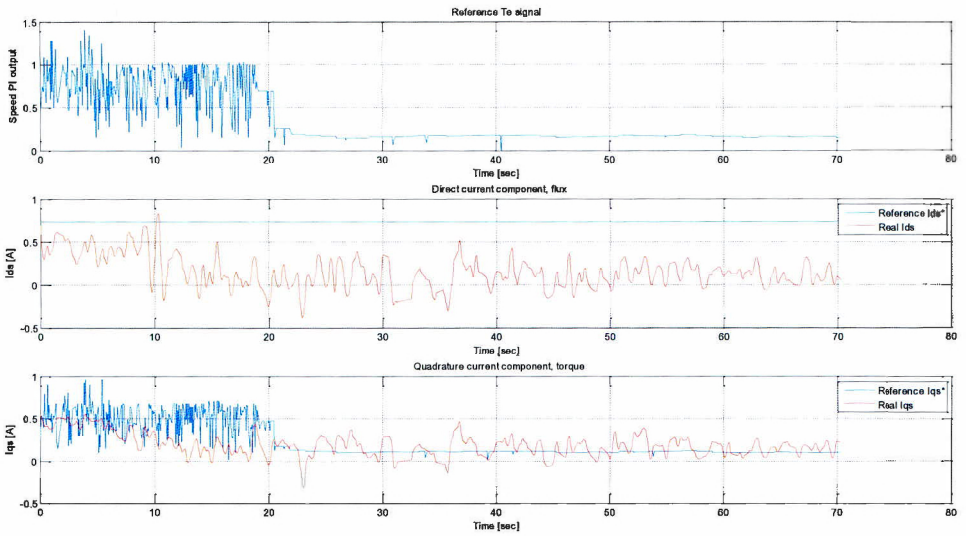

Figure 134. Speed PI output and curreent components Iq, Id. 900 RPM

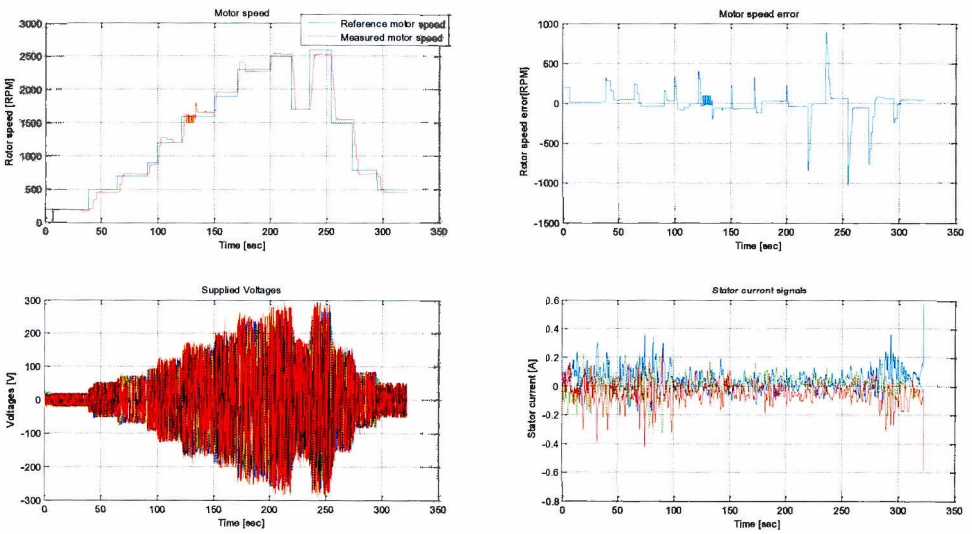

Figure 135. Speed reference variation, with load

MSE in steady state is 41.7675 RPM

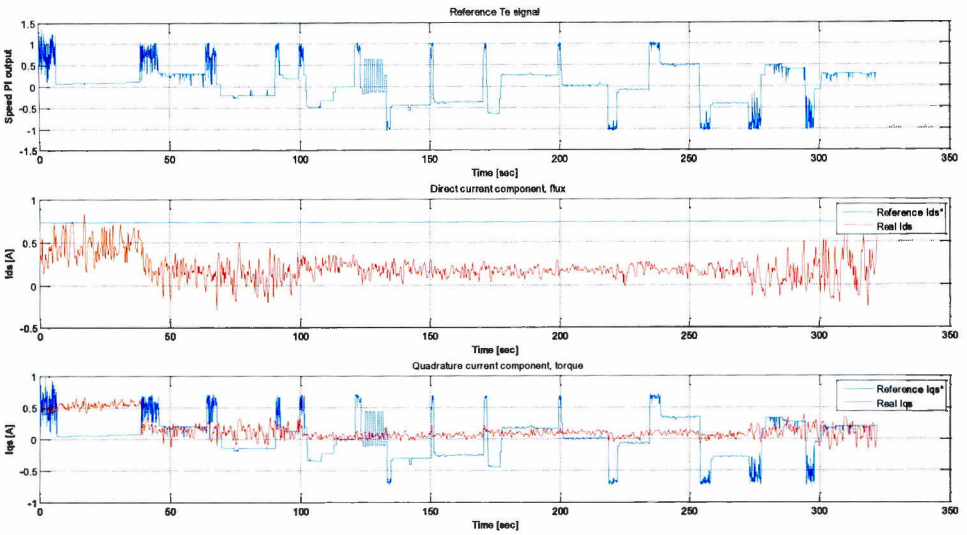

Figure 136. Speed PI output and curreent components Iq, Id.

Since several tests were performed, the results are summarized in Table 6 and Table 7.

Table 6. Motor test with no load

Speed [RPM]	MSE [RPM]
100	34.1672
200	34.2013
300	20.9048
400	7.55
500	8.0905
600	9.5382
700	20.1764
800	2.6825
900	13.7637
Variable setpoints	37.7991

Table 7. Motor test with load, 1Nm

Speed [RPM]	MSE [RPM]
100	34.0875
200	34.1862
300	14.4232
400	33.9582
500	33.1834
600	33.3084
700	35.3973
800	33.9635
900	34.78
Variable setpoints	41.7675

In order to compare the results obtained from the tests with load and no load is depicted the Figure 137, where is possible to see how the no load results keep a low profil in comparison with the loaded tests.

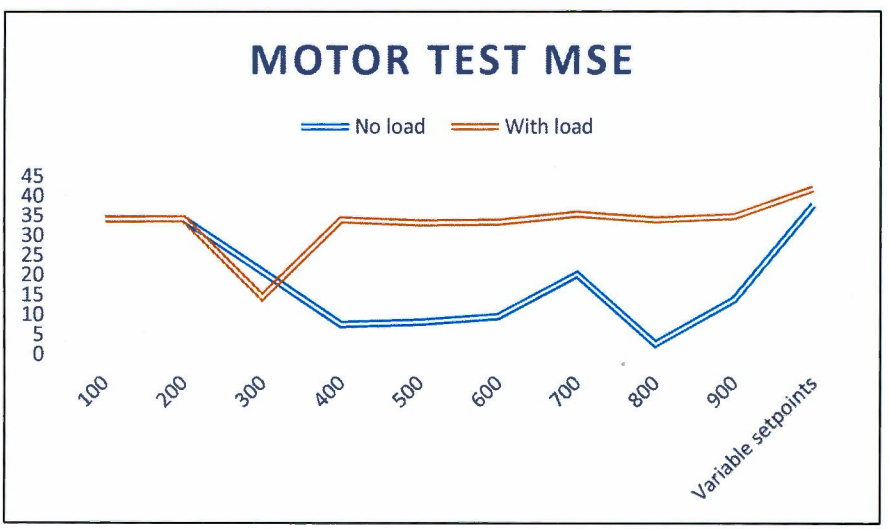

Figure 137. Motor tests with and without load

Next, it is evaluated the results for the intelligence vector control in the co-simulation environment.

4.2.3 Co-Simulation Results

The results obtained from the co-simulation with Multisim model as depicted in the Figure 138 to Figure 140.

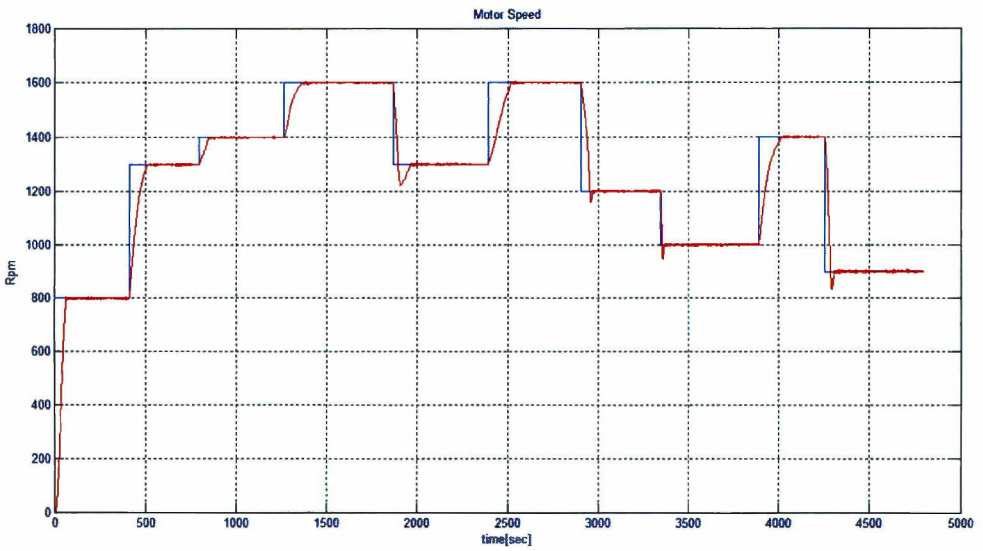

Figure 138. Reference and measured motor speed, co-simulation intelligent vector control

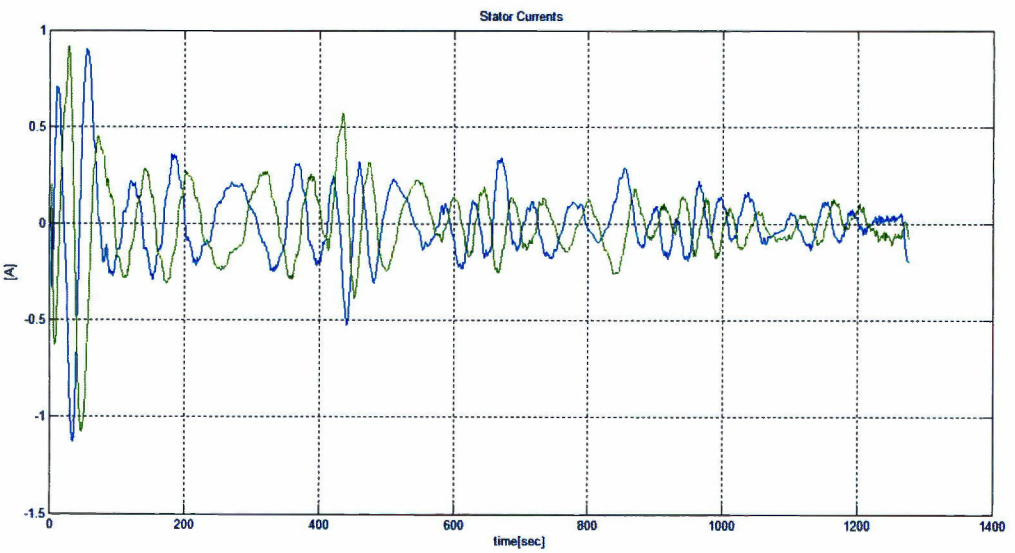

Figure 139. Stator currents, co-simulation intelligent vector control

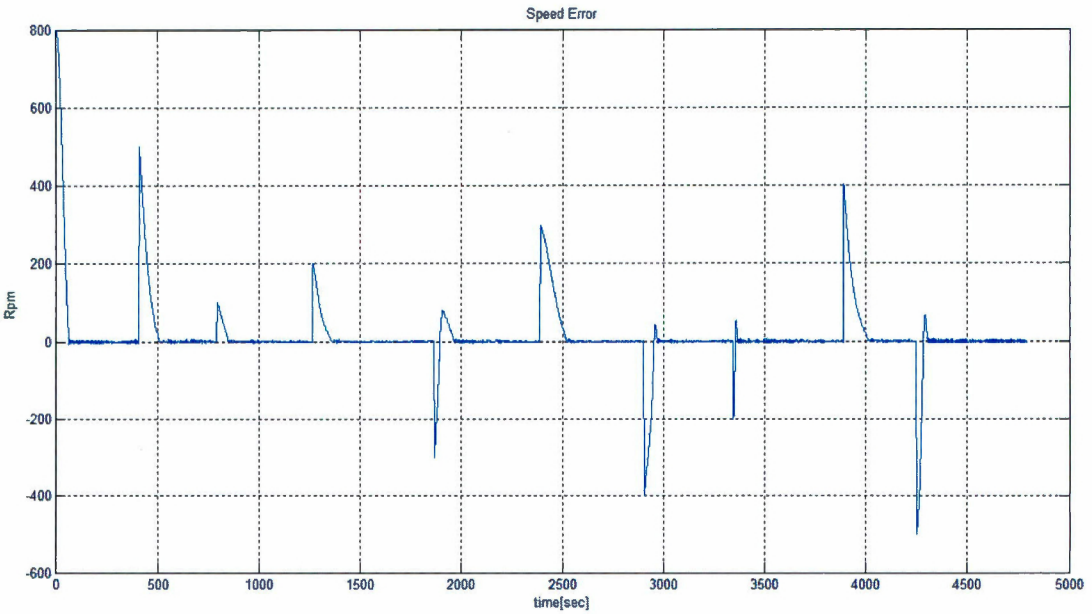

Figure 140. Motor speed error, co-simulation intelligent vector control

The mean square error obtained for the co-simulation is 23.438 rpm. All the steps involved during the programming phase were depicted in this section and also the results obtained for the experimental implementation and co-simulation. It was showed that acceptable results were obtained from each controller and it was demonstrated how useful the implementation of a co-simulation tool for control design is.

The implementation of SMC and fuzzy logic helps to obtain acceptable results with a low error margin. It is valuable to mention that one important result from the implementation of fuzzy logic is the mitigation of torque chattering produced from the SMC controller. Thus, a second test in the co-simulation environment was performed in order to show the reduction in torque pulsations. Figure 141 shows load variations applied to the motor using vector control working with SMC for the speed controller and PI's controllers for the current loops in the co-simulation environment. Some chattering is perceptible in the torque response, especially in the portion after 3 sec.

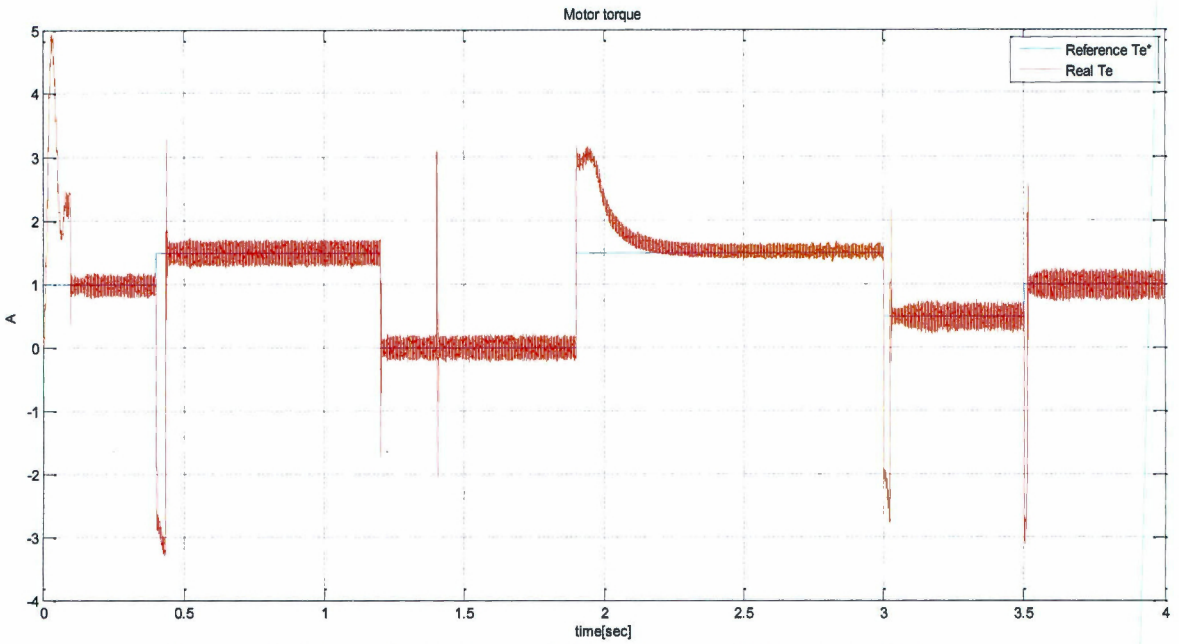

Figure 141. Torque load changes. SMC and normal PI's, co-simulation

The reference current component i_q obtained from equation (4.5) is calculated based on the torque reference signal from the SMC controller. From Figure 142 is notable the torque ripple during load variations, which in real applications can represent efficiency losses. SMC can introduce chattering since one state must track the S surface (see chapter 3, section 3.1). Thus, fuzzy logic contributes to eliminate part of the chattering produced by SMC.

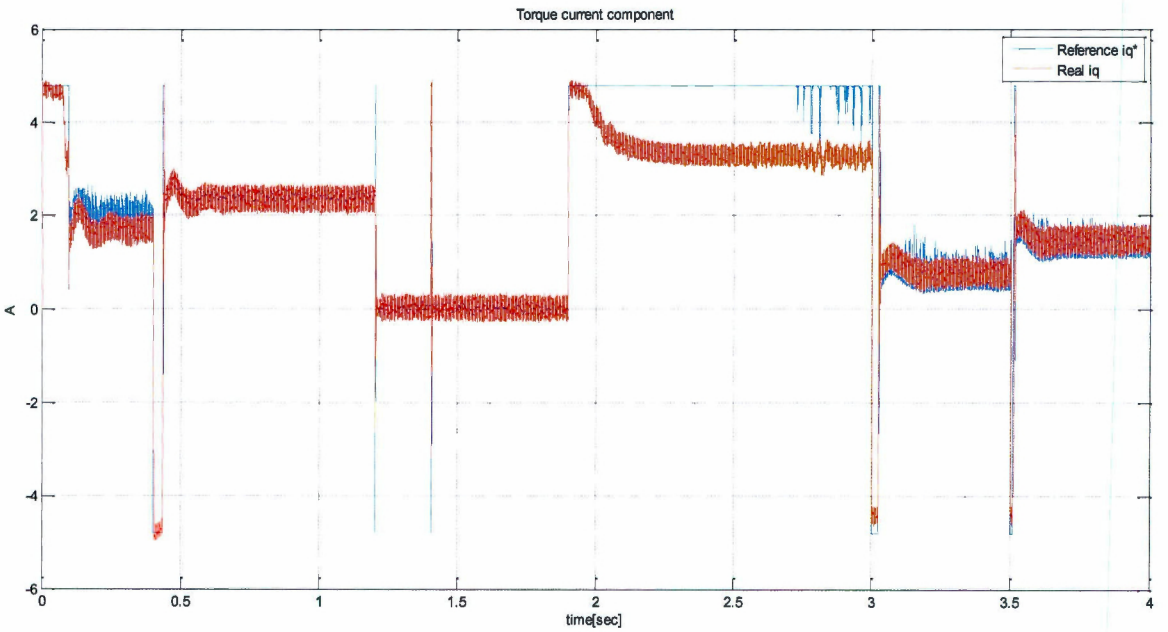

Figure 142. Iq torque current response. SMC and normal PI's, co-simulation

For the same torque load changes the intelligent vector control with SMC and fuzy logic controllers is tested. The load changes are presented in Figure 143, where is possible to note a similar graphical response. However, comparing with Figure 141 is possible to see how the chattering was reduced, more visual in the same portion mentioned before, after 3 sec

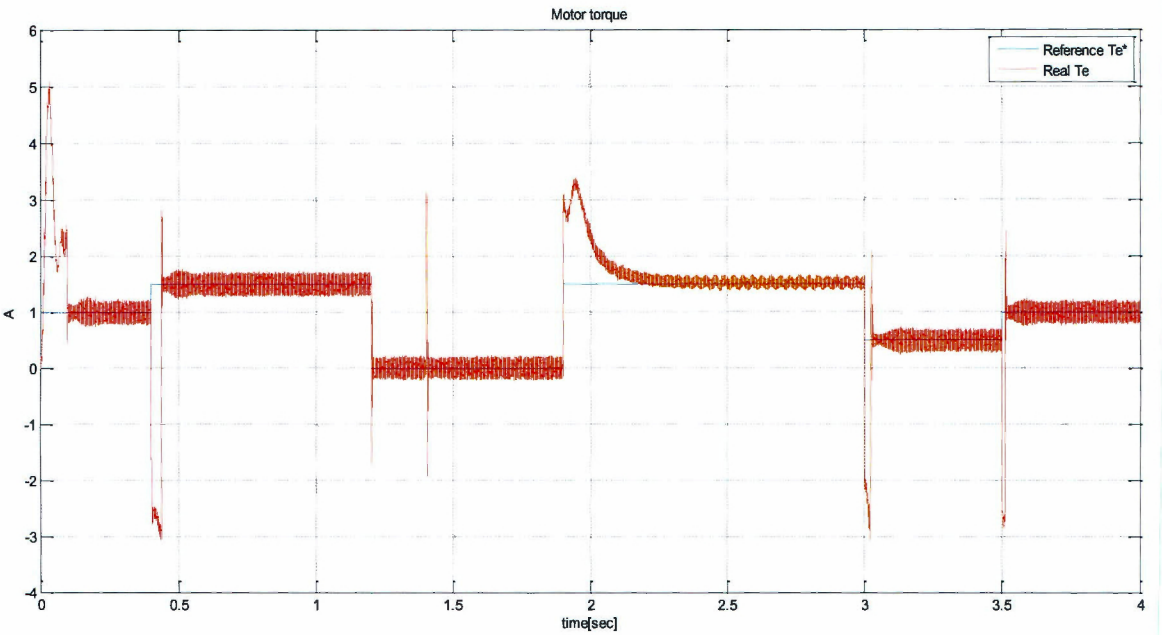

Figure 143. Torque load changes. Intelligent vector control, co-simulation

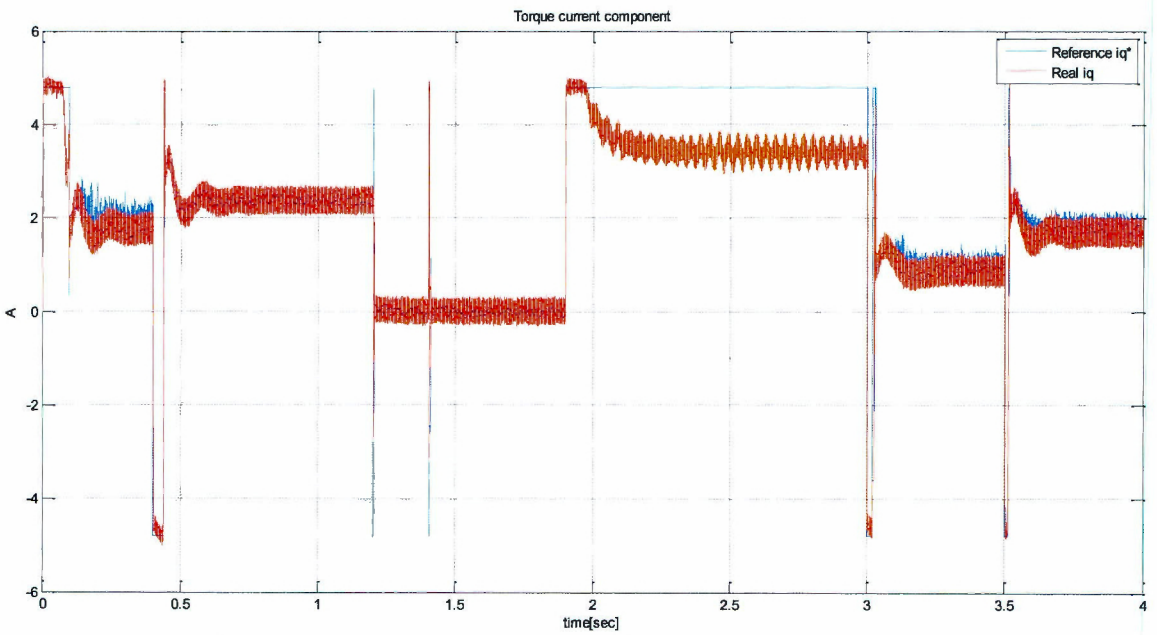

Figure 144. Iq torque current response. Intelligent vector control, co-simulation

Figure 144 clearly presents how the blue signal that corresponds to the reference current torque component has a relevant ripple reduction which of course is reflected in less torque chattering. This is one important contribution from fuzzy logic to the entire control performance. Thanks to a better current control loops response, it is possible to decrease ripple introduction from the inherent nature of a SMC. For real applications, this is a desire response since, it will help to increase AC electric machine service life, and will help to keep low efficiency losses.

Chapter 5: Results and Implementation Discussion

5.1 Results Discussion

In this thesis work was presented the development and implementation of a vector control technique and a vector control with artificial intelligent and robust control methods; both controllers were tested with an induction motor and simulated for an electric vehicle powertrain. All these aspects were evaluated and simulated thanks to Mathworks Matlab and National Instruments LabVIEW and Multisim tools. Now the results obtained and the experience gained during this development is summarized in this section.

5.1.1 Simulation tests

- An EV Peugeot Scooter was modeled and the powertrain was controlled with a conventional vector control technique. This controller was tested with a FUDS driving cycle and also with a regular test where vehicle speed variations were simulated. For both tests, satisfactory results were obtained, from the simulation for the conventional vector controller with a MSE of 8.4482 km/h, and for the FUDS driving cycle and a MSE of 8.2934 km/h for the regular setpoint variations. Taking in consideration that variations of vehicle's speed above 60 km/h (close to 100km/h the higher variation) were performed in order to test acceleration/deceleration and controller response within the driving cycle, a MSE below 10 km/h for the entire test is pretty decent.
- As mentioned in chapter 1, one of the objectives of this work is to walk the reader (e.g. ungraduated student, engineer, interested, etc.) through the vector control design and implementation for AC electric machine applications. This was achieved in this part, since all the simulation phase helped to consolidate the theory explained at the beginning of chapter 2 and was possible to consider all the important element that composed an EV and vector control modelling and design, like the motor selection, the transmission system and driveline configuration. The latter was possible thanks to the calculation of the tractive forces that define an idea of the power requirements.
- In this work the SVPWM was used to work with the vector control, even though popular methods like the hysteresis-band current control PWM is frequently used for vector control. As it was implemented in chapter 2, section 2.1.2.3.2, where the indirect vector control was first simulated in this thesis. This PWM technique is so popular due to its reduction in mathematical complexity (i.e. it is not necessary to transform q-d currents components to stator voltage components, possible to note in the 10 steps explanation in section 2.1.2.3.2), the problem with this technique is the present of harmonic ripple in motor current. On the other hand, the SVPWM, allows a DC bus voltage usage up to 86.6%, as presented in chapter 2, which is higher than other PWM techniques. Also, as a result of a convenient distribution of V0 and V7 vectors during the activation sequence, it is possible to form symmetrical pulse width, hence minimal output harmonics are present in the commanded current waves.
- The results obtained from the vector control in the simulation environment illustrate how oscillations in the stator motor current will be reflected in the motor torque output, and vice versa. This is possible to note in Figure 65 and Figure 66, where the control obeys the speed and torque commanded. Though, the vehicle speed MSE is relatively low for both cases (8.4482 km/h for FUDS test and 8.2934 km/h for vehicular speed variations), the variations in the motor current waves are quite different among each other tests, and this is closely related to the torque variations and the voltage regulator operation (i.e. calculation of q-d voltage components). Thus, the simulation exercise helps to understand how important is to implement motor current filters

in order to obtain a signal with fundamental information, in this case, with a sinusoidal current wave without higher harmonics and therefore lower torque ripple.

- Even though in the simulations performed in this thesis, was not included the thermodynamic effects over the stator and rotor resistance, it is possible to note the implications of the voltage regulator. The SVPWM implementation introduced the q-d components coupled effect among each other (i.e. coupled relation among voltage components illustrated in equation (4.12) and (4.13)). Once the relation among the voltage components is understood in the simulation, it is possible to take that information into account in order to design the vector control for real experimental tests. Therefore, thanks to the initial design stage in the simulation environment was possible to note how important is to decouple voltage components for a smooth motor/control performance.
- In the simulation environment is encouraged to students and researchers to simulate thermic effects that will produce motor parameters variations in order to emulate real world implications in the simulation model. This can certainty improves the vector control design and increase control robustness.

5.1.2 Co-simulation tests

- The first and second objectives defined in this thesis are accomplished thanks to the control validation in a co-simulation environment. Since an intelligent vector control is designed and implemented in LabVIEW (objective 1) based on the conventional vector control defined in the initial simulation phase but now adding fuzzy logic and robust control features to the controller, also a powerful design tool is included in order to validate the correct control performance with real time considerations, Circuit Design Suite Multisim (objective 2).
- Two co-simulation tests were performed in this thesis, the first one at the end of chapter 3, where was used the EV simulated in chapter 2, and the second one performed just with the electric motor model in chapter 4 in order to compare results with the real experiment. For the first test, including the EV model, a MSE of 5.9414 km/h was obtained for the second test, just considering the electric motor, a MSE of 23.438 rpm was obtained for the motor speed changes in rpm.
- Decent results were obtained with the co-simulation test compared with the simulation result obtained in chapter 2 for the EV with MSE of 8.2934 km/h for the Matlab simulation vs. MSE of 5.9414 km/h with the co-simulation. Smooth variations in speed and torque were obtained in the co-simulation tests thanks to the artificial intelligence techniques and sliding mode control incorporate in the indirect vector control.
- In the co-simulation environment part of the model is in the discrete time domain in order to have faster responses from the transfer functions (e.g. integral, rotor flux response) involved. This environment ease to export the controller to the real testing environment. Again, thanks to design aid tools as LabVIEW and Circuit Design Suite Multisim, was possible to shape the controller design with real time considerations in order to have a final indirect vector control.
- Real time experiment with the NI FPGA involves, mandatory use of fixed point variable type. Thanks to the rapid design and development allowed by the NI tools in a co-simulation environment. It was possible to evaluate probable overshoots during the calculations due to fixed point (e.g. 32,6 FXP; 6-integer word length and 32-word length) data configuration. Once, it was validated that overshoots (i.e. operation among fixed points data) were not presented for different operation conditions, was possible to jump to the real time experimentation with the proper setup for a conventional vector control.
- After a detailed theory explanation for SMC and Fuzzy logic, was possible to see how beneficial in terms of control performance, is the implementation of intelligent and robust techniques for

electric motor applications. Also, this part of the thesis helps to contribute with the objective 2, since students or interested people in AC motor control, can learn from the co-simulation design process.

- It is the intention for future works to implement in real time the intelligent vector control evaluated in co-simulation in this thesis, and see the motor response for low speeds operation and hyper speeds (field weakening region). Also, evaluate the torque for different conditions and the chattering reduction by implementing FLC. Of course that other robust control approach are welcome to compare to SMC and FLC for indirect vector control

5.1.3 Experimental tests

- The conventional vector control was tested with an induction motor using a two level inverter. This controller was run through all the motor speed range, and acceptable results were obtained from low range speed tests with and without load. The MSE in steady state varied from 3 rpm up to 41 rpm as a maximum error obtained, which illustrates the control programming work in a real time environment.
- Figure 137 shows the comparison among loaded and no loaded tests, where no loaded motor tests showed a lower MSE profile compared to the loaded motor tests. Behavior that is completely reasonable due to the load effect over the motor speed. Also, when the motor speed setpoint is variated the MSE among tests have a pretty close behavior.
- From the experience obtained during the vector control design phase, it is concluded the following points:
    - Rotor flux position: the integration method implemented to compute the flux angle must be pretty well defined, since the minimum error will directly affect coordinates transformation and hence the other calculations will not be carried out in the correct coordinates framework (e.g. q-d actual stator current components and therefor Vq and Vd PI's outputs). Another important parameter related to the rotor flux is the sample period defined for the integration, period that is defined based on the hardware clock implemented. The integration method implemented was the Euler backward integration, which gave an acceptable control performance under a reasonable low mathematical complexity for the memory space available. It is possible to say that this is the most important parameter to take into account during a vector control development process. For future works, it can be evaluated the inference of the temperature at high speed conditions, this may be overcome by using observers to estimate rotor inductance and resistance, parameters that directly affect the correct rotor flux calculation.
    - Measurement frequency: in order to allow the control to develop all the computation phase, must be well defined the clock period at which will be measured the motor currents and speed signals. A correct desfinition of this parameter will gives the correct communication among the three parts of a vector control: measurement, control and PWM computation.
    - PI's sampling frequency: The vector control implemented in this work used three PI's which control speed and currents variables. Due to the response time inherent to the motor speed variable (mechanical variable) a higher sampling period is needed. On the other hand, the currents variables i_{qs} and i_{ds} have a lower sample period due to their fast time response. Therefore, the hardware implemented should offer enough speed (e.g. FPGA implemented has a 40MHz clock) in order to track the behavior of these current components and guarantee the correct control performance.
    - SVPWM times: The space vector modulation technique depends enormously on an accurate times vector calculation, that is, T1, T2 and T0. These parameters calculation depend on the accurate voltage reference vector position computation, equation (2.80).

Therefore, similar as was explained for the rotor flux position, here a good integration method with a precisely sample period is preponderant. Future improvements on the SVPWM implementation in real time is the elimination of trigonometric functions by calculating the unit vector sings (i.e. $[\hat{\imath}, \hat{\jmath} \,\&\, \hat{k}]$) and therefore defining the rotatory voltage vector location.

- The flux and torque components are the core of vector control. The reason of this is illustrated in equation (4.5), where is possible to note how is desire to have a constant rotor flux response while the torque is regulated by the quadrature stator current component. This behavior is reflected in Figure 116 and Figure 136 where the torque follows the Iq commands while the rotor flux has a stable constant performance. This is also possible to confirm in all the tests results plotted for no loaded and loaded motor. As a future work, for real time vector control implementation must be interesting to evaluate the vector control operation under field weakening conditions, that is, setting motor speed above its nominal value and evaluate motor parameters variations and torque response.

Chapter 6: Conclusions

In this thesis work is presented the design and implementation processes of the vector control technique, tested in an EV powertrain model, with help of simulations, and in an induction motor. All these were complemented with the use of artificial intelligence and robust control techniques in order to achieve an intelligent vector control for EV powertrain, tested by co-simulation among two NI software. Simulation and real-time implementation tools were used to show the complete design process from the theory to the real experimental deployment.

A detailed description of each design phase was presented through all the chapters with their corresponding demonstration. Even though, there is plenty of literature regarding vector control, in this work is address the AC electric motor control from a wide perspective of control and pulse wide modulation alternative techniques, with main focus on vector control and SVPWM. This is considered the highest added value of this work, the condensation of theory, demonstration, design and implementation through simulation and real experiments. Also, two important methods from robust control such as Sliding mode and intelligent control like Fuzzy Logic, were introduced in vector control and tested by co-simulation. The latter, gives a relevant value to this work in terms of the possible benefits that can represent for undergraduate or graduate students that want to explorer the world of electric machines control.

Alternative energy sources are quite important for different application and it was presented in this work how is possible to implement electric motor controllers by means of simulation and experimental tools. It is also the desire of this work to be useful for other researchers as a knowledge source in order to keep improving on the green energy transportation and to keep developing science in favor of alternative energy implementation for several applications.

Electric vehicles applications are quite important for the future of transportation and it is the desire of this work to contribute with a detailed theory, simulation, co-simulation and experimentation deployment to motivate students and researchers interested in AC motors control to propose efficient and less complex alternatives of vector control to be implemented in commercial EV at a large production scale. Therefore, this work encourage students to develop AC motor bed test and prototype EV using AC motors in order to erase the idea that AC drives are equal to difficult and complex control laws.

Glossary

ADVISOR: It is a powertrain simulation tool developed by the National Renewable Energy Laboratory (NREL) that is used to study.----------23,71,72

Alternative energies: Different technologies implemented to generate renewable energy solutions.---14, 18

Artificial Intelligence: The capability to understand by itself establishing relations among works and tasks.

ANFIS: Adaptive Neuro-Fuzzy Inference System combines the benefits of a neural networks with the benefits of the fuzzy inference system in a single model.----------34

Balanced systems: For electric motor applications the loads are distributed evenly as is practical between three phases.----------31

Blaschcke equations: The equations that describes the flux rotor components in the current method implemented for direct vector control.----------52

Block diagram: It represents the language that describes the interaction of components within a system. The principal parts or functions are represented by blocks connected by lines that show the relationships of the block.----------62

Capacitors: these are implemented for power electronic applications to filter voltage signals and store energy. ----------25

Cascaded H-bridge: It is a topology implemented usually for multilevel voltage-source inverter.--------32

Rectifier: It is an electrical device that converts alternating current (AC), which periodically reverses direction, to direct current (DC), which flows in only one direction.----------22
Regenerative rectifiers: These kinds of rectifiers allow the energy regeneration back to the electrical grid.
Rotor flux: It is the magnetic flux generated in the rotor. ----------33
Scalar control: It is a control technique that plays with the voltage and frequency ratio and it is based on the equivalent circuit of the induction motor.----------47
Semiconductor switch: It is a semiconductor device used as a switch or rectifier in power electronics.--29
SHE-PWM: Selective harmonic elimination is a low switching frequency PWM method developed for traditional converters. ----------31
Sine PWM: A PWM technique that used reference and carrier signals to generate multiple pulse. -------31
Sliding mode control: A nonlinear control technique method that alters the dynamics of a nonlinear system by application of a discontinuous control signal that forces the system to "slide" along a cross-section of the system's normal behavior. ----------11
SVPWM: Space Vector PWM is a modulation algorithm which translates phase voltage (phase to neutral) references, coming from the controller, into modulation times/duty-cycles to be applied to the PWM peripheral. ----------68
Switching frequency: It is the duty cycle that is defined for the semiconductor of an inverter. ----------32
Testbed: The set of components that define an experimental configuration. In this work the testbed is defined with induction motor, inverter, Ac module and electromagnetic break. ----------81
Thyristors: It is a solid-state semiconductor device with four layers of alternating N and P-type material. 29
Tractive effort: This is the force propelling the vehicle forward transmitted to the ground through the drive wheels. ----------71
Ultracapacitors: A high technology device to storage electrical energy for EV applications. ----------22
Vector control: A control technique for AC motors also known as Field Oriented Control that uses current and magnetic flux vectors to control rotor flux and motor torque variables.----------18
VHDL: VHSIC Hardware Description Language is a low level programming method implemented for FPGAs. ----------91
Voltage model: A model implemented in direct vector control to calculate the stator fluxes components and then rotor fluxes. ----------53

References

Akatsu, Kan, Atsuo Kawamura, and Senior Member. 2000. "Sensorless Very Low-Speed and Zero-Speed Estimations with Online Rotor Resistance Estimation of Induction Motor." *IEEE TRANSACTIONS ON INDUSTRY APPLICATIONS,* 36 (3): 764–71.

Amjadi, Z., and S.S. Williamson. 2010. "Power-Electronics-Based Solutions for Plug-in Hybrid Electric Vehicle Energy Storage and Management Systems." *IEEE Transactions on Industrial Electronics* 57 (2): 608–16. doi:10.1109/TIE.2009.2032195.

Banerjee, Archis, Aritra Banerjee, D P Saikat Rana, and K N Shubhanga. 2015. "A Study of Starting Methods for an Induction Motor Using an Arbitrary Waveform Generator." In *3rd International Conference on Advances in Electrical Engineering*, 34–37.

Blaschke, Felix. 1972. "The Principle of Field Orientation as Applied to the New TRANSVECTOR Closed LoopControl System for Rotating Field Machines." *Siemens Review* 39 (5): 217–20.

Bose, Bimal K. 2002. *Modern Power Electronics and AC Drives*. Prentice Hall PTR.

Burke, Andrew F. 2007. "Batteries and Ultracapacitors for Electric, Hybrid, and Fuel Cell Vehicles." *Proceedings of the IEEE. Electric, Hybrid & Fuel Cell Vehicles* 95 (4): 806–20. doi:10.1109/JPROC.2007.892490.

Carrara, G., S. Gardella, M. Marchesoni, R. Salutari, and G. Sciutto. 1992. "A New Multilevel PWM Method: A Theoretical Analysis." *IEEE Transactions on Power Electronics* 7 (3): 497–505. doi:10.1109/63.145137.

Chan, C. C. 2007. "The State of the Art of Electric, Hybrid, and Fuel Cell Vehicles." *Proceedings of the IEEE. Electric, Hybrid & Fuel Cell Vehicles* 95 (4): 704–18. doi:10.1109/JPROC.2007.892489.

Chen, Xia, and Zhongchao Wei. 2008. "A New Modeling and Simulation Platform-Mworks for Electrical Machine Based on Modelica." In *International Conference onElectrical Machines and Systems, 2008. ICEMS*, 4065–67.

Depenbrock, Manfred. 1987. Direct self-control of the flux and rotary moment of a rotary-field machine, issued 1987.

Dunnigan, M.W., S. Wade, B.W. Williams, and X. Yu. 1998. "Position Control of a Vector Controlled

Induction Machine Using Slotine's Sliding Mode Control Approach." *IEE Proceedings - Electric Power Applications* 145 (3): 231. doi:10.1049/ip-epa:19981834.

Enjeti, Prasad N., Phoivos D. Ziogas, and James F. Lindsay. 1990. "Programmed PWM Techniques to Eliminate Harmonics: A Critical Evaluation." *IEEE Transactions on Industry Applications* 26 (2): 302–16. doi:10.1109/28.54257.

Ernest, Emil, Rafal Sztylka, Bartlomiej Ufnalski, and Wlodzimierz Koczara. 2007. "Methods in Teaching Modern AC Drives: Inverter-Fed Motor System with Internet-Based Remote Control Panel." In *EPE-PEMC 2006: 12th International Power Electronics and Motion Control Conference, Proceedings*, 2130–33. doi:10.1109/EPEPEMC.2006.283176.

Esposito, F, V Isastia, and S Meo. 2010. "PSO Based Energy Management Strategy for Pure Electric Vehicles with Dual Energy Storage Systems." In *International Review of Electrical Engineering*, 5:1862–72.

Farrokhi, M. Mohebbi, M. 2005. "Optimal Fuzzy Control of Parallel Hybrid Electric Vehicles." In *Automation and Systems*, 252–56. Ieee. doi:10.1109/VPPC.2005.1554566.

Fraile-Ardanuy, Jesús, Pedro Ángel García-Gutiérrez, Cristina Gordillo-Iracheta, and Jesús Maroto-Reques. 2011. "Development of an Integrated Virtual-Remote Lab for Teaching Induction Motor Starting Methods: Evaluation of the ECTS Really Devoted to Study." In *Promotion and Innovation with New Technologies in Engineering Education, FINTDI 2011, Conference Proceedings*, 8:77–81. doi:10.1109/FINTDI.2011.5936419.

Franquelo, L.G, Jose Rodríguez, Jose I Leon, Samir Kouro, Ramon Portillo, and Maria A M Prats. 2008. "The Age of Multilevel Converters Arrives." *Industrial Electronics Magazine, IEEE* 2 (2): 28–39.

Ghanes, M, J De Leon, and A Glumineau. 2006. "Observability Study and Observer-Based Interconnected Form for Sensorless Induction Motor." In *45th IEEE Conference on Decision & Control*, 1240–45.

———. 2007. "A Sensorless Flux-Speed Sliding Mode Controller for Induction Motor with Experimental Results." In *16th IEEE International Conference on Control Applications*, 1185–90.

Goldberg, Saul, William F Horton, and Thomas Agayoff. 2001. "Teaching Power Conversion in a Virtual Laboratory." In *Power Engineering Society Summer Meeting*, 0:1515–19.

Gupta, Aayush, Taehyung Kim, Taesik Park, and Cheol Lee. 2009. "Intelligent Direct Torque Control of Brushless DC Motors for Hybrid Electric Vehicles." In *Vehicle Power and Propulsion Conference*, 116–20.

Hasse, Karl. 1968. "Zum Dynamischen Verhalten Der Asynchronmaschine Bei Betrieb Mit Variabler Ständerfrequenz Und Ständerspannung."

———. 1969. "Zur Dynamik Drehzahlgeregelter Antriebe Mit Stromrichtergespeisten Asynchron-Kurzschlublaufermaschinen." Darmstadt Tech. Hochsch.

———. 2001. "Feldorientierte Regelung Im Rückblick." In *IEEE IAS/PELS/IES German Chapter Meeting, Braunschweig, 22.*

Hoekstra, Douwe. 2005. "Conceptual Design of Energy Exchange Systems for Hybrid Vehicles." Technische Universiteit Eindhoven.

Holtz, J. 1994. "Pulsewidth Modulation for Electronic Power Conversion." *Proceedings of the IEEE* 82 (8): 1194–1214. doi:10.1109/5.301684.

Hou, Jun, and Xuexun Guo. 2008. "Modeling and Simulation of Hybrid Electric Vehicles Using HEVSIM and ADVISOR." In *IEEE Vehicle Power and Propulsion Conference (VPPC)*, 1–5.

Ibtiouen, R. 2003. "Estimation of the Rotor Resistance in Induction Motor by Application of the Spiral

Vector Theory Associate to Extended Kalman Filter." In *The 35th Southeastern Symposium on System Theory*, 211–16.

Jiang, Weige, and Jiuchun Xia. 2002. "CNG Engine Air-Fuel Ratio Control Using Fuzzy Neural Networks." In *The 2nd International Workshop on Autonomous Decentralized System, 2002.*, 156–61. IEEE Comput. Soc. doi:10.1109/IWADS.2002.1194665.

Karanayil, Baburaj, Muhammed Fazlur Rahman, and Colin Grantham. 2007. "Online Stator and Rotor Resistance EstimationScheme Using Artificial Neural Networks for VectorControlled Speed Sensorless Induction Motor Drive." *IEEE TRANSACTIONS ON INDUSTRIAL ELECTRONICS* 54 (1).

Lai, J. S., and Z. F. Peng. 1996. "Multilevel Converters. A New Breed of Power Converters." *IEEE Transactions on Industry Applications* 32: 509–17.

Larminie, James, and John Lowry. 2003. *Electric Vehicle Technology Explained.* Chichester, UK: John Wiley & Sons, Ltd. doi:10.1002/0470090707.

Liang, Zhang, Zhang Xin, Tian Yi, and Zhang Xinn. 2009. "Intelligent Energy Management Based on the Driving Cycle Sensitivity Identification Using SVM." In *2009 Second International Symposium on Computational Intelligence and Design*, 513–16. Ieee. doi:10.1109/ISCID.2009.274.

Luk, P C K, and L C Rosario. 2006. "Power and Energy Management of a Dual- Energy Source Electric Vehicle - Policy Implementation Issues." In *Power Electronics and Motion Control Conference*, 5–10.

Majdi, Laila, Ali Ghaffari, and Nima Fatehi. 2009. "Control Strategy in Hybrid Electric Vehicle Using Fuzzy Logic Controller." In *2009 IEEE International Conference on Robotics and Biomimetics (ROBIO)*, 842–47. Ieee. doi:10.1109/ROBIO.2009.5420563.

Majumdar, G, H Hussein, M Fukada, J Yama, and T Kikunaga. 2001. "High-Functionality Compact Intelligent Power Unit (IPU)." In *International Symposium on Proceedings of the 13th*, 315–18.

Markel, T, A Brooker, T Hendricks, V Johnson, K Kelly, B Kramer, M O Keefe, S Sprik, and K Wipke. 2002. "ADVISOR : A Systems Analysis Tool for Advanced Vehicle Modeling." *ELSEVIER Journal of Power Sources* 110: 255–66.

Mohebbi, M., M. Charkhgard, and M. Farrokhi. 2005. "Optimal Neuro-Fuzzy Control of Parallel Hybrid Electric Vehicles." In *2005 IEEE Vehicle Power and Propulsion Conference*, 252–56. Ieee. doi:10.1109/VPPC.2005.1554566.

Nash, J.N. 1997. "Direct Torque Control, Induction Motor Vector Control without an Encoder." *IEEE Transactions on Industry Applications* 33 (2): 333–41. doi:10.1109/28.567792.

Pacheco, Juliano De O, Flabio A B Batista, and Clovis A. Petry. 2012. "Multi-Platform Education System of Frequency Inverters." In *2012 10th IEEE/IAS International Conference on Industry Applications, INDUSCON 2012*. doi:10.1109/INDUSCON.2012.6451391.

Park, Kang Hyo, Cheol Moon, Kee Hyun Nam, Mun Kyu Jung, and Young Ahn Kwon. 2011. "State Observer with Parameter Estimation for Sensorless Induction Motor." In *SICE*, 2967–70.

Park, M. K., I. H. Suh, S. J. Byoun, and S. R. Oh. 1996. "An Intelligent Coordinated Control System for Steering and Traction of Electric Vehicles." In *International Conference on Proceedings of the 1996 IEEE IECON 22nd*, 1972–77.

Pérez, Daniel, J. Balcells, M. Lamich, N. Berbel, J. Zaragoza, and J. Mon. 2008. "Training Kit for Power Electronics Teaching." In *Proceedings - 34th Annual Conference of the IEEE Industrial Electronics Society, IECON 2008*, 3541–45. doi:10.1109/IECON.2008.4758532.

Ponce, Pedro, Mario Pacas, and Arturo Molina. 2012. "Real Time Systems for Teaching Induction Motor

Drives." In *6th IEEE International Conference One-Learning in Industrial Electronics (ICELIE)*, 65–73. IEEE.

Ponce, Pedro, and Lopez Sampé. 2008. *Máquinas Eléctricas Y Técnicas Modernas de Control*. Alfaomega.

Raed H. Ahmad, George G. Karady, Tracy D. Blake, Peter Pinewski. 1997. "Comparison of Space Vector Modulation Techniques Based on Performance Indexes and Hardware Implementation." In *Industrial Electronics, Control and Instrumentation, 1997. IECON 97. 23rd International Conference on*, 682–87.

Rodriguez, J., L.G. Franquelo, S. Kouro, J.I. Leon, R.C. Portillo, M.A.M. Prats, and M.A. Perez. 2009. "Multilevel Converters : An Enabling Technology for High-Power Applications." *Proceedings of the IEEE* 97 (11): 1786–1817.

Rodríguez, J, J Pontt, G Alzamora, N Becker, O Einenkel, J L Cornet, and A Weinstein. 2001. "Novel 20 MW Downhill Conveyor System Using Three-Level Converters." In *IEEE, Industry Applications Conference*, 0:1396–1403.

Rosario, Leon C, and Patrick C K Luk. 2006. "Implementation of a Modular Power and Energy Management Structure for Battery-Ultracapacitor Powered Electric Vehicles." In *Hybrid Vehicle Conference*, 141–56.

Rosario, Leon, Patrick Chi, and Kwong Luk. 2007. "Applying Management Methodology to Electric Vehicles with Multiple Energy Storage Systems." In *Machine Learning and Cybernetics Conference*, 19–22.

Santini, D J. 2011. "Electric Vehicle Waves of History : Lessons Learned about Market Deployment of Electric Vehicles."

Sepe, R. B., and N. Short. 2000. "Web-Based Virtual Engineering Laboratory (VE-LAB) for Collaborative Experimentation on a Hybrid Electric Vehicle Starter/alternator." *IEEE Transactions on Industry Applications* 36 (4): 1143–50. doi:10.1109/28.855972.

Sepe, R.B., M. Chamberland, and N. Short. 1999. "Web-Based Virtual Engineering Laboratory (VE-LAB) for a Hybrid Electric Vehicle Starter/alternator." In *Conference Record of the 1999 IEEE Industry Applications Conference. Thirty-Forth IAS Annual Meeting (Cat. No.99CH36370)*, 4:2642–48. doi:10.1109/IAS.1999.799210.

Shoorehdeli, M.a., M. Teshnehlab, and A.K. Sedigh. 2006. "A Novel Training Algorithm in ANFIS Structure." In *2006 American Control Conference*, 6 pp. Ieee. doi:10.1109/ACC.2006.1657525.

Slotine, J. J. E. 1984. "Sliding Controller Design for Non-Linear Systems." *International Journal of Control, Taylor & Francis* 40 (2): 421–34.

Slotine, J. J. E., and L. Welping. 1991. *Applied Nonlinear Control*. Prentice Hall.

Takahashi, Isao, and Toshihiko Noguchi. 1986. "A New Quickresponse and High-Efficiency Control Strategy of an Induction Motor." *IEEE Transactions on Industry Applications* 1A–22 (5): 420–29.

Tant, Jeroen, Jeroen Zwysen, Kristof Engelen, Niels Leemput, Juan Van Roy, Sam Weckx, and Johan Driesen. 2012. "Power Electronics for Electric Vehicles: A Student Laboratory Platform." In *2012 IEEE 13th Workshop on Control and Modeling for Power Electronics, COMPEL 2012*. doi:10.1109/COMPEL.2012.6251778.

Tao, Wu, and Zhao Liang. 2011. "Simulation of Vector Control Frequency Converter of Induction Motor Based on Matlab / Simulink." In *Third International Conference on Measuring Technology and Mechatronics Automation*, 2–5. doi:10.1109/ICMTMA.2011.637.

Teodorescu, R., F. Blaabjerg, J. K. Pedersen, E. Cengeli, S. Sulistijo, B. Woo, and P. Enjeti. 1999.

"Multilevel Converters a Survey." In *Power Electronics Conference*.

Thornton, Edward J, and J Kirk Armintor. 2003. "The Fundamental of AC Electric Induction Motor Design and Application." In *Proceedings of Twentieth International Pump Users Symposium*.

Tiitinen, Pekka. 1996. "The next Generation Motor Control Method, DTC Direct Troque Control." In *Power Electronics, Drives and Energy Systems for Industrial*, 37–43.

Timmermans, Jean-marc, Hasan Culcu, Thierry Coosemans, Joeri Van Mierlo, and Philippe Lataire. 2009. "Test Platform for Hybrid Electric Power Systems : Use for Design Project for Students." In *Power Electronics and Applications, 2009. EPE '09. 13th European Conference on*, 1–7. http://ieeexplore.ieee.org/xpl/login.jsp?tp=&arnumber=5279064&url=http://ieeexplore.ieee.org/xpls/abs_all.jsp?arnumber=5279064.

Trigg, T, P Telleen, R Boyd, and F Cuenot. 2013. "Global EV Outlook: Understanding the Electric Vehicle Landscape to 2020." *Iea*, no. April: 1–41. http://www.iea.org/publications/freepublications/publication/name-37024-en.html%5Cnhttp://scholar.google.com/scholar?hl=en&btnG=Search&q=intitle:Global+EV+Outlook:+Understanding+the+Electric+Vehicle+Landscape+to+2020#0.

Utkin, V. 1977. "Variable Structure Systems with Sliding Modes." *IEEE Transactions on Automatic Control* 22 (2): 212–22.

Vandermeulen, Aaron, and John Maurin. 2010. "Current Source Inverter vs . Voltage Source Inverter Topology."

Vas, Peter. 1998. *Sensorless Vector and Direct Torque Control*. Oxford University Press.

Veiga, Emiliano, Jacson Oliveira, Ademir Nied, and Jose De Oliveira. 2012. "Web-Based Learning of Electrical Machines Simulation Tool - IMotor." In *Proceedings - 2012 6th IEEE International Conference on E-Learning in Industrial Electronics, ICELIE 2012*, 74–79. doi:10.1109/ICELIE.2012.6471150.

Wang, Dazhi, Renyuan Tang, and Jie Yang. 2004. "HEV Control System Based on Adaptive Hierarchical Supervisory Control Strategy." In *Control Conference*, 283–87.

Wipke, K B, M R Cuddy, and S D Burch. 1999. "ADVISOR 2 . 1 : A User-Friendly Advanced Powertrain Simulation Using a Combined Backward / Forward Approach." *Preprint Prepared for IEEE Transactions on Vehicular Technology: Special Issues on Hybrid and Electric Vehicles*, no. August.

Wipke, Keith, Matthew Cuddy, Desikan Bharathan, Steve Burch, Valerie Johnson, Tony Markel, and Sam Sprik. 1998. "ADVISOR 2 . 0 : A Second-Generation Advanced Vehicle Simulator for Background : Applications of ADVISOR." In *North American EV & Infrastructure*.

Wishart, Jeffrey Daniel. 2008. "Modelling, Simulation, Testing, and Optimization of Advanced Hybrid Vehicle Powertrains." University of Victoria.

Xiaolan, Wu, Cao Binggang, Wen Jianping, and Wang Zhanbin. 2008. "Application of Particle Swarm Optimization for Component Sizes in Parallel Hybrid Electric Vehicles." In *IEEE World Congress on Computational Intelligence).*, 2874–78.

Yang, Yee-pien, and Chuan-feng Fang. 1994. "Adaptive Speed Control of AC Servo Induction Motors with On-Line Load Estimation." In *American Control Conference*, 2030–34.

Yi, Tian, Zhang Xin, Zhang Liang, and Zhang Xinn. 2009. "Intelligent Energy Management Based on Driving Cycle Identification Using Fuzzy Neural Network." In *2009 Second International Symposium on Computational Intelligence and Design*, 501–4. Ieee. doi:10.1109/ISCID.2009.271.

Zadeh, L. A. 1965. "Fuzzy Sets." *Information and Control* 8 (3): 338–353.

Zhang, Danhong, Yan Zhou, Kai-Pei Liu, and Qing-Quan Chen. 2009. "A Study on Fuzzy Control of Energy Management System in Hybrid Electric Vehicle." In *2009 Asia-Pacific Power and Energy Engineering Conference*, 1–4. Ieee. doi:10.1109/APPEEC.2009.4918119.

Zhao, Tao Zhao Tao, and Qunjing Wang Qunjing Wang. 2005. "Application of MATLAB/SIMULINK and PSPICE Simulation in Teaching Power Electronics and Electric Drive System." In *International Conference on Electrical Machines and Systems*, 3:2037–2041. doi:10.1109/ICEMS.2005.202919.

Zorgani, Y Agrebi, Y Koubaa, M Boussak, and Senior Member. 2010. "Simultaneous Estimation of Speed and Rotor Resistance in Sensorless ISFOC Induction Motor Drive Based on MRAS Scheme." In *XIX International Conference on Electrical Machines -*.

Zorzano, Luis F, Jose Zorzano, Abelardo Martinez, Antonio Zorzano, and Javier Vicunia. 2007. "Virtual Laboratory for Intelligent Vector Control of AC Machines." In *Intelligent Signal Processing, 2007. WISP . IEEE International Symposium on*.